

Is an Ultra Large Natural Image-Based Foundation Model Superior to a Retina-Specific Model for Detecting Ocular and Systemic Diseases?

Qingshan Hou^{1,2,3*}, Yukun Zhou^{4,5,6*}, Jocelyn Hui Lin Goh^{1,3,7*}, Ke Zou^{1,3}, Samantha Min Er Yew^{1,3}, Sahana Srinivasan^{1,3}, Meng Wang^{1,3}, Thaddaeus Lo⁷, Xiaofeng Lei⁸, Siegfried K. Wagner^{5,9}, Mark A. Chia^{5,9}, Dawei Yang¹⁰, Hongyang Jiang¹⁰, AnRan Ran¹⁰, Rui Santos^{11,12}, Gabor Mark Somfai^{11,12,13}, Juan Helen Zhou^{14,15}, Haoyu Chen^{16,17}, Qingyu Chen¹⁸, Carol Yim-Lui Cheung¹⁰, Pearse A. Keane^{5,9†}, Yih Chung Tham^{1,3,7,19†}

***contributed equally as first author**

†contributed equally as last author

¹ Department of Ophthalmology, Yong Loo Lin School of Medicine, National University of Singapore, Singapore

² School of Computer Science and Engineering, Northeastern University, Shenyang, China

³ Centre for Innovation and Precision Eye Health, Yong Loo Lin School of Medicine, National University of Singapore, Singapore

⁴ Centre for Medical Image Computing, University College London, London, United Kingdom.

⁵ NIHR Biomedical Research Centre at Moorfields Eye Hospital NHS Foundation Trust, London, UK

⁶Department of Medical Physics and Biomedical Engineering, University College London, London, United Kingdom.

⁷ Singapore Eye Research Institute, Singapore National Eye Centre, Singapore

⁸ Institute of High-Performance Computing (IHPC), Agency for Science, Technology and Research (A*STAR), Singapore, Singapore.

⁹ Institute of Ophthalmology, University College London, London, UK

¹⁰ Department of Ophthalmology and Visual Sciences, Chinese University of Hong Kong, Hong Kong, China

¹¹ Department of Ophthalmology, Stadtspital Zürich, Zurich, Switzerland

¹² Spross Research Institute, Zurich, Switzerland

¹³ Department of Ophthalmology, Semmelweis University, Budapest, Hungary

¹⁴ Centre for Sleep and Cognition & Centre for Translational MR Research, Yong Loo Lin School of Medicine, National University of Singapore, Singapore

¹⁵ Department of Electrical and Computer Engineering, National University of Singapore, Singapore

¹⁶ Joint Shantou International Eye Center, Shantou University and the Chinese University of Hong Kong, Shantou, Guangdong, China

¹⁷ Shantou University Medical College, Shantou, Guangdong, China

¹⁸ Department of Biomedical Informatics and Data Science, Yale School of Medicine, Yale University, New Haven, USA

¹⁹ Ophthalmology and Visual Sciences (Eye ACP), Duke-NUS Medical School, Singapore

Correspondence:

Dr Yih Chung Tham

Yong Loo Lin School of Medicine, National University of Singapore.

Level 13, MD1 Tahir Foundation Building, 12 Science Drive 2, Singapore 117549

Tel: +65 65767298, Fax: +65 6225 2568

Email: thamyc@nus.edu.sg

Abstract

The advent of foundation models (FMs) is transforming medical domain. In ophthalmology, RETFound, a retina-specific FM pre-trained sequentially on 1.4 million natural images and 1.6 million retinal images, has demonstrated high adaptability across clinical applications. Conversely, DINOv2, a general-purpose vision FM pre-trained on 142 million natural images, has shown promise in non-medical domains. However, its applicability to clinical tasks remains underexplored. To address this, we conducted head-to-head evaluations by fine-tuning RETFound and three DINOv2 models (large, base, small) for ocular disease detection and systemic disease prediction tasks, across eight standardized open-source ocular datasets, as well as the Moorfields AlzEye and the UK Biobank datasets. DINOv2-large model outperformed RETFound in detecting diabetic retinopathy (AUROC=0.850–0.952 vs. 0.823–0.944, across three datasets, all $P \leq 0.007$) and multi-class eye diseases (AUROC=0.892 vs. 0.846, $P < 0.001$). In glaucoma, DINOv2-base model outperformed RETFound (AUROC=0.958 vs 0.940, $P < 0.001$). Conversely, RETFound achieved superior performance over all DINOv2 models in predicting heart failure, myocardial infarction, and ischaemic stroke (AUROC =0.732–0.796 vs. 0.663–0.771, all $P < 0.001$). These trends persisted even with 10% of the fine-tuning data. These findings showcase the distinct scenarios where general-purpose and domain-specific FMs excel, highlighting the importance of aligning FM selection with task-specific requirements to optimise clinical performance.

Introduction

The advent of foundation models (FMs) have ushered in a paradigm shift in medical deep learning (DL) approaches[1][2][3][4]. Driven by the availability of large-scale high-quality unstructured datasets and advanced self-supervised learning methods, FMs excel in performing multiple tasks with high adaptability and generalizability to new, unseen tasks, often requiring minimal fine-tuning [5][6]. In ophthalmology, the introduction of RETFound, the first retina-specific FM developed by Zhou et al. [7] in 2023, led to a significant transformation in DL approaches for medical image analysis. Using a Vision Transformer (ViT) [8][9] backbone and a Masked Autoencoder (MAE)-based [10] self-supervised learning approach, RETFound was pre-trained on a diverse dataset of 1.4 million natural images (ImageNet-1K), ~900,000 color fundus photographs (CFPs), and ~730,000 OCT scans. This pretraining approach enabled RETFound to effectively extract and learn retinal features and representations, enhancing diagnostic performance, data efficiency, and generalizability across ophthalmic and systemic clinical tasks [11][12][13].

In parallel, DINOv2 is a general-purpose vision FM developed by Meta AI, pre-trained on 142 million natural images from the LVD-142M dataset [14]. With its sheer scale and versatile feature representation capabilities, DINOv2 has demonstrated strong adaptability across some medical domains, such as pathology [15][16] and radiology[17]. However, the applicability of DINOv2 to ophthalmic tasks remains largely unexplored, and a direct comparison with RETFound in fine-tuning for retinal image analysis has not yet been performed.

To address these gaps, we conducted a head-to-head performance comparison between three DINOv2 models (large, base, small) and RETFound across a range of ocular disease detection and systemic disease prediction tasks. For a fair and standardized comparison, we replicated the RETFound study's original fine-tuning methodology on all three DINOv2 models (**Fig. 1**). The models' comparative performances were evaluated across eight open-source datasets for ocular disease detection tasks including diabetic retinopathy (APTOS-2019, IDRID, MESSIDOR2), glaucoma (PAPILA, Glaucoma Fundus), and multi-class eye diseases (JSIEC, Retina, OCTID). For systemic disease prediction tasks (3-year incidence of heart failure, myocardial infarction, ischemic stroke), we fine-tuned all models on the Moorfields AlzEye dataset, and externally tested on the UK Biobank dataset. Model performance was primarily measured using the area under receiver operator characteristics curve (AUROC), and the significant differences in AUROC values between models were determined through two-sided t-tests with Bonferroni correction. This comprehensive evaluation provides critical insights into the respective strengths and optimal applications of general-purpose and retina-specific FMs, contributing new understanding to the utilization of FM in ophthalmology and beyond.

Results

The demographic characteristics and details of study datasets utilized are detailed in **Supplementary Table 1 and 2**.

Comparative Performance of Models in Ocular Disease Detection Tasks:

DINOv2 fine-tuned models generally outperformed RETFound across ocular disease detection tasks in internal and external testing (**Fig.2, Extended Data Fig. 1-4, and Supplementary Table 3-4**).

For diabetic retinopathy (DR) detection task, DINOv2-Large achieve higher AUROC values across the datasets. For example, after fine-tuning and internally validating using the APTOS2019 dataset, DINOv2-Large achieved an AUROC of 0.952 (95% CI: 0.950–0.954), surpassing RETFound (AUROC: 0.944, 95% CI: 0.941–0.946, all $P < 0.001$, **Fig. 2 and Extended Data Fig. 1**). Consistently, in the MESSIDOR-2 dataset, DINOv2-Large achieved an AUROC of 0.906 (95% CI: 0.902–0.910), higher than RETFound (AUROC: 0.883, 95% CI: 0.878–0.889, $P < 0.001$). Similarly, in the IDRID dataset, DINOv2-Large obtained an AUROC of 0.850 (95% CI: 0.836–0.865), outperforming RETFound (AUROC: 0.823, 95% CI: 0.809–0.836, $P = 0.007$). Similarly, in external validations, where cross-evaluation was performed by fine-tuning models on one dataset and testing them on the other two (repeating this permutation across all three datasets), DINOv2 models generally performed better than RETFound (**Extended Data Fig. 3 and Supplementary Table 4**). For instance, when fine-tuned on APTOS2019 and externally tested MESSIDOR2, DINOv2-Large achieved the highest AUROCs of 0.817, outperforming RETFound (AUROCs: 0.725 in MESSIDOR2, **Extended Data Fig. 3a**, all $p < 0.001$). When fine-tuned on IDRID and tested on APTOS2019, DINOv2-Large (AUROC:0.783) and DINOv2-Small (AUROC:0.808) outperformed RETFound (AUROC:0.752, all $P < 0.001$). Evaluations based on accuracy, Kappa values, and F1-score, consistently showed that DINOv2 models outperformed RETFound in most scenarios (**Extended Data Fig. 3b-3d**).

For the glaucoma detection task, when fine-tuned and internally validated on the Glaucoma_fundus dataset, DINOv2 models achieved higher AUROC scores than RETFound (**Fig.2**). Specifically, DINOv2-Base and -Small achieved AUCs of 0.958 (95% CI: 0.955–0.961), outperforming RETFound (AUROC: 0.940, 95% CI: 0.936–0.945, all $P < 0.001$, **Fig. 2 and Extended Data Fig. 1**). Similarly, in external validation, when fine-tuned on the Glaucoma_fundus dataset and tested on the PAPILA dataset, DINOv2-Large achieved the highest performance with an AUROC of 0.625, surpassing RETFound's 0.558 ($P < 0.001$, **ExtendedDataFig.4a, Supplementary Table 4**). Evaluations based on accuracy, Kappa values,

and F1-score, consistently largely showed that DINOv2 models outperformed RETFound in most scenarios (**Extended Data Fig. 4b-4d**).

For the multi-class eye disease classification tasks, the models were finetuned and validated internally on datasets containing CFPs (the JSIEC and Retina datasets) and OCT scans (**Fig.2**). In the JSIEC CFP dataset, all models were comparable and achieved AUROC scores close to 1. In the Retina CFP dataset, the DINOv2 models achieved AUROC scores ranging from 0.874 (DINOv2-Base: 95% CI: 0.864–0.883) to 0.892 (DINOv2-Large: 95% CI: 0.883–0.902), surpassing RETFound's performance (AUROC: 0.846, 95% CI: 0.836–0.856, all $P \leq 0.001$). For the OCTID dataset with OCT scans, all models showed comparable performance.

Comparative Performance of Models in Predicting 3-year incidence of Systemic Diseases:

We further evaluated the comparative performance of DINOv2 and RETFound models in predicting three cardiovascular-related systemic diseases - heart failure, myocardial infarction, and ischemic stroke. Across all three systemic disease outcomes, the models were fine-tuned and tested internally on the Moorfields AlzEye study dataset, and externally validated using the UK Biobank dataset (**Fig. 3 & Extended Data Fig. 5-6 & Supplementary Table 5**).

For heart failure prediction, in internal testing, RETFound significantly outperformed all DINOv2 variants, achieving an AUROC of 0.796 (95% CI: 0.767-0.827), compared to DINOv2-Base's 0.771 (95% CI: 0.738-0.807), the best-performing DINOv2 model ($P < 0.001$, **Fig 3**). For myocardial infarction prediction, RETFound achieved the highest AUROC of 0.732 (95% CI: 0.663-0.805), significantly outperforming the best DINOv2 model, DINOv2-Large (AUROC: 0.711, 95% CI: 0.638-0.784, $P < 0.001$). For ischemic stroke prediction, RETFound demonstrated consistent superiority with an AUROC of 0.754 (95% CI: 0.684-0.838), surpassing the best DINOv2 model, DINOv2-base (AUROC: 0.714, 95% CI: 0.633-0.789, $P < 0.001$).

In the external validation using the UK Biobank dataset (**Extended Data Fig.6**), RETFound consistently outperformed all DINOv2 models across the three systemic disease prediction tasks. For heart failure prediction, RETFound achieved the highest AUROC (0.674), surpassing all DINOv2 models (AUROC: 0.615-0.623, all $P < 0.001$). Similarly, for myocardial infarction prediction, RETFound maintained its advantage with an AUROC of 0.594, outperforming all DINOv2 models (AUROC: 0.523-0.559, all $P < 0.001$). In ischemic stroke prediction, RETFound achieved an AUROC of 0.586, exceeding DINOv2-Base (0.556) and DINOv2-Small (0.519) (all $P \leq 0.008$). Secondary metric, including accuracy, further reinforced RETFound's superiority, with higher values compared to all DINOv2 models across all three systemic outcomes (**Extended Data Fig. 6**).

Comparative Performance in Label Efficiency:

To investigate the impact of training data size on FMs performance, we conducted an in-depth analysis using varying proportions of training/ fine-tuning data (10%, 20%, 50%, 90%, and 100%) across different ocular and systemic disease prediction tasks (**Fig. 4 and Supplementary Table 6-7**).

For DR detection task, in the APTOS2019 dataset, the DINOv2 models and RETFound achieved comparable AUROC performance, with minimal variation across different proportions of training data (**Fig. 4 and Supplementary Table 6**). However, in the MESSIDOR2 and IDRID datasets, the DINOv2 models consistently outperformed RETFound, achieving higher AUROCs as the training data proportion decreased. Furthermore, in the APTOS2019 and MESSIDOR2 datasets, the performances of DINOv2 models remained relatively stable (i.e. no significant drop) despite decrease in training data size. In the multi-class eye disease detection tasks (e.g., JSIEC, Retina, OCTID), DINOv2 models consistently exhibited higher AUROCs than RETFound across nearly all training data proportions. Notably, DINOv2 models required fewer training samples to achieve superior performance (particularly in the OCTID dataset), demonstrating better label efficiency in these multi-class tasks. Nevertheless, in glaucoma detection task, all models largely showed similar performances across the scenarios.

On the other hand, in systemic disease prediction tasks, RETFound exhibited a distinct advantage where it consistently achieved higher AUROC values across all training data proportions (**Fig. 4 and Supplementary Table 7**). Notably, as training data decreased, RETFound maintained relatively stable or similar performances across the three systemic prediction tasks, reflecting its robustness. At lower training proportions (e.g., 10%–50%), DINOv2 models, particularly DINOv2-Small, exhibited more variability and consistently underperformed compared to RETFound.).

Comparison of Calibration Performance between DINOv2 and RETFound Models

We compared the calibration performance of DINOv2 models (Large, Base, and Small) with RETFound across ocular and systemic disease tasks using corresponding datasets. Overall, we observed that DINOv2 models generally demonstrated better calibration for ocular diseases, while RETFound exhibited superior calibration for systemic disease predictions.

For DR detection task, in the APTOS2019 dataset, it was revealed that DINOv2-Base and -Small were better calibrated than RETFound, as indicated by their calibration curves being closer to the perfectly calibrated line and their lower expected calibration error (ECE) values (**Fig. 5 &**

Extended Data Fig. 7–8). In the IDRID dataset, DINOv2-Small demonstrated the best calibration performance with its curve closely following the diagonal line. Similarly in glaucoma detection, DINOv2-Base (ECE: 0.015) performed best, especially in high-probability regions in the Glaucoma_fundus dataset, while DINOv2-Large (ECE:0.040) achieved superior overall calibration on the PAPILA dataset, outperforming RETFound (ECE=0.065). On the other hand, for datasets covering multiple retinal diseases, such as Retina, DINOv2-small (ECE:0.013) had more superior calibration than RETFound (ECE:0.027). In the JSIEC and OCTID datasets, all models exhibited fluctuations and had similar calibration.

Across the tasks of predicting heart failure and myocardial infarction (**Fig. 5**), RETFound demonstrates stable calibration performance. Its calibration curves were closer to the perfectly calibrated line, and it achieved ECE values mostly lower than DINOv2 models' values. Nevertheless, when predicting ischemic stroke, RETFound exhibited poorer calibration compared to its performance in other systemic disease tasks, with an ECE of 0.212. By contrast, DINOv2-Base achieved the best calibration among all models with an ECE of 0.024, followed by DINOv2-Small (ECE = 0.125). DINOv2-Large, however, displayed the highest calibration error among all models, with an ECE of 0.312, indicating substantial miscalibration in its probability estimates for ischemic stroke prediction.

Discussion

In this study, we evaluated the comparative performance and label efficiency between fine-tuning on DINOv2, a general-purpose vision FM, with RETFound, a retina-specific FM, across a range of ocular disease detection and systemic disease prediction tasks. We ensured a standardized and robust comparison with RETFound by replicating RETFound study's original fine-tuning methodology on all three DINOv2 models (large, base, small). This is a rare feat and has not been conducted prior. Overall, in ocular disease detection tasks, we observed that DINOv2-large outperformed RETFound and with better label efficiency. Additionally, DINOv2-base and -small models generally required three times less computing resources compared to RETFound. Conversely, in systemic disease prediction tasks, RETFound generally achieved superior performance and better label efficiency than all the DINOv2 models. This comprehensive head-to-head evaluation highlights distinct scenarios where general-purpose and domain-specific FMs excel, offering practical information to users on the optimal application of these FMs for task-specific fine-tuning.

In ocular disease detection tasks, DINOv2 generally outperformed RETFound, when fine-tuned on the complete dataset, highlighting the transferability of DINOv2 to these tasks. Additionally, DINOv2 demonstrated exceptional label efficiency, maintaining robust AUROC performance even with limited training data (**Fig. 4 and Supplementary Table 6**). DINOv2's superior performance may be attributed to its pretraining strategy. First, its exposure to a large corpus of 142 million natural images enabled DINOv2 to learn diverse visual patterns and contexts, enhancing its feature extraction capabilities and thereby establishing a stronger foundation for various downstream visual tasks. This could have contributed to DINOv2's exceptional transfer learning capabilities, a finding consistent with prior research on AMD and DR detection[20][21]. Secondly, DINOv2 employs a self-distillation process where knowledge transfer occurs between the teacher and student network, enabling the model efficiently learn refined visual representations. This broad knowledge of visual representations acquired during its larger pretraining could have enhanced DINOv2's generalizability to ocular disease detection tasks. Altogether, this suggests that DINOv2 could serve as a competitive alternative to RETFound particularly in low-data resource settings for specific ocular diseases detection tasks.

Interestingly, while DINOv2 demonstrated superior performance over RETFound in the ocular disease diagnosis task, this trend was not fully replicated in all external validations (**Extended Data Figures 3 and 4**). Our observation highlighted a common challenge in model generalizability, where variations in data distribution between datasets can impact model reliability and performance especially when the models are deployed in a new real-world environment. Therefore, addressing these issues of model generalization would help researchers to determine the clinical applicability of these FMs in real-world practice.

Additionally, in terms of computational resource consumption (**Supplementary Table 8**), RETFound required more GPU RAM during the fine-tuning phase but had a lower inference speed (i.e. took more time to process the same number of images) as compared to the DINOv2-small and -base. DINOv2-small (22M parameters) and DINOv2-base (86M parameters) are significantly smaller models compared to RETFound and DINOv2-large (both models have 303M parameters). As such, when tested on 100 retinal images (with 224×224 resolution and processed on a single A100 GPU), DINOv2-small (0.48 seconds) and DINOv2-Base (0.64 seconds), both had lower inference time compared to RETFound (1.48 seconds) and DINOv2-Large (1.70 seconds). This underscores the potential of smaller and more computational resource efficient general-purpose vision FMs like DINOv2-small and base as a competitive alternative to RETFound for ocular disease detection tasks under resource-scarce settings. More importantly, it highlights the need to consider the trade-off between model performance and computational resource requirements depending on unique deployment sites.

On the other hand, in systemic disease prediction tasks, RETFound consistently outperformed the DINOv2 models across all varying proportions of fine-tuning data used, indicating RETFound's superior label efficiency and its ability to detect subtle retinal changes associated with systemic diseases. (**Fig. 3 - 4 and Supplementary Table 5 and 7**). This superior performance could be attributed to its pretraining strategy, which harnessed domain-specific knowledge from 900,000 unlabeled retinal images using the MAE-supervised learning approach [7]. The MAE approach involves having the model reconstruct highly masked input images, forcing the model to infer missing information from the masked patches of the images during training. Through this iterative training process, the model learns to extract subtle, fine-grained vasculature patterns and features from the masked retinal images, thereby potentially contributing to RETFound's retina-specific domain knowledge. Overall, these findings suggest the advantages of incorporating domain-specific data in the pretraining process of FMs. For ophthalmology tasks, RETFound superior label efficiency demonstrated its potential as an effective pre-trained model, especially well-annotated data still remain scarce and expensive to curate.

Our study's key strength lies in replicating the intricate methodology of the original RETFound experiments, ensuring consistent and robust head-to-head evaluation between DINOv2 and RETFound across diverse ocular disease detection and systemic disease prediction tasks. We fine-tuned the DINOv2 models using multiple open-source datasets, applying the same fine-tuning and test data split as applied in RETFound's task-specific adaptations. To our knowledge, such a benchmarking evaluation of a general-purpose vision FM and RETFound has never been conducted to date. This open approach provides credibility to the repeatability of our study findings, and would help to facilitate comparable benchmarking evaluations for future FMs.

Nevertheless, this study has a few limitations. In this study, the range of detection tasks included was limited by the availability of annotated open-source CFP and OCT datasets with specific disease labels. Therefore, the comparative performance of DINOv2 and RETFound models was not demonstrated on other modalities such as ultra-wide field retinal imaging. Furthermore, even though we evaluated the models' performance in detecting multiple ocular diseases and predicting multiple systemic diseases, other rare ocular (e.g. Retinitis Pigmentosa) and systemic diseases were not included in this study. Future work should include benchmarking of the performance of FMs on other conditions such as dementia and coronary artery diseases. Additionally, due to the rarity of open-source datasets with systemic disease annotation, the performance of DINOv2 and RETFound models in predicting the 3-year incidence of heart failure, myocardial infarction and ischemic stroke was evaluated using the private MEH-AlzEye and the UK Biobank datasets. This implies that a benchmarking dataset that encompasses a broader spectrum of use cases, including ocular diseases, systemic disease prediction, general medical conditions, and rare diseases, would be essential for standardizing performance evaluation of these FMs. The reliance on private datasets implies that future benchmarking evaluations on these systemic disease outcomes would necessitate obtaining relevant data access approvals from the respective institutions.

Building on our findings, to deepen insights on the clinical applicability of these FMs, it will be critical to evaluate their comparative performance using datasets that are representative of real-world setting. Specifically, there is a need to further investigate novel methods to improve the performance, generalizability and efficiency of these FMs in scarce-data and resource conditions (i.e. the real-world clinical challenge). One method could be the use of multimodality to synergize feature-rich image data and contextual information-rich text data from electronic health records in the pre-training phase, hence allowing the models to learn underlying dynamic relationship between the different data type [20]. Future work would involve iterative refinement and continuous validations of these FMs for diverse clinical task scenarios across the medical domain to broaden their application to wider healthcare contexts. Globally, this will require collaborative efforts from researchers worldwide to curate diverse datasets, adopt standardized reporting practices to ensure reproducibility and comparability, and engage stakeholders in collectively democratizing access to datasets and advanced FMs [21].

Conclusion

This study provides a comprehensive evaluation of general-purpose vision FMs (DINOv2 models) and a domain-specific FM (RETFound), highlighting DINOv2's optimal adaptability for ocular disease detection tasks and RETFound's superior performance in systemic disease prediction. These findings provide new insights into the optimal utilisation of general-purpose vision FM and retina-specific FM, highlighting the importance of aligning FM selection with task-specific requirements and resource considerations to achieve optimal clinical performance.

Method

Details of pretraining datasets for DINOv2 models

All three model versions of DINOv2 - Small, Base, and Large - were pretrained on the LVD-142M dataset, which is a large-scale unannotated dataset with a total of 142,109,386 natural images [14]. This massive dataset was curated from multiple open-source natural image databases, including the ImageNet-22k (56,788,344 images, 40.0%), the ImageNet-1K[22] (40,997,344 images, 28.8%), the Google Landmarks v2 (6,321,880 images, 4.4%), and Mapillary SLS (1,434,262 images, 1.0%) datasets, and the remaining 36,567,556 images (25.8%) obtained through retrieval and augmentation of multiple smaller datasets. To ensure data quality and diversity, researchers employed self-supervised image retrieval and clustering methods to filter and rebalance the curated dataset, which provided rich visual feature learning resources for pretraining of the DINOv2 models.

Task-specific datasets for ocular disease detection.

We evaluated model performance on multiple publicly available ophthalmological datasets covering various eye diseases. For DR detection, we used three datasets, the IDRiD (India)[23][24], MESSIDOR-2 (France)[25][26][27], and APTOS-2019 (India) datasets[28]. The DR grading for these datasets were based on the International Clinical Diabetic Retinopathy Severity Scale, which indicated five stages of severity from no DR to proliferative DR. For detection of glaucoma, we used the PAPILA (Spain)[29] and Glaucoma Fundus (Korea)[30] datasets. Both datasets have glaucoma labels of three classes, non-glaucoma, early glaucoma (suspected glaucoma), and late-stage glaucoma. For detection of multi-category eye diseases, we used two CFP datasets including the JSIEC dataset (China)[31] which comprises 1,000 images covering 39 classes of common referable fundus diseases and conditions, and the Retina dataset [32], comprising 601 images with normal, glaucoma, cataract, and retinal diseases annotations. An additional OCT dataset, the OCTID dataset (India)[33], containing 470 OCT scans with labels including normal, macular hole, age-related macular degeneration (AMD), central serous retinopathy, and DR was also used. For more detailed information about the datasets used, please refer to Supplementary Table 1.

Task-specific datasets for incidence prediction of systemic diseases.

For incidence prediction of systemic diseases, we focused on three cardiovascular disease outcomes: heart failure, myocardial infarction, and ischemic stroke. We used retinal images to predict the risk of these three cardiovascular diseases occurring within the next 3 years. All models were fine-tuned on a curated private dataset from the Moorfields AlzEye[34] study (MEH-AlzEye) and internally evaluated on a held-out test dataset. The MEH-AlzEye study is a large-scale retrospective cohort study that linked the ophthalmological data of 353,157 patients seen at Moorfields Eye Hospital between 2008 and 2018 with systemic health data across England. These

systemic health data primarily come from the Hospital Episode Statistics (HES) data that documented hospital records of patients receiving inpatient care. Additionally, we leveraged the UK Biobank for external evaluation of three systemic diseases, a large-scale biomedical database that includes data from 502,665 participants aged 40 to 69 years who are registered with the UK National Health Service. Among them, 82,885 participants underwent retinal imaging and OCT examination, and a total of 171,500 retinal images were obtained. For consistency, we selected one left-eye retinal image per patient visit for model training, to avoid bias caused by inconsistent individual visits. We divided patient data into training, validation, and test sets for model training, tuning, and evaluation. This approach allowed us to assess the potential of retinal images in predicting these important systemic diseases, providing new insights for early intervention and personalized medical strategies. For more detailed information about the datasets, please refer to Supplementary Table 2.

DINOv2 model architecture and implementation

DINOv2 employs Vision Transformer (ViT) as its backbone network with three different model size scales: Small, Base, and Large. DINOv2-Small (21M parameters) is based on the ViT-S/14 architecture, with an embedding dimension of 384, with 6 attention heads, and 12 Transformer blocks. DINOv2-Base (86M parameters) utilized the ViT-B/14 architecture, featuring an embedding dimension of 768, with 12 attention heads, and 12 Transformer blocks. DINOv2-Large (303 M parameters) was built on the ViT-L/14 architecture, with the largest embedding dimension of 1024, along with 16 attention heads, and 24 Transformer blocks. All three model versions use a patch size of 14×14 . During training, DINOv2 employs the AdamW optimizer with an initial learning rate of $1e-3$, a batch size of 2048, and a total of 625k iterations. To enhance performance, LayerScale technology was introduced with an initial value of $1e-5$. Weight decay follows a cosine schedule ranging from 0.04 to 0.2. Learning rate warm-up lasts for 100k iterations, while the teacher network momentum also adopts a cosine schedule, gradually increasing from 0.994 to 1. The models were primarily trained in float16 precision, but the gradients for DINO heads were computed in float32 precision to ensure accuracy. The feed-forward network layers used a multilayer perceptron (MLP) structure with a dropout rate of 0 to maximize information transfer. These models were distilled from a larger ViT-G/14 model, effectively learning and extracting powerful visual feature representations while maintaining training efficiency.

Details on task-specific fine-tuning of the DINOv2 models.

When adapting to downstream tasks, we used all three versions of the DINOv2 model (Large, Base, or Small) to generate high-level features from the retinal images, and added an MLP block to each model. The MLP block takes these high-level features as input and generates probability scores (ranging from 0 to 1) as outputs in each ocular disease or systemic disease incidence prediction task. The number of neurons in the last layer of the MLP block is determined by the number of categories in each task. To enhance the models' generalization, we also applied various

data augmentation techniques, including random cropping, horizontal flipping, vertical flipping, rotation, and adjustments to brightness and contrast. The batch size was set to 32 and training was conducted over 100 epochs. The first 10 epochs was a learning rate warm-up phase, increasing from 0 to 5×10^{-3} . For the subsequent 90 epochs, a cosine annealing scheduling was applied, gradually decreasing the learning rate from 5×10^{-3} to 1×10^{-6} . We used the AdamW optimizer with weight decay set to 0.05. After each training epoch, the models were evaluated on the validation set and the model iteration with the highest AUROC on the validation set was used for all downstream evaluation. These model weights were then implemented for independent internal and external evaluations. For RETFound, we utilized the publicly available pre-trained weights of the model for each specific task.

For the cross-dataset evaluation of DR, glaucoma detection, and systemic disease prediction, we employed the same fine-tuning strategy but trained and tested the models on different dataset combinations. Specifically, the datasets used for DR include APTOS-2019, MESSIDOR-2, and IDRiD; for glaucoma, Glaucoma_fundus and PAPILA; and for systemic diseases, Moorfields AlzEye and UK Biobank.

In the label efficiency analyses, we applied varying percentages of training data (from 10% to 100%) and finetuned the models for ocular and systemic disease prediction tasks. This label efficiency analysis was repeated across all datasets (eight open-source ocular disease datasets and the Moorfields AlzEye dataset), and all models were internally validated on held-out test sets. This enabled a comprehensive analysis of the models' performance in scenarios with limited labeled data for task-specific finetuning.

Performance evaluation and statistical analysis

For all tasks, we used the area under receiver operating characteristics curve (AUROC) to evaluate the models' diagnostic performance. For multi-class detection tasks, including detection of DR (5 classes), glaucoma (3 classes), multi-category eye diseases and systemic diseases, we calculated the AUROC for each class and then averaged across the number of classes to obtain the overall AUROC. We calculated the mean and standard deviation of the AUROC by randomly sampling 20% of the data in each iteration across 100 bootstrap replicates. The standard error was obtained by dividing the standard deviation by $\sqrt{100}$, and the 95% confidence interval was computed as the mean $\pm 1.96 \times$ standard error. Normality was evaluated using the Shapiro-Wilk test applied to the AUROC derived from 100 bootstrapped replicate samples, with the majority demonstrating a normal distribution. To establish statistical differences in the AUROC performance between the DINOv2 and RETFound models, we computed the p-value (P) using the two-sided t-test with Bonferroni correction. Statistical significance was defined as P less than $0.05/3$ ($P=0.017$), accounting for multiple pairwise comparisons between RETFound and the DINOv2 models. To evaluate the model calibration performance, we calculated the Expected Calibration Error (ECE) and plotted the reliability diagrams to ensure that the model's predictive accuracy matches its

confidence level. For external evaluations of ocular and systemic diseases, we also reported metrics such as Kappa, F1-score, and accuracy.

Ethics statement

This study, approved by the London-Central Research Ethics Committee (18/LO/1163, 1 August 2018), the Advanced Statistical Modelling of Multimodal Data Project (20/HRA/2158, 5 May 2020), and the Confidential Advisory Group (18/CAG/0111, 13 September 2018), received final approval from the NHS Health Research Authority on 13 September 2018. De-identification was validated by Moorfields Eye Hospital NHS Foundation Trust, and only de-identified retrospective data were used, with no direct patient involvement.

Data availability

The AlzEye dataset is governed by contractual restrictions between NHS Digital, Moorfields Eye Hospital, and University College London, limiting access to the AlzEye research team. While collaborations are welcomed, individual-level systemic health data can only be analyzed by AlzEye researchers. Detailed information about data curation can be found in the RETFound paper and its supplementary materials. For more information about the dataset and potential collaborations, please visit https://readingcentre.org/studies/artificial_intelligence/alzeye or refer to the comprehensive documentation in Nature (<https://www.nature.com/articles/s41586-023-06555-x#Sec10>) and its supplementary figures (https://static-content.springer.com/esm/art%3A10.1038%2Fs41586-023-06555-x/MediaObjects/41586_2023_6555_MOESM1_ESM.pdf). UK Biobank data can be accessed at <https://www.ukbiobank.ac.uk/>.

Publicly available datasets for ocular disease experiments include:

IDRID: <https://ieee-dataport.org/open-access/indian-diabetic-retinopathy-image-dataset-idrid>;

MESSIDOR-2: <https://www.adcis.net/en/third-party/messidor2/>;

APTOS-2019: <https://www.kaggle.com/competitions/aptos2019-blindness-detection/data>;

PAPILA: <https://figshare.com/articles/dataset/PAPILA/14798004/1>;

Glaucoma Fundus:

<https://dataverse.harvard.edu/dataset.xhtml?persistentId=doi:10.7910/DVN/1YRRAC>;

JSIEC: <https://zenodo.org/record/3477553>;

Retina: <https://www.kaggle.com/datasets/jr2ngb/cataractdataset>;

OCTID: <https://borealisdata.ca/dataverse/OCTID>.

Code availability

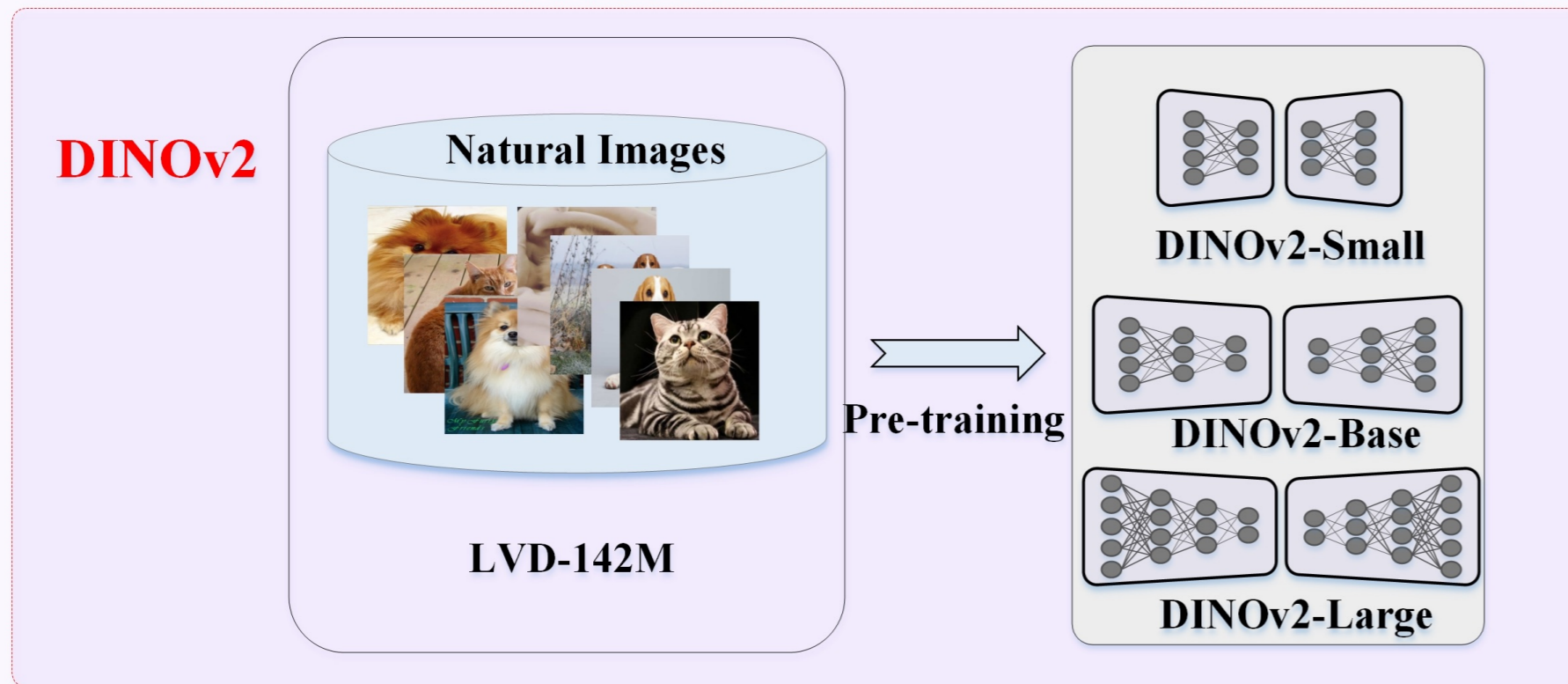
The training, fine-tuning, and evaluation code for RETFound, provided by Y.Z. and built on PyTorch, is available at https://github.com/rmaphoh/RETFound_MAE. The corresponding code for DINOv2 is available at <https://github.com/HouQingshan/DINOv2>.

Reference

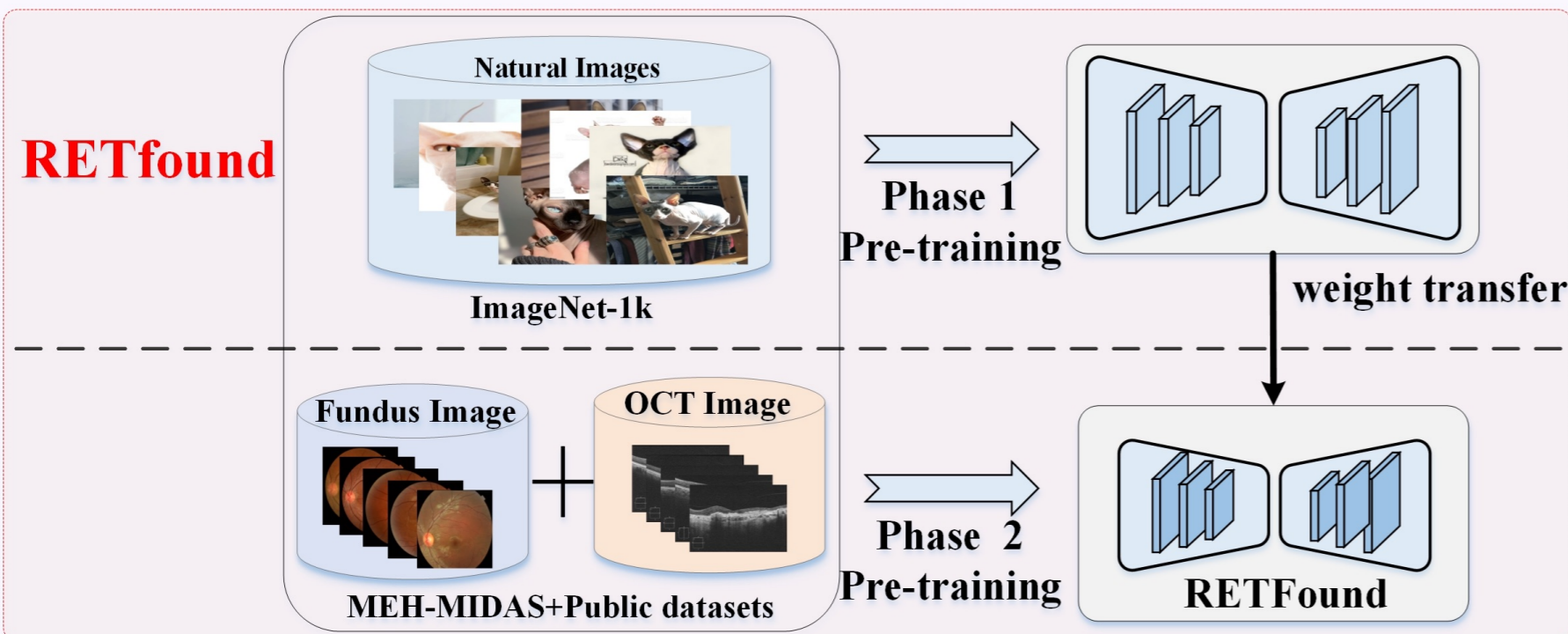
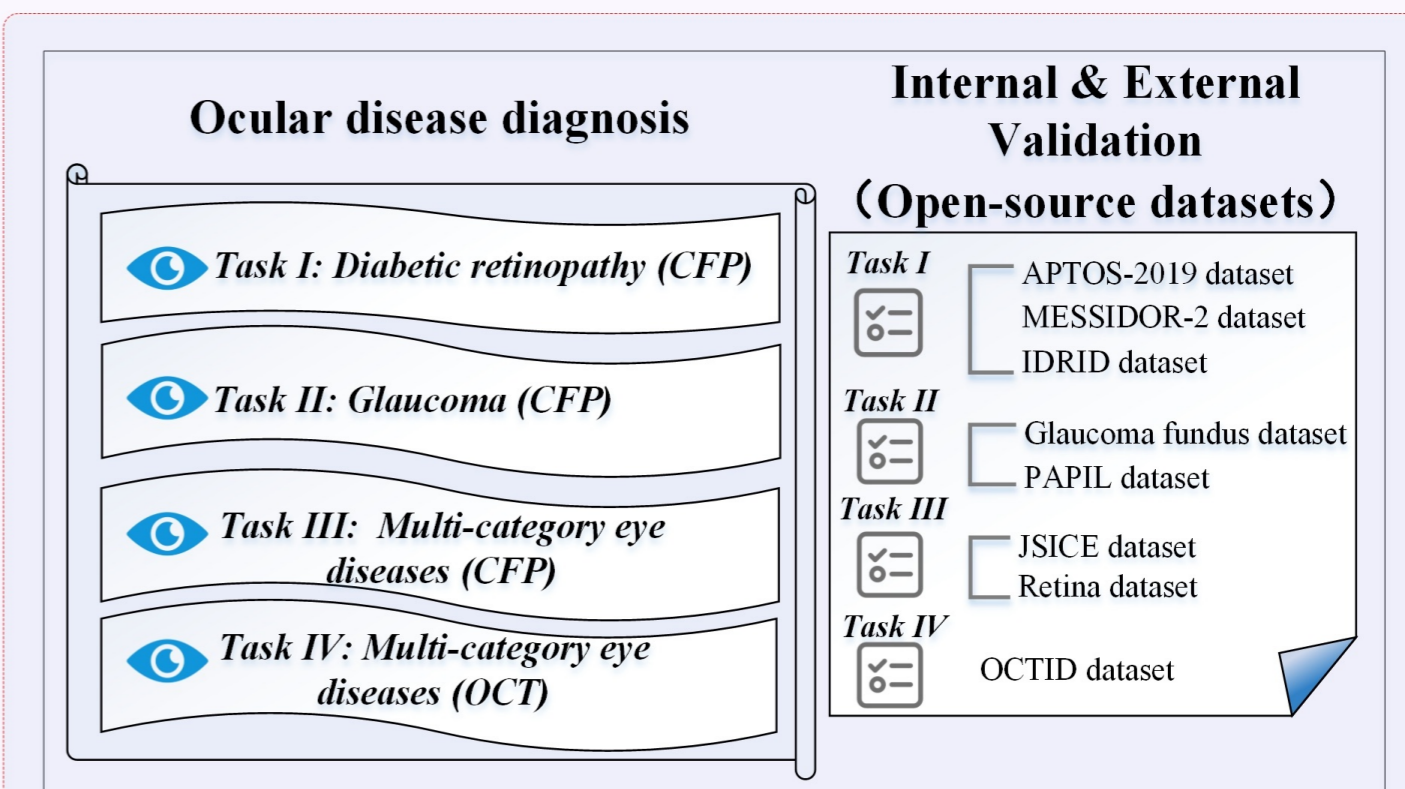
- [1] Azad, B., Azad, R., Eskandari, S., Bozorgpour, A., Kazerouni, A., Rekik, I., & Merhof, D. (2023). Foundational models in medical imaging: A comprehensive survey and future vision. arXiv preprint arXiv:2310.18689.
- [2] Achiam, J., Adler, S., Agarwal, S., Ahmad, L., Akkaya, I., Aleman, F. L., ... & McGrew, B. (2023). Gpt-4 technical report. arXiv preprint arXiv:2303.08774.
- [3] Moor, M., Banerjee, O., Abad, Z. S. H., Krumholz, H. M., Leskovec, J., Topol, E. J., & Rajpurkar, P. (2023). Foundation models for generalist medical artificial intelligence. *Nature*, 616(7956), 259-265.
- [4] Qiu, J., Wu, J., Wei, H., Shi, P., Zhang, M., Sun, Y., ... & Yuan, W. (2023). Visionfm: a multi-modal multi-task vision foundation model for generalist ophthalmic artificial intelligence. arXiv preprint arXiv:2310.04992.
- [5] Roth, B., Koch, V., Wagner, S. J., Schnabel, J. A., Marr, C., & Peng, T. (2024). Low-resource finetuning of foundation models beats state-of-the-art in histopathology. arXiv preprint arXiv:2401.04720.
- [6] Awais, M., Naseer, M., Khan, S., Anwer, R. M., Cholakkal, H., Shah, M., ... & Khan, F. S. (2025). Foundation Models Defining a New Era in Vision: a Survey and Outlook. *IEEE Transactions on Pattern Analysis and Machine Intelligence*.
- [7] Zhou, Y., Chia, M. A., Wagner, S. K., Ayhan, M. S., Williamson, D. J., Struyven, R. R., ... & Keane, P. A. (2023). A foundation model for generalizable disease detection from retinal images. *Nature*, 622(7981), 156-163.
- [8] Han, K., Wang, Y., Chen, H., Chen, X., Guo, J., Liu, Z., ... & Tao, D. (2022). A survey on vision transformer. *IEEE transactions on pattern analysis and machine intelligence*, 45(1), 87-110.
- [9] Dosovitskiy, A. (2020). An image is worth 16x16 words: Transformers for image recognition at scale. arXiv preprint arXiv:2010.11929.
- [10] He, K., Chen, X., Xie, S., Li, Y., Dollár, P., & Girshick, R. (2022). Masked autoencoders are scalable vision learners. In *Proceedings of the IEEE/CVF conference on computer vision and pattern recognition* (pp. 16000-16009).
- [11] Zhang, J., Lin, S., Cheng, T. et al. RETFound-enhanced community-based fundus disease screening: real-world evidence and decision curve analysis. *npj Digit. Med.* 7, 108 (2024). <https://doi.org/10.1038/s41746-024-01109-5>
- [12] Teresa Araújo, Guilherme Moreira Aresta, Ursula Schmidt-Erfurth, Hrvoje Bogunovic; Robust deep learning for automated AMD screening and staging based on a retinal foundation model. *Invest. Ophthalmol. Vis. Sci.* 2024;65(7):2833.
- [13] Nikhil Varma Gadiraju, David Kuo, Vahid Ownagh, Terry Lee, Lindsey A Chew, Grant A. Justin, Nita Valikodath, Stephanie Hsu, Miroslav Pajic, Majda Hadziahmetovic, Lejla Vajzovic; Evaluating Performance of ResNet-50 and RETFound Image Classification Algorithms on Ultra-widefield Fundus Images. *Invest. Ophthalmol. Vis. Sci.* 2024;65(7):1605.
- [14] Oquab, M., Darcet, T., Moutakanni, T., Vo, H., Szafraniec, M., Khalidov, V., ... & Bojanowski, P. (2023). Dinov2: Learning robust visual features without supervision. arXiv preprint arXiv:2304.07193.
- [15] Dippel, J., Feulner, B., Winterhoff, T., Schallenberg, S., Dernbach, G., Kunft, A., ... & Alber, M. (2024). RudolfV: a foundation model by pathologists for pathologists. arXiv preprint arXiv:2401.04079.
- [16] Xu, H., Usuyama, N., Bagga, J., Zhang, S., Rao, R., Naumann, T., ... & Poon, H. (2024). A whole-slide foundation model for digital pathology from real-world data. *Nature*, 1-8.
- [17] Fan, W., Yang, Y., Qi, J., Zhang, Q., Liao, C., Wen, L., ... & Zhang, D. (2024). A deep-learning-based framework for identifying and localizing multiple abnormalities and assessing cardiomegaly in chest X-ray. *Nature Communications*, 15(1), 1347.

- [18] Huang, Y., Zou, J., Meng, L., Yue, X., Zhao, Q., Li, J., ... & Fu, G. (2024). Comparative Analysis of ImageNet Pre-Trained Deep Learning Models and DINOv2 in Medical Imaging Classification. arXiv preprint arXiv:2402.07595.
- [19] Nakayama, L. F., Restrepo, D., Matos, J., Ribeiro, L. Z., Malerbi, F. K., Celi, L. A., & Regatieri, C. S. (2024). BRSET: a Brazilian multilabel ophthalmological dataset of retina fundus photos. medRxiv.
- [20] Huang, S. C., Pareek, A., Seyyedi, S., Banerjee, I., & Lungren, M. P. (2020). Fusion of medical imaging and electronic health records using deep learning: a systematic review and implementation guidelines. *NPJ digital medicine*, 3(1), 136.
- [21] Topol, E. J. (2019). High-performance medicine: the convergence of human and artificial intelligence. *Nature medicine*, 25(1), 44-56.
- [22] Russakovsky, O., Deng, J., Su, H., Krause, J., Satheesh, S., Ma, S., ... & Fei-Fei, L. (2015). Imagenet large scale visual recognition challenge. *International journal of computer vision*, 115, 211-252.
- [23] Porwal, P., Pachade, S., Kokare, M., Deshmukh, G., Son, J., Bae, W., ... & Meriaudeau, F. (2020). Idrid: Diabetic retinopathy–segmentation and grading challenge. *Medical image analysis*, 59, 101561.
- [24] Porwal, P., Pachade, S., Kamble, R., Kokare, M., Deshmukh, G., Sahasrabudhe, V., & Meriaudeau, F. (2018). Indian diabetic retinopathy image dataset (IDRiD): a database for diabetic retinopathy screening research. *Data*, 3(3), 25.
- [25] Decencière, E., Zhang, X., Cazuguel, G., Lay, B., Cochener, B., Trone, C., ... & Klein, J. C. (2014). Feedback on a publicly distributed image database: the Messidor database. *Image Analysis & Stereology*, 231-234.
- [26] Abramoff, M. D., Folk, J. C., Han, D. P., Walker, J. D., Williams, D. F., Russell, S. R., ... & Niemeijer, M. (2013). Automated analysis of retinal images for detection of referable diabetic retinopathy. *JAMA ophthalmology*, 131(3), 351-357.
- [27] Krause, J., Gulshan, V., Rahimy, E., Karth, P., Widner, K., Corrado, G. S., ... & Webster, D. R. (2018). Grader variability and the importance of reference standards for evaluating machine learning models for diabetic retinopathy. *Ophthalmology*, 125(8), 1264-1272.
- [28] APTOS 2019 Blindness Detection [Internet]. Available from: <https://kaggle.com/competitions/aptos2019-blindness-detection>
- [29] Kovalyk, O., Morales-Sánchez, J., Verdú-Monedero, R., Sellés-Navarro, I., Palazón-Cabanes, A., & Sancho-Gómez, J. L. (2022). PAPILA: Dataset with fundus images and clinical data of both eyes of the same patient for glaucoma assessment. *Scientific Data*, 9(1), 291.
- [30] Ahn, J. M., Kim, S., Ahn, K. S., Cho, S. H., Lee, K. B., & Kim, U. S. (2018). A deep learning model for the detection of both advanced and early glaucoma using fundus photography. *PloS one*, 13(11), e0207982.
- [31] Cen, L. P., Ji, J., Lin, J. W., Ju, S. T., Lin, H. J., Li, T. P., ... & Zhang, M. (2021). Automatic detection of 39 fundus diseases and conditions in retinal photographs using deep neural networks. *Nature communications*, 12(1), 4828.
- [32] Retina [Internet]. Available from: <https://www.kaggle.com/datasets/jr2ngb/cataractdataset>
- [33] Gholami, P., Roy, P., Parthasarathy, M. K., & Lakshminarayanan, V. (2020). OCTID: Optical coherence tomography image database. *Computers & Electrical Engineering*, 81, 106532.
- [34] Wagner, S. K., Hughes, F., Cortina-Borja, M., Pontikos, N., Struyven, R., Liu, X., ... & Keane, P. A. (2022). AlzEye: longitudinal record-level linkage of ophthalmic imaging and hospital admissions of 353 157 patients in London, UK. *BMJ open*, 12(3), e058552.

Stage 1: Self-supervised learning for pre-training



Stage 2: Supervised fine-tuning for clinical tasks



Fine-tuning

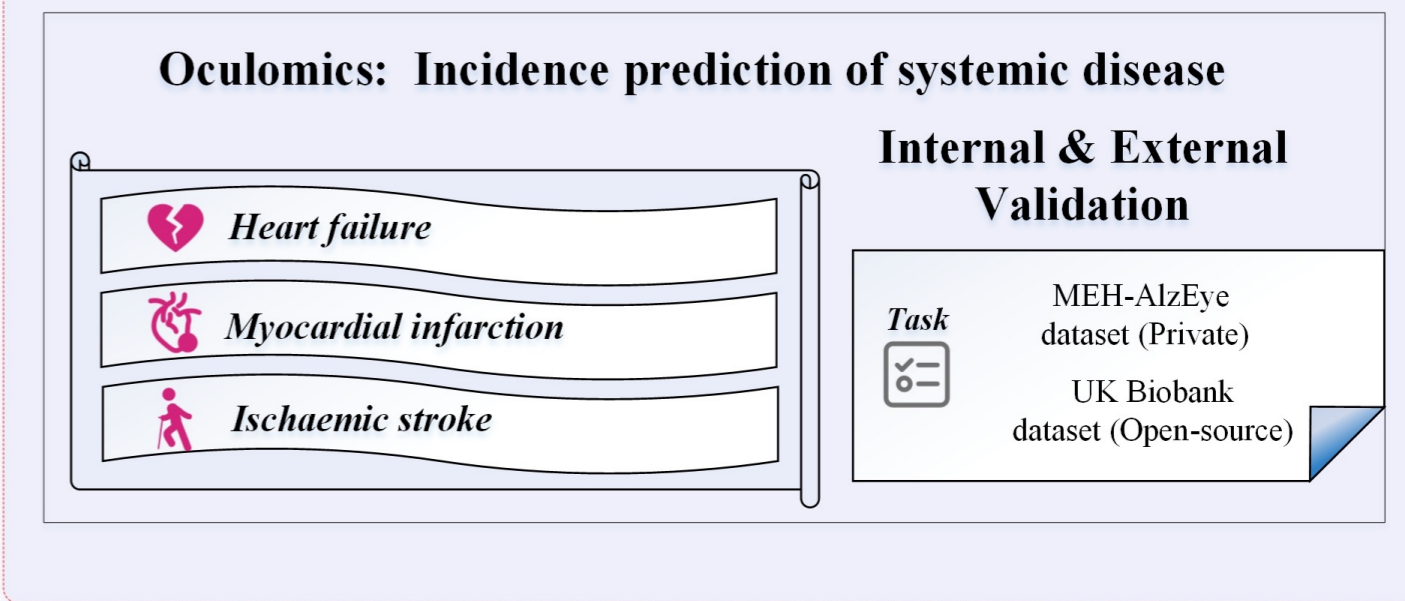


Figure 1. Overview of the development and evaluation of the DINOv2 and RETFound models. Stage 1 illustrates the pre-training phase of DINOv2 and RETFound models through self-supervised learning on respective natural and ophthalmic image datasets. Stage 2 covers the supervised fine-tuning of the pre-trained models for adaptation to specific downstream ocular disease diagnosis and systemic disease incidence prediction tasks.

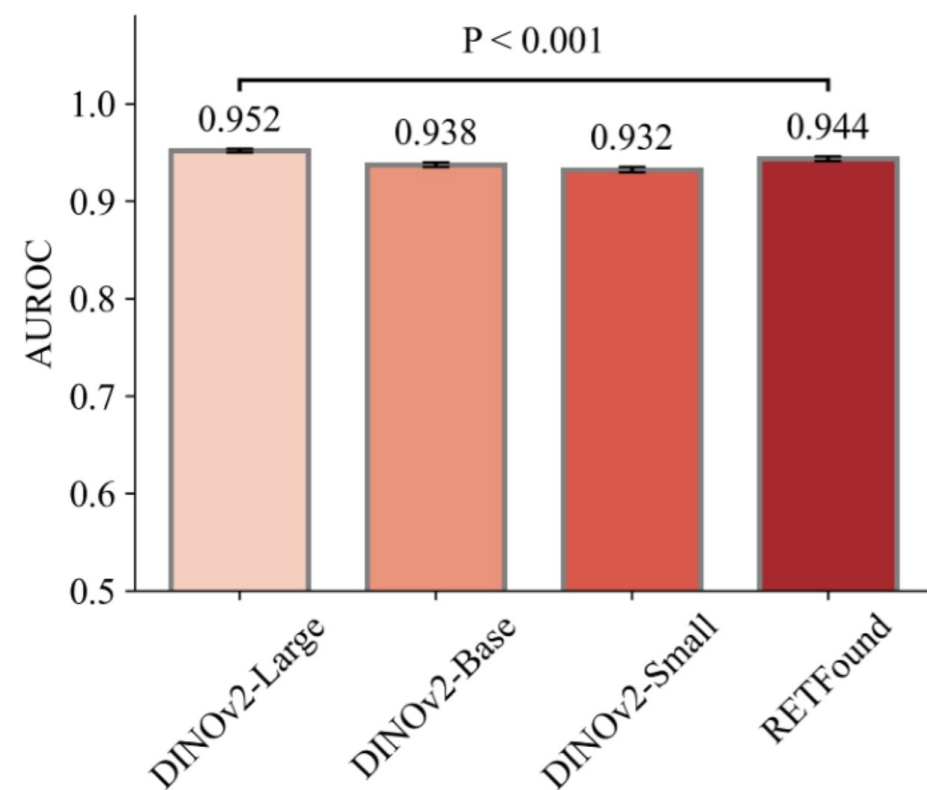
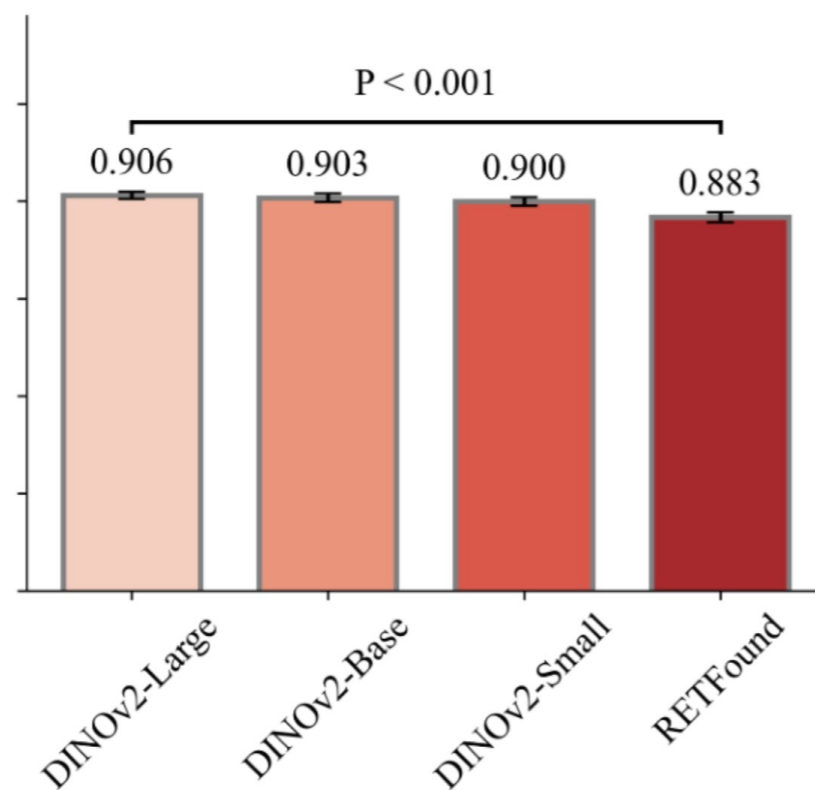
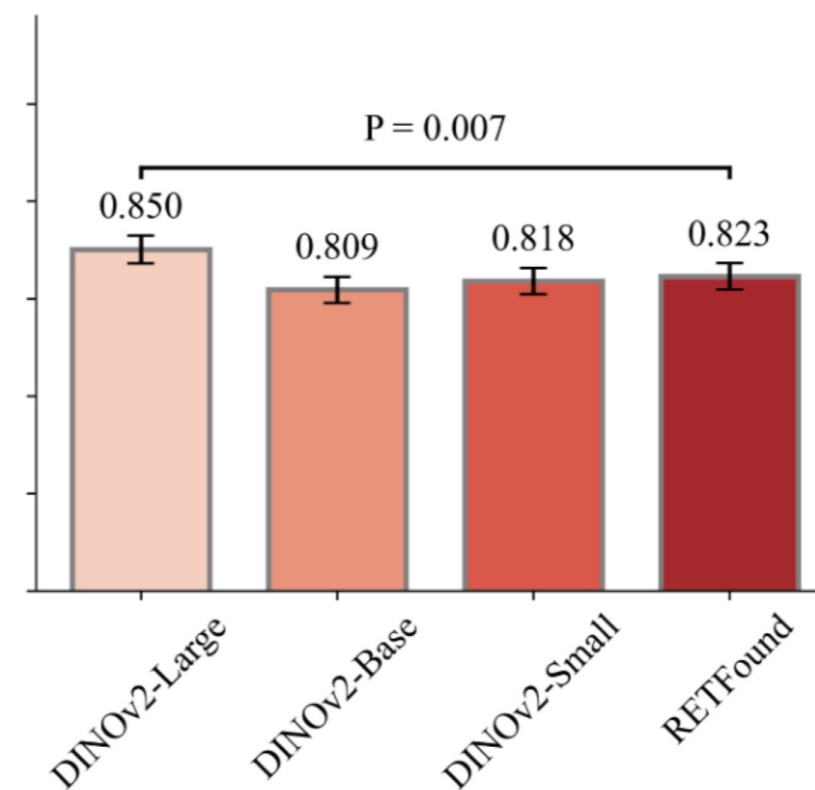
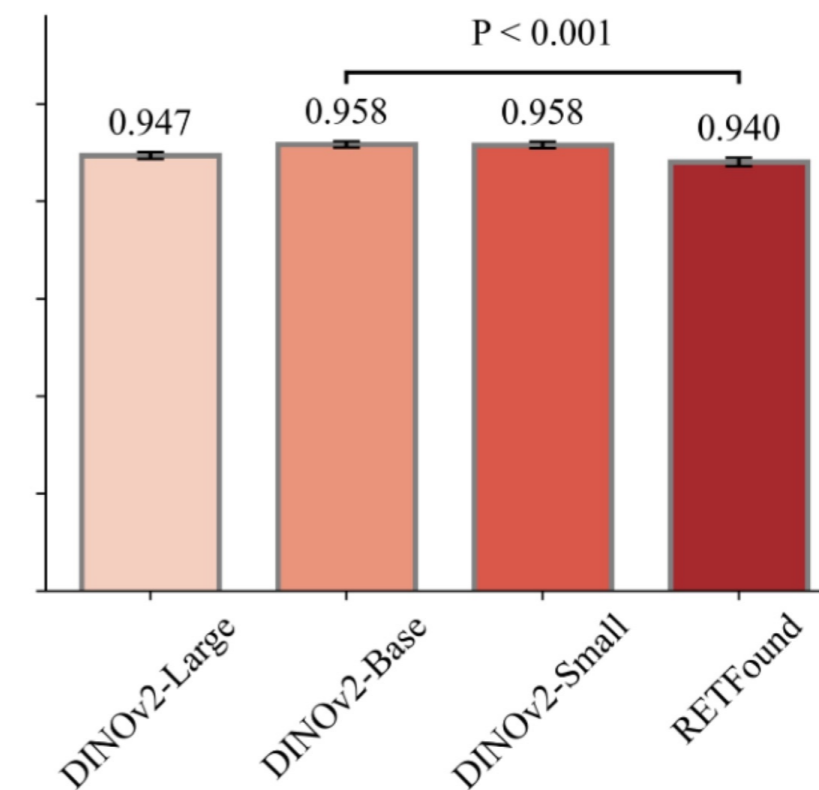
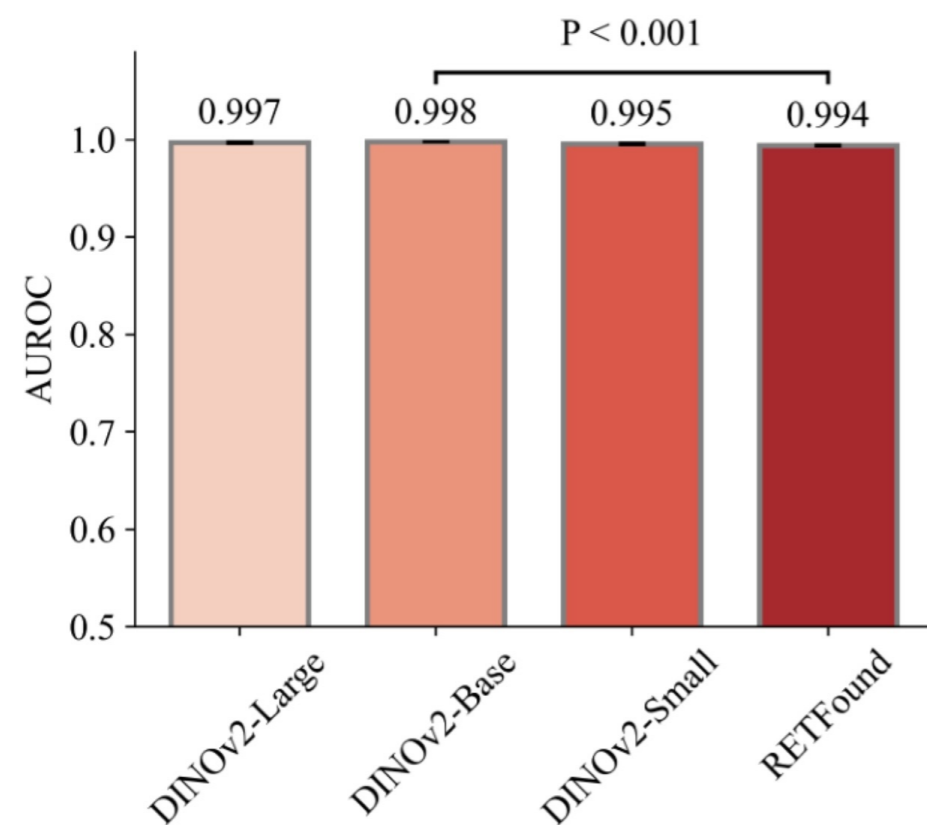
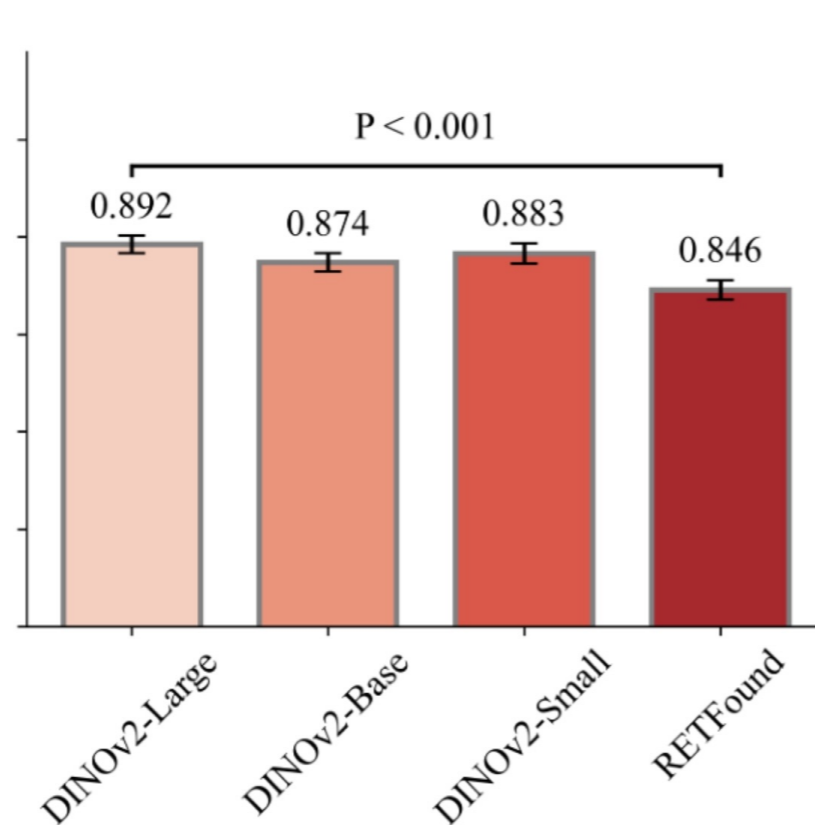
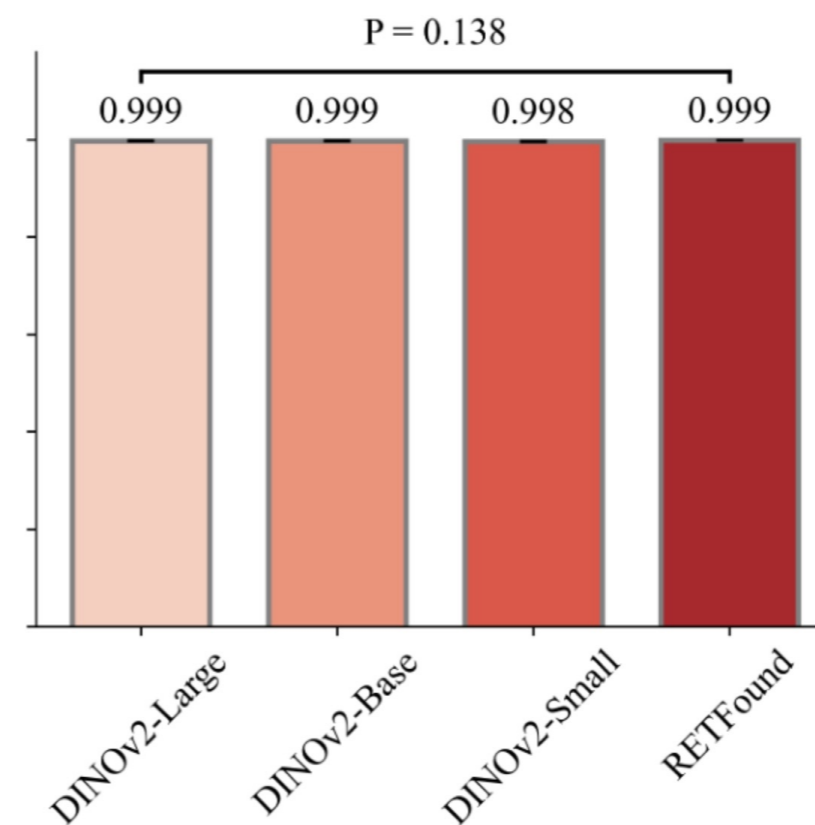
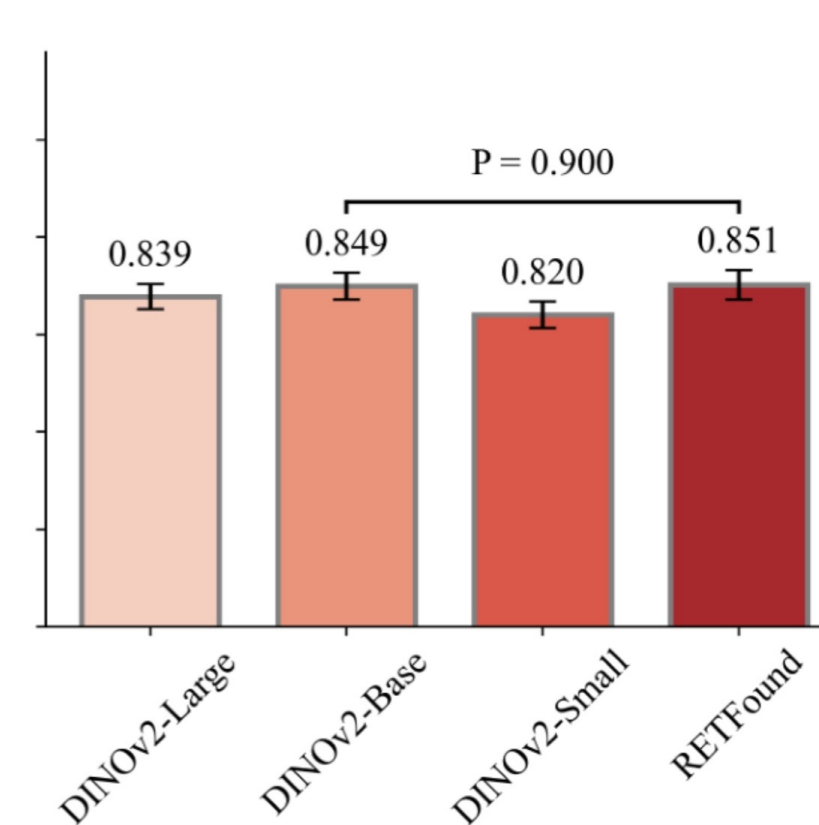
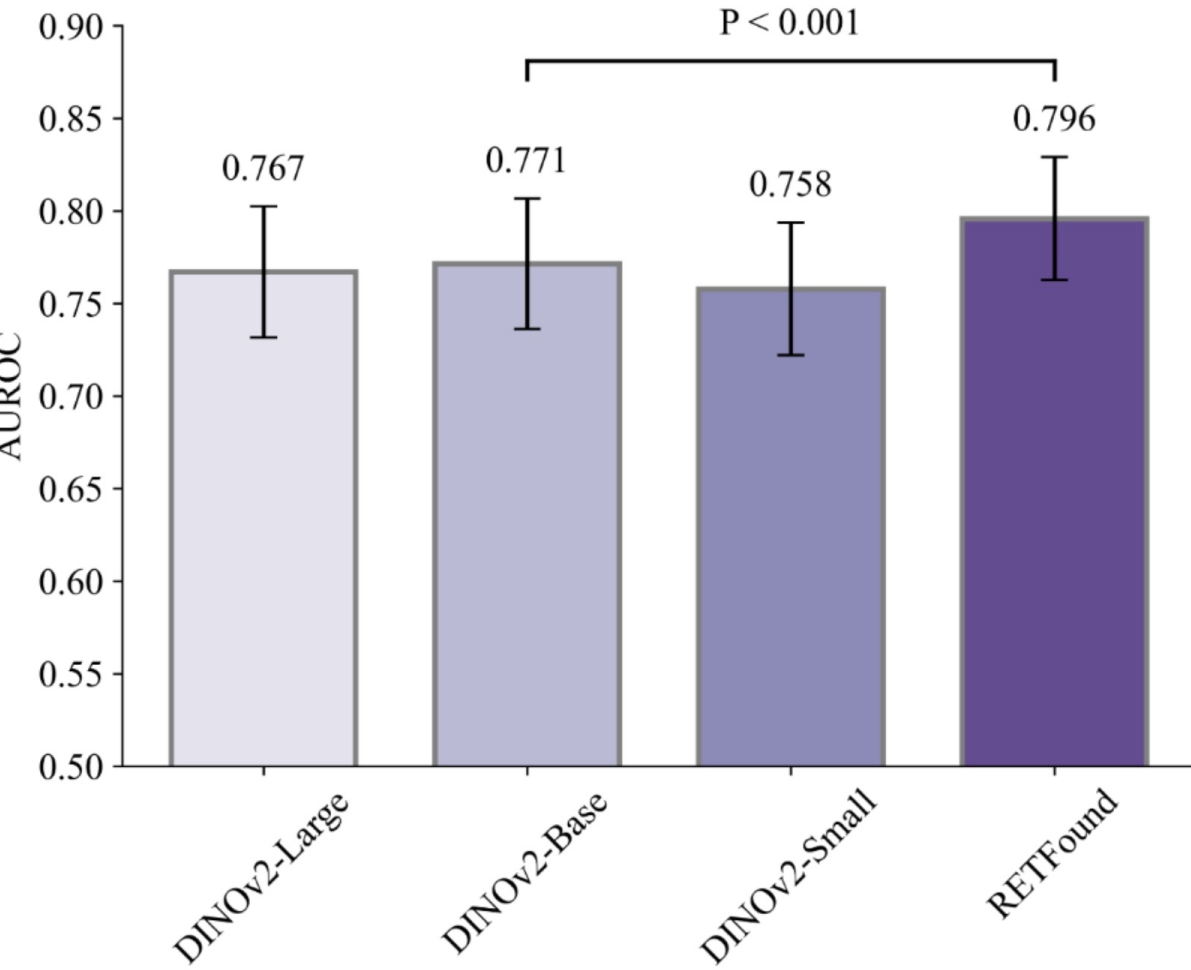
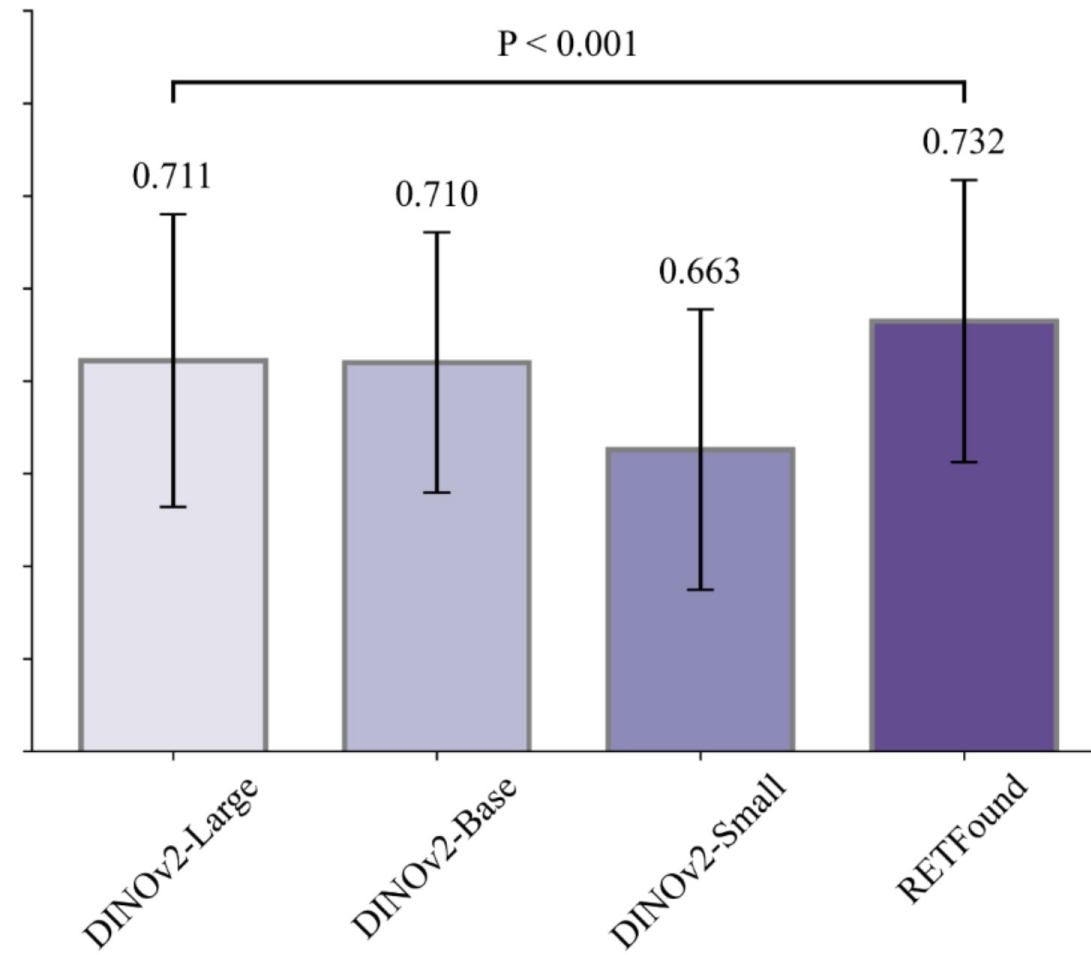
Task IDiabetic retinopathy (CFP)
APTOS2019Diabetic retinopathy (CFP)
MESSIDOR2Diabetic retinopathy (CFP)
IDRID**Task II**Glaucoma (CFP)
Glaucoma_fundus**Task III**Multi-category eye disease (CFP)
JSIECMulti-category eye disease (CFP)
Retina**Task IV**Multi-category eye disease (OCT)
OCTIDGlaucoma (CFP)
PAPILA

Figure 2. AUROC performance of DINOv2 and RETFound for ocular disease diagnostic tasks in the internal tests. We fine-tuned DINOv2-Large, DINOv2-Base, DINOv2-Small, and RETFound models separately to adapt to each dataset, and internally evaluated them on hold-out test data for ocular disease diagnostic tasks, including diabetic retinopathy, glaucoma, multi-category eye diseases. For each task, statistical significance of AUROC differences was evaluated using 100 bootstrap replicates, randomly sampling 20% of the data. Error bars show 95% confidence intervals, and bar centers represent the mean AUROC values.

Heart failure



Myocardial infarction



Ischaemic stroke

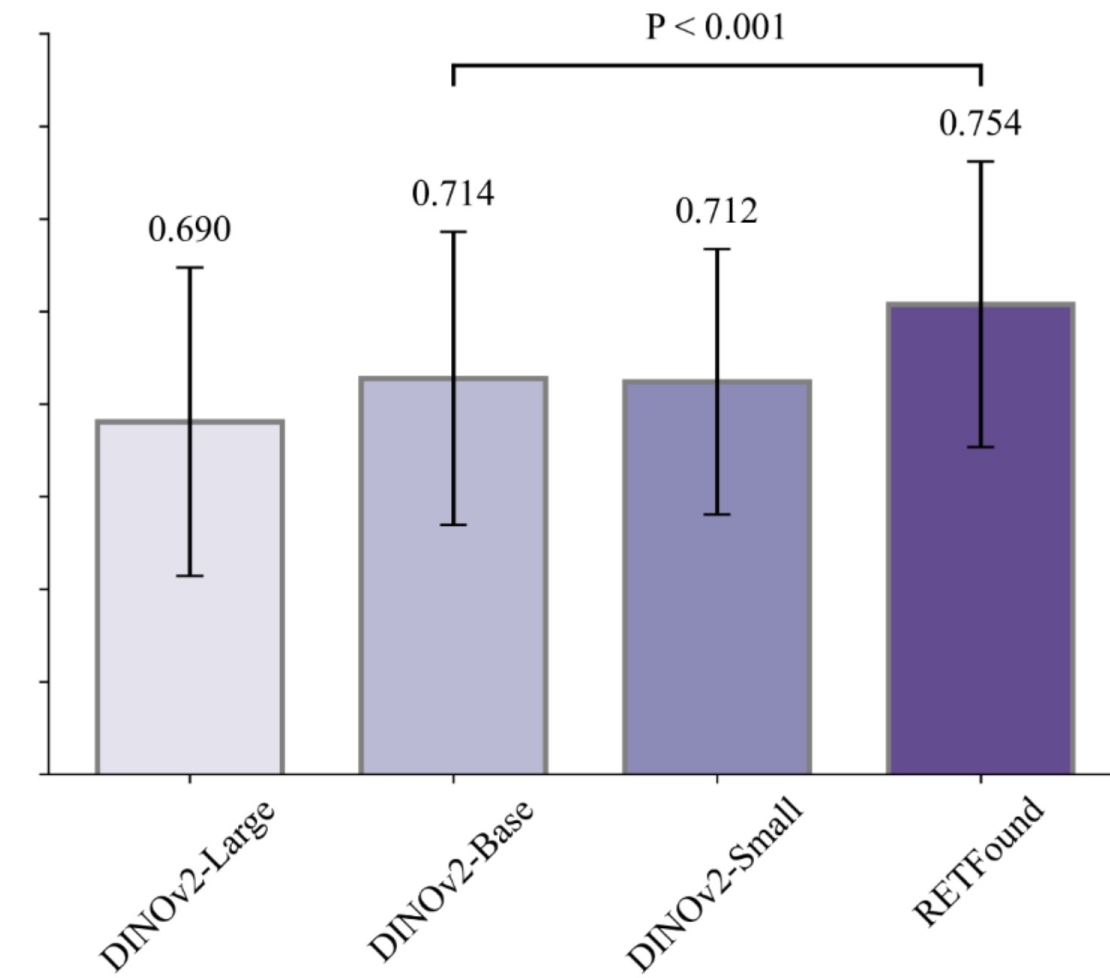
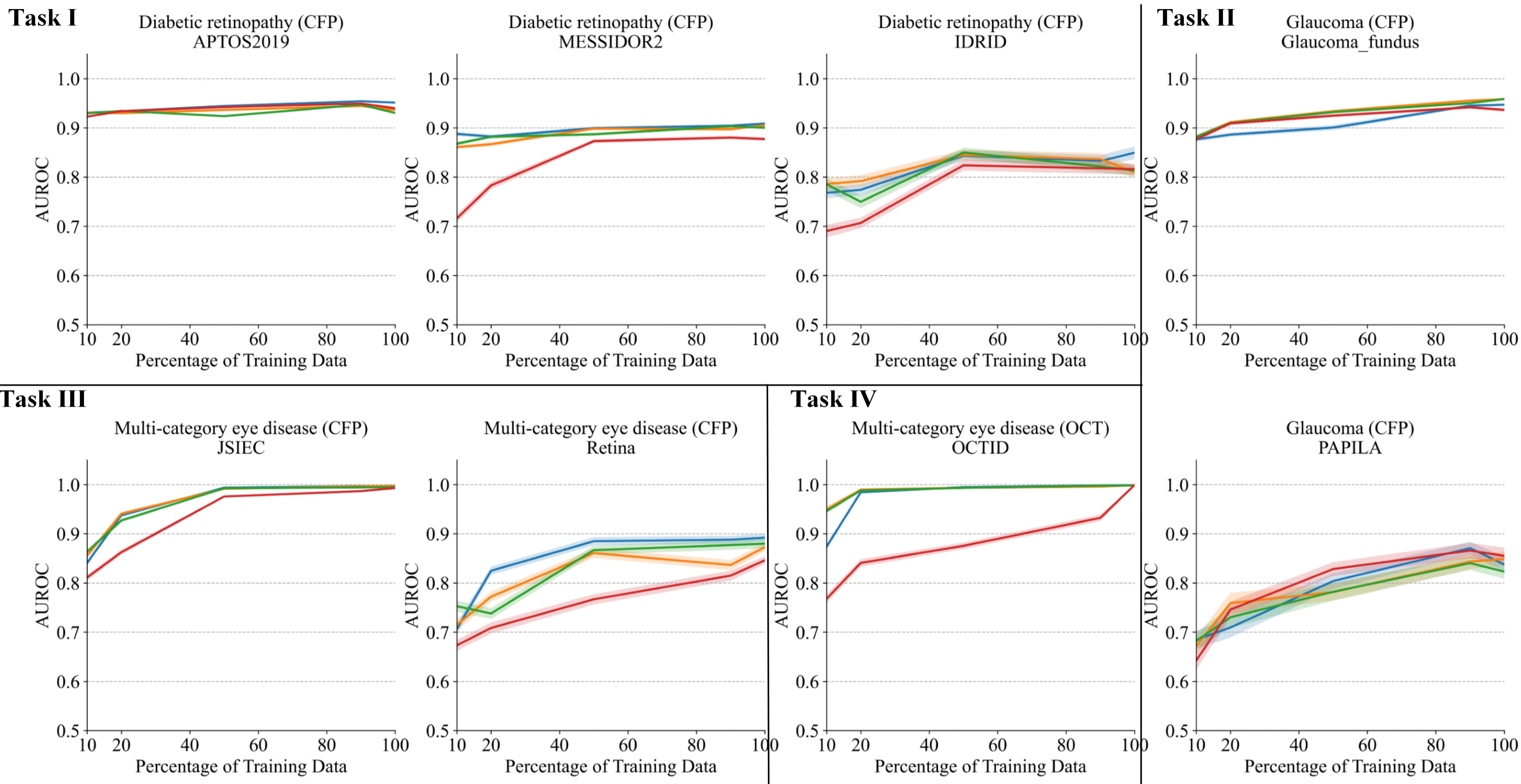


Figure 3. AUROC performance of DINOv2 and RETFound in predicting 3-year incidence of systemic diseases using retinal images in the internal tests. The models were fine-tuned to adapt to curated datasets from MEH-AlzEye and internally evaluated on hold-out test data. For each task, statistical significance of AUROC differences was evaluated using 100 bootstrap replicates, randomly sampling 20% of the data. Error bars show 95% confidence intervals, and bar centers represent the mean AUROC values.

Label efficiency for ocular disease diagnostic tasks

— DINOv2-Large — DINOv2-Base — DINOv2-Small — RETFound



Label efficiency for systemic disease diagnostic tasks

— DINOv2-Large — DINOv2-Base — DINOv2-Small — RETFound

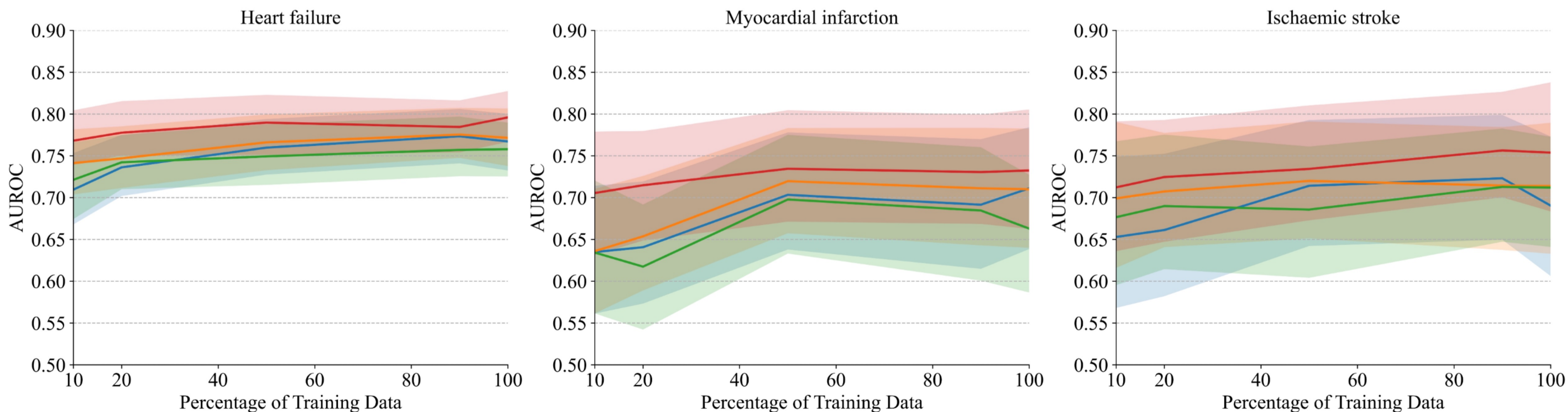
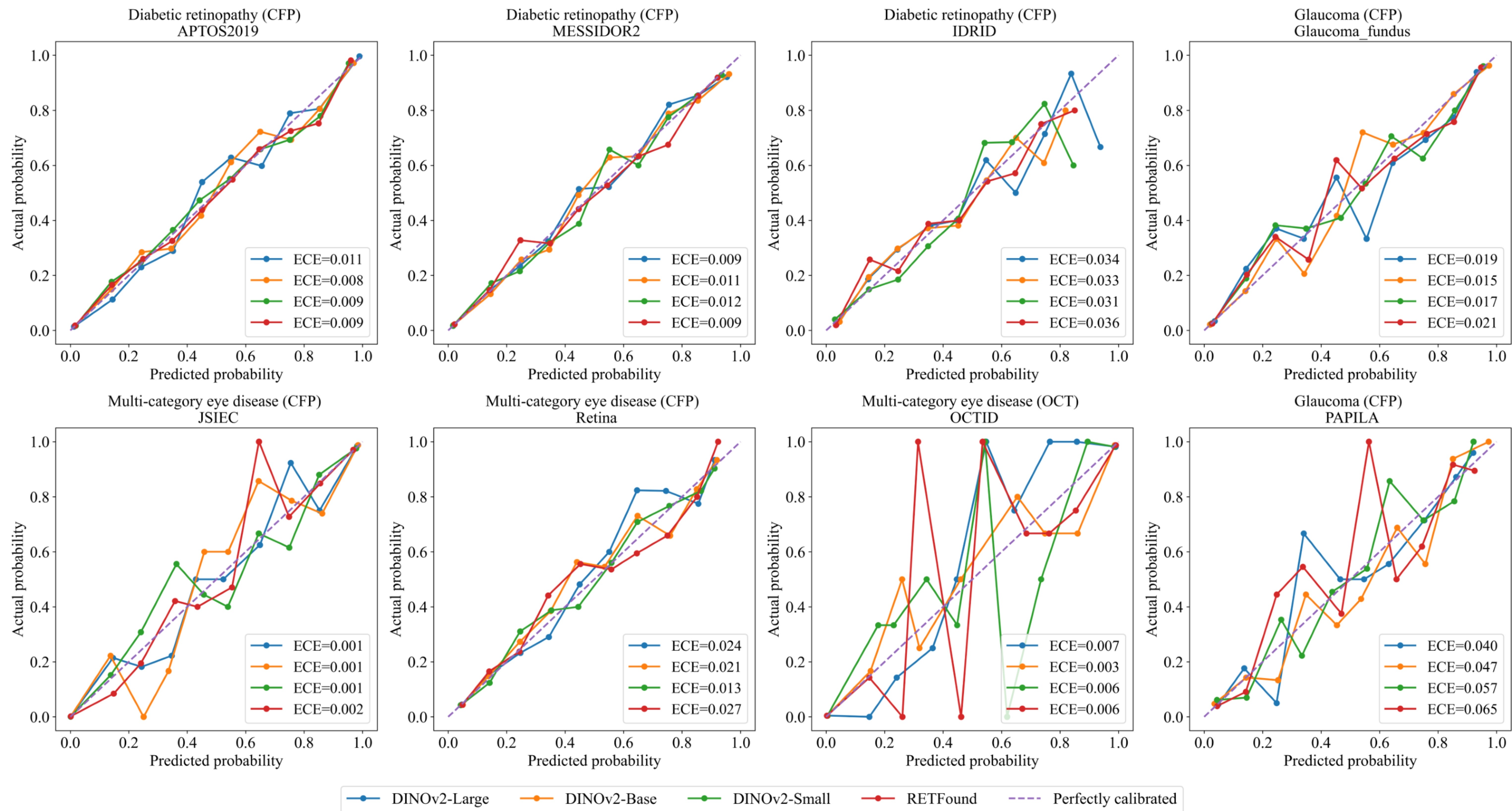


Figure 4. Label efficiency in clinical applications: Label efficiency assesses model performance using varying proportions of training data. Such analysis is key in optimizing the amount of data required to reach target performance levels.

Expected calibration error for ocular disease diagnostic tasks



Expected calibration error for systemic disease diagnostic tasks

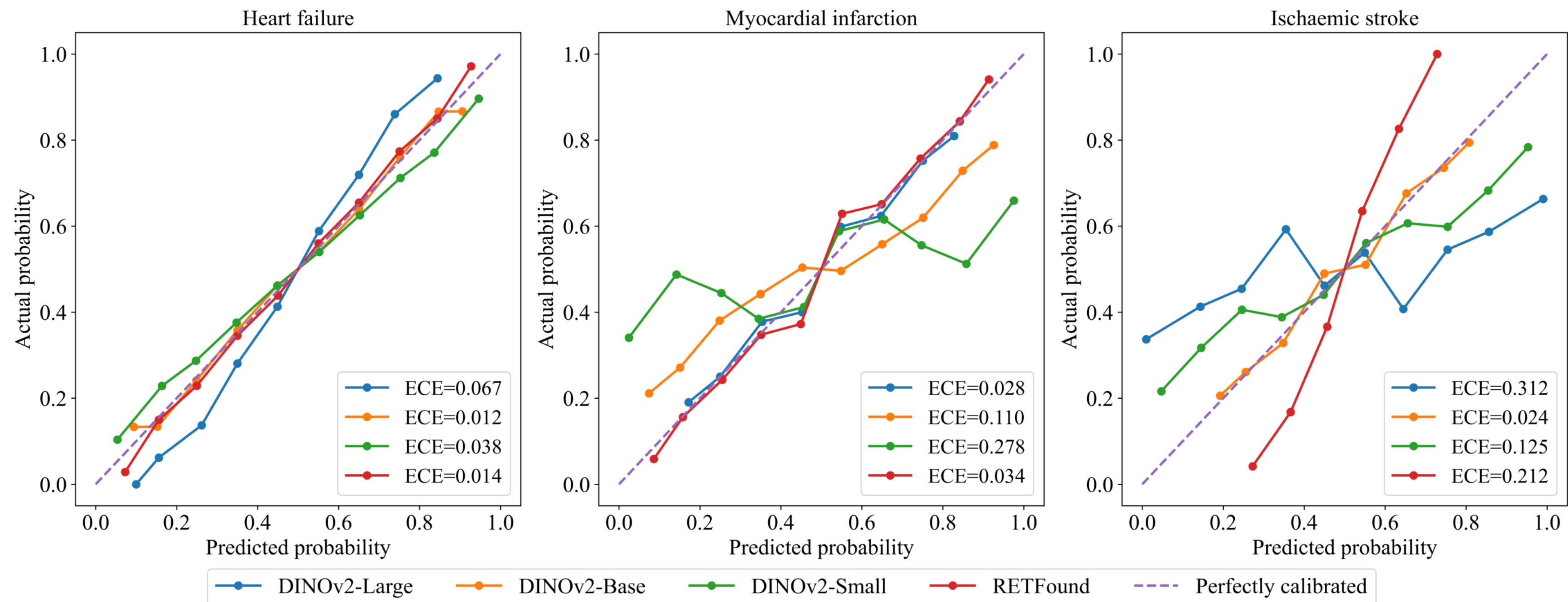
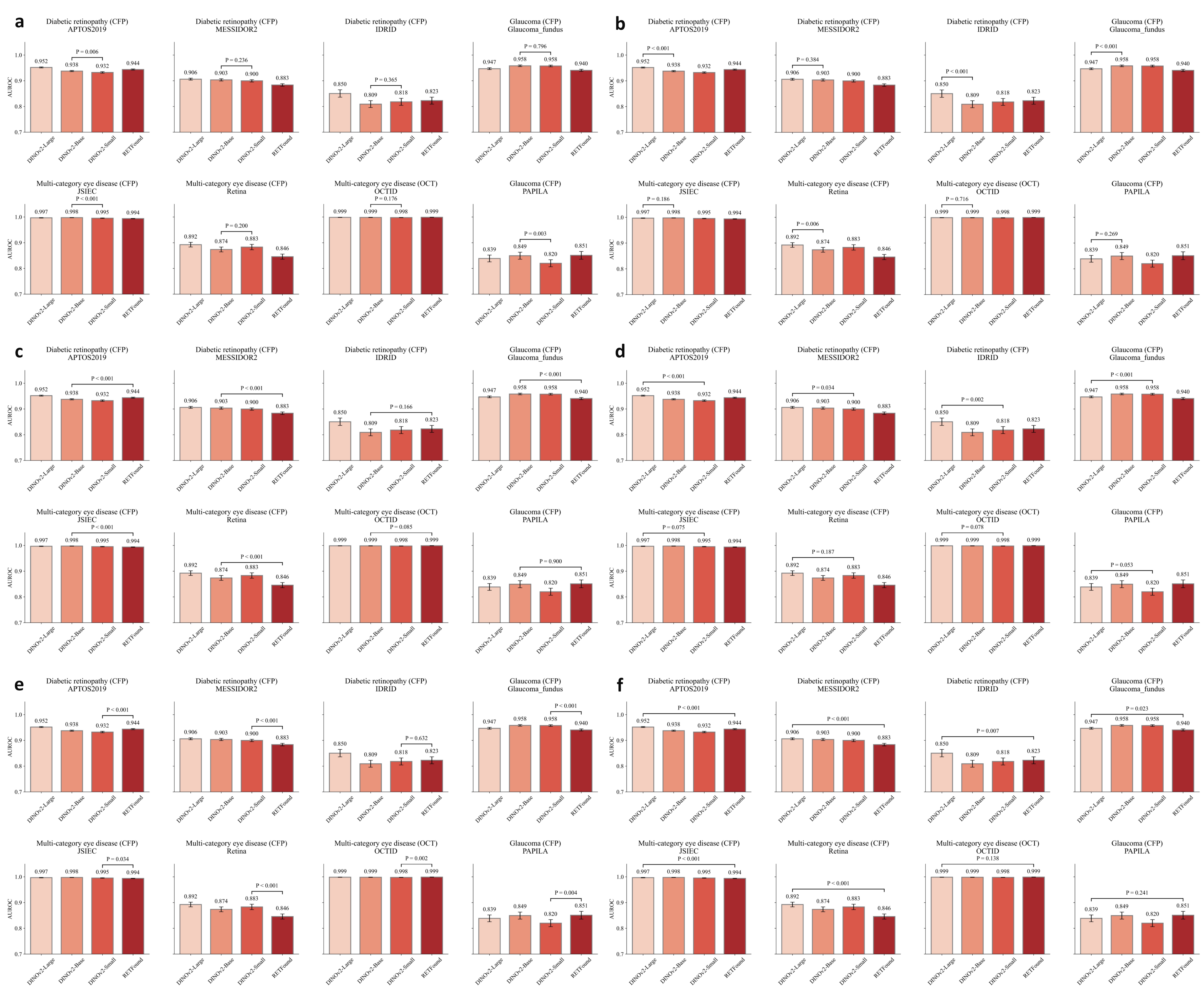


Figure 5. Reliability diagrams and expected calibration error (ECE) for ocular disease and systemic diagnostic tasks. Calibration plots (10 bins, full test set) are shown for DINOv2 (Large, Base, Small) and RETFound models, with the dashed diagonal line representing perfect calibration. The ECE values quantify model miscalibration, where lower values indicate better alignment. These plots highlight performance differences among models across eight open-source ocular disease datasets and the Moorfields AlzEye dataset for systemic diseases. The DINOv2 models generally performed comparably or better than RETFound with lower ECE values in ocular disease tasks. While RETFound largely achieved lower ECE values than the DINOv2 models in systemic disease tasks, with an exception when compared to DINOv2-Base in predicting ischemic stroke.

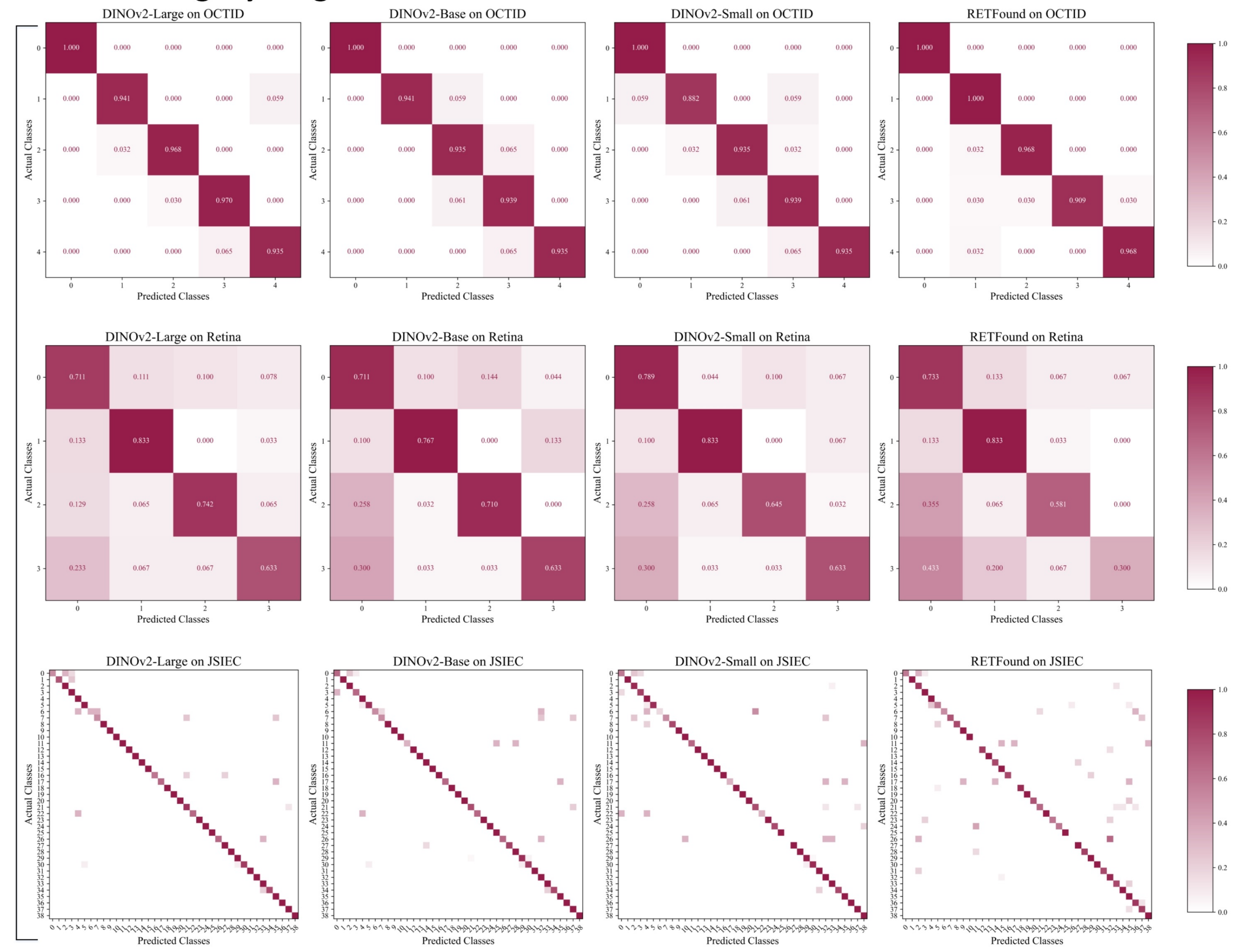


Extended Data Fig.1 Permutated pair-wise AUROC comparison between all models for ocular disease diagnosis tasks. Each subplot shows P-value comparison between paired models across the internal tests with, a) DINOv2-Base vs DINOv2-Small. b) DINOv2-Large vs DINOv2-Small. c) DINOv2-Large vs DINOv2-Base. d) RetFound vs DINOv2-Small. e) RetFound vs DINOv2-Base. f) RetFound vs DINOv2-Large. For each task and scenario, statistical significance of AUROC differences was evaluated using 100 bootstrap replicates, randomly sampling 20% of the data. Error bars show 95% confidence intervals, and bar centers represent the mean AUROC values.

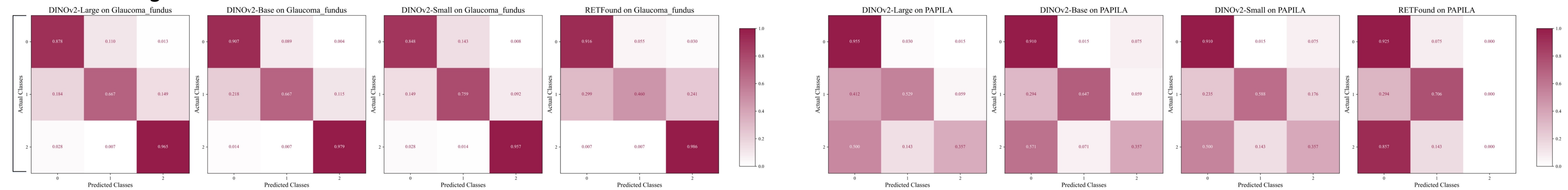
a Diabetic retinopathy grading



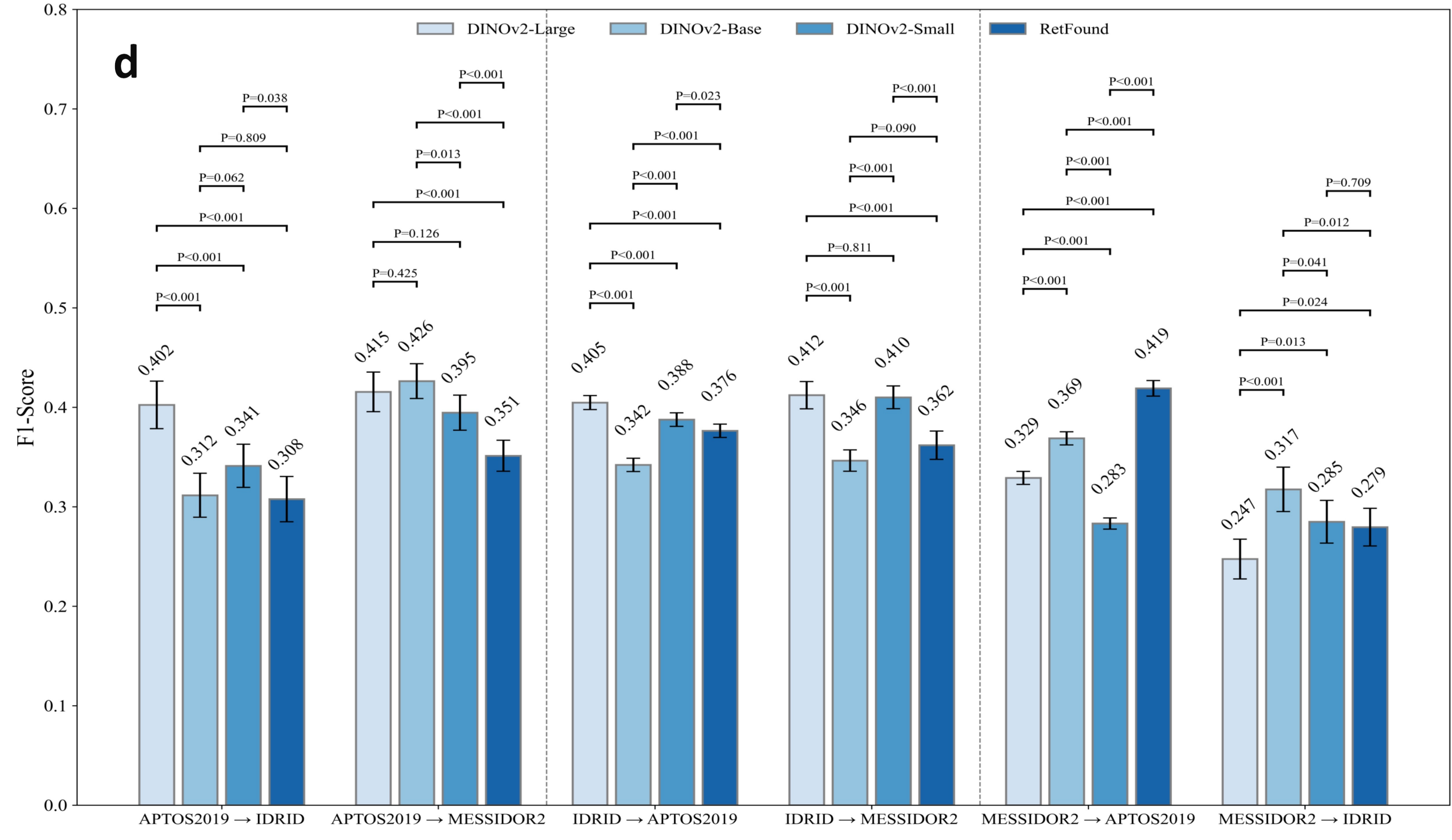
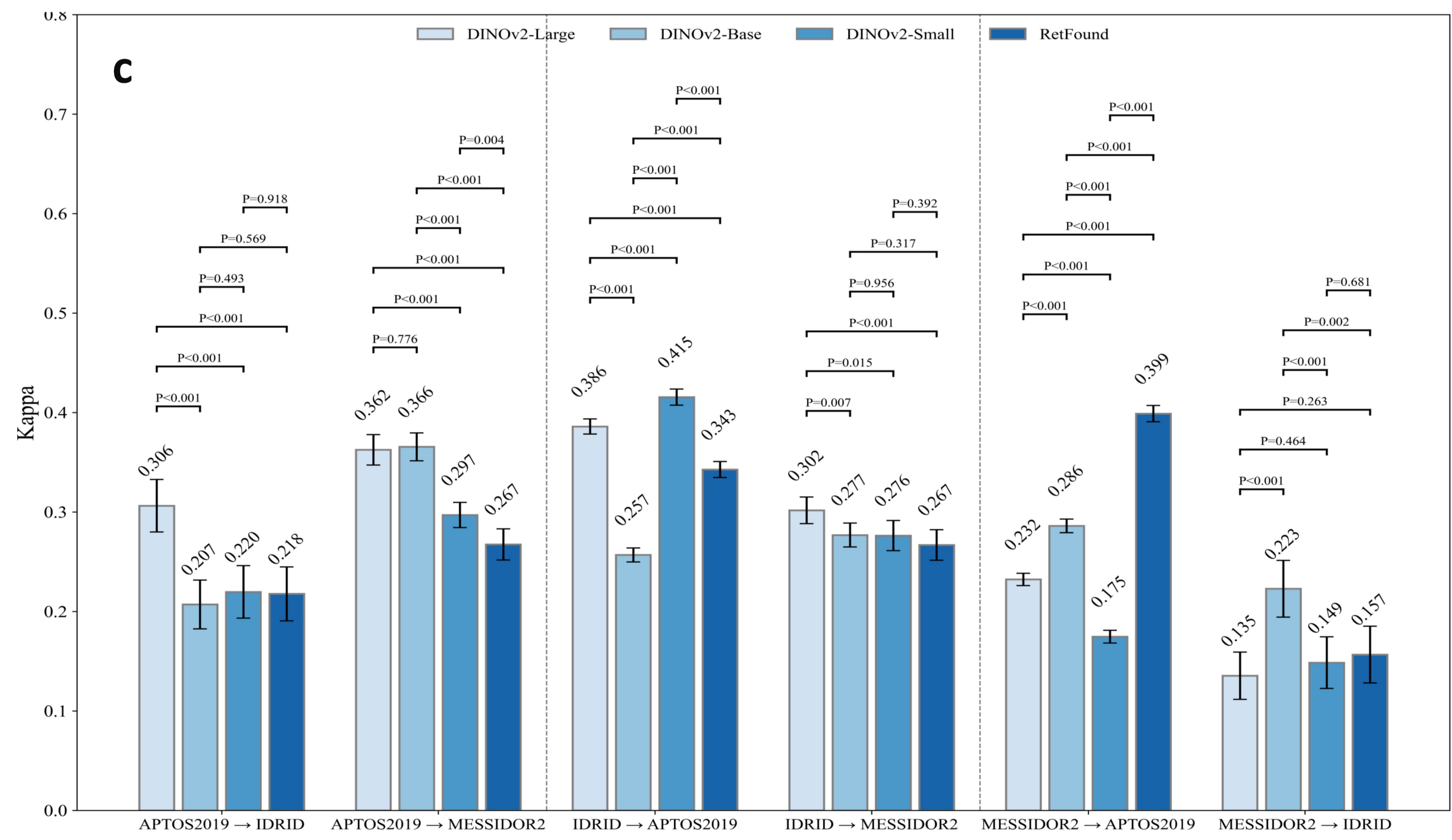
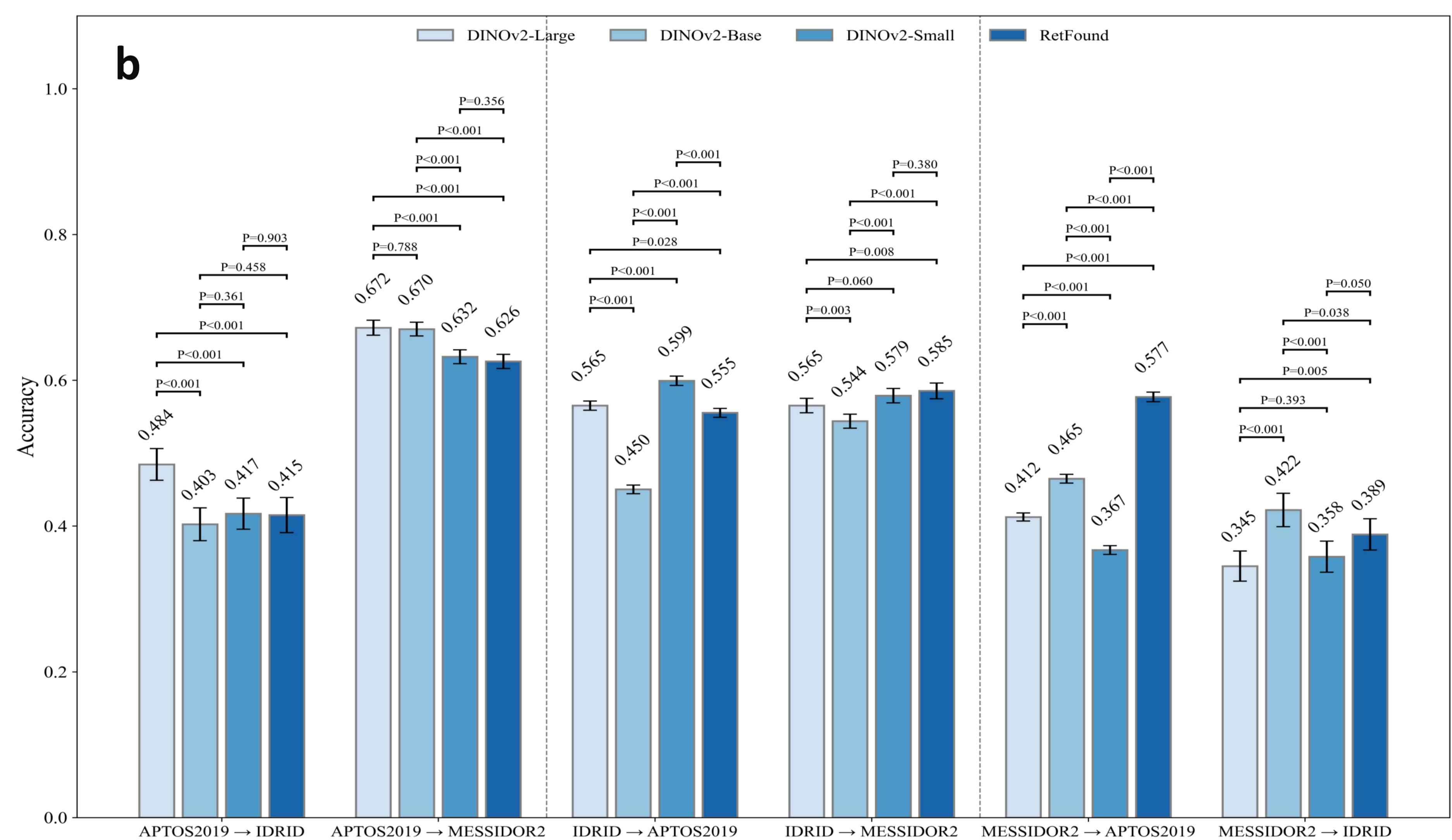
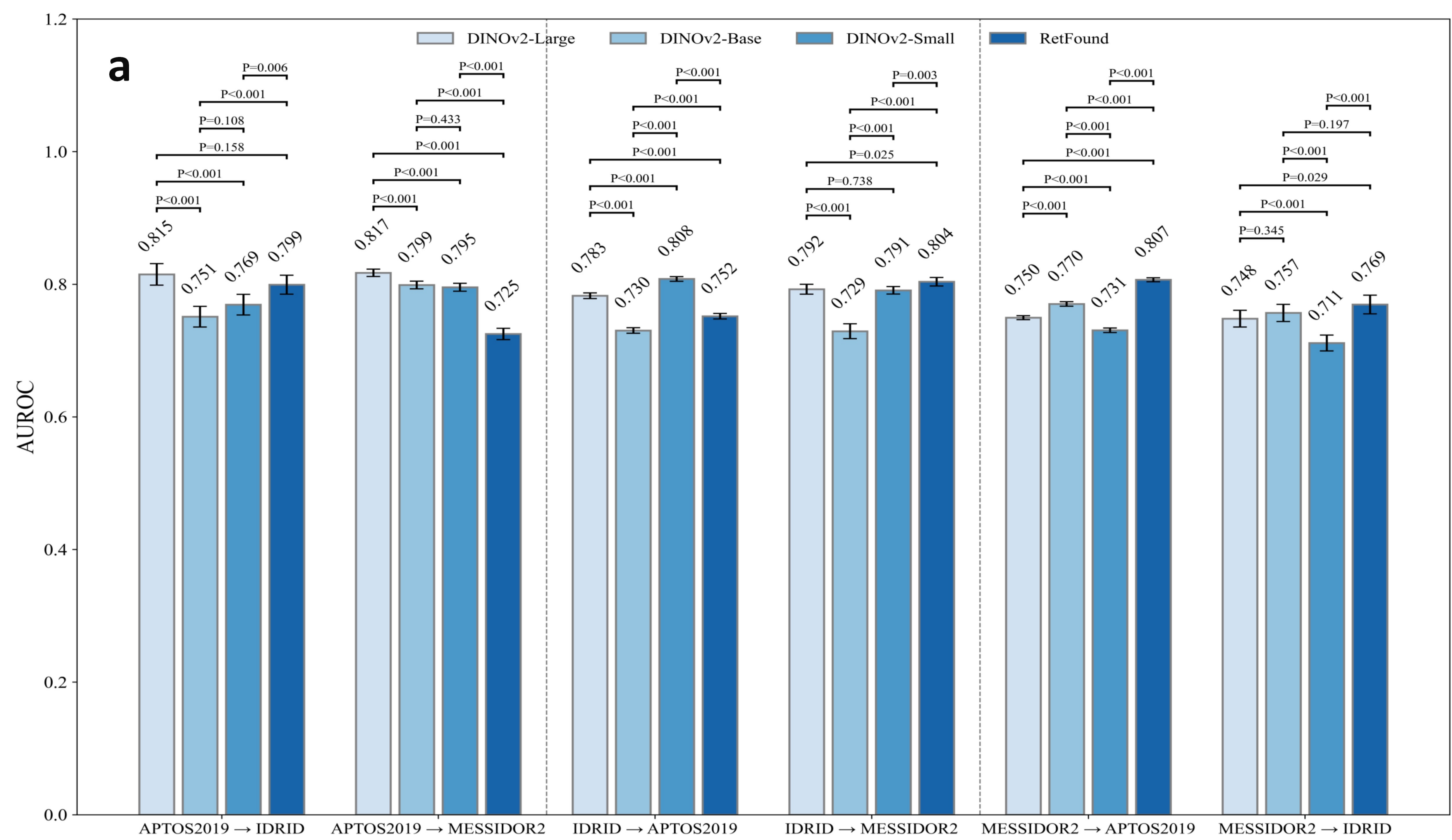
b Multi-category diagnosis of fundus diseases



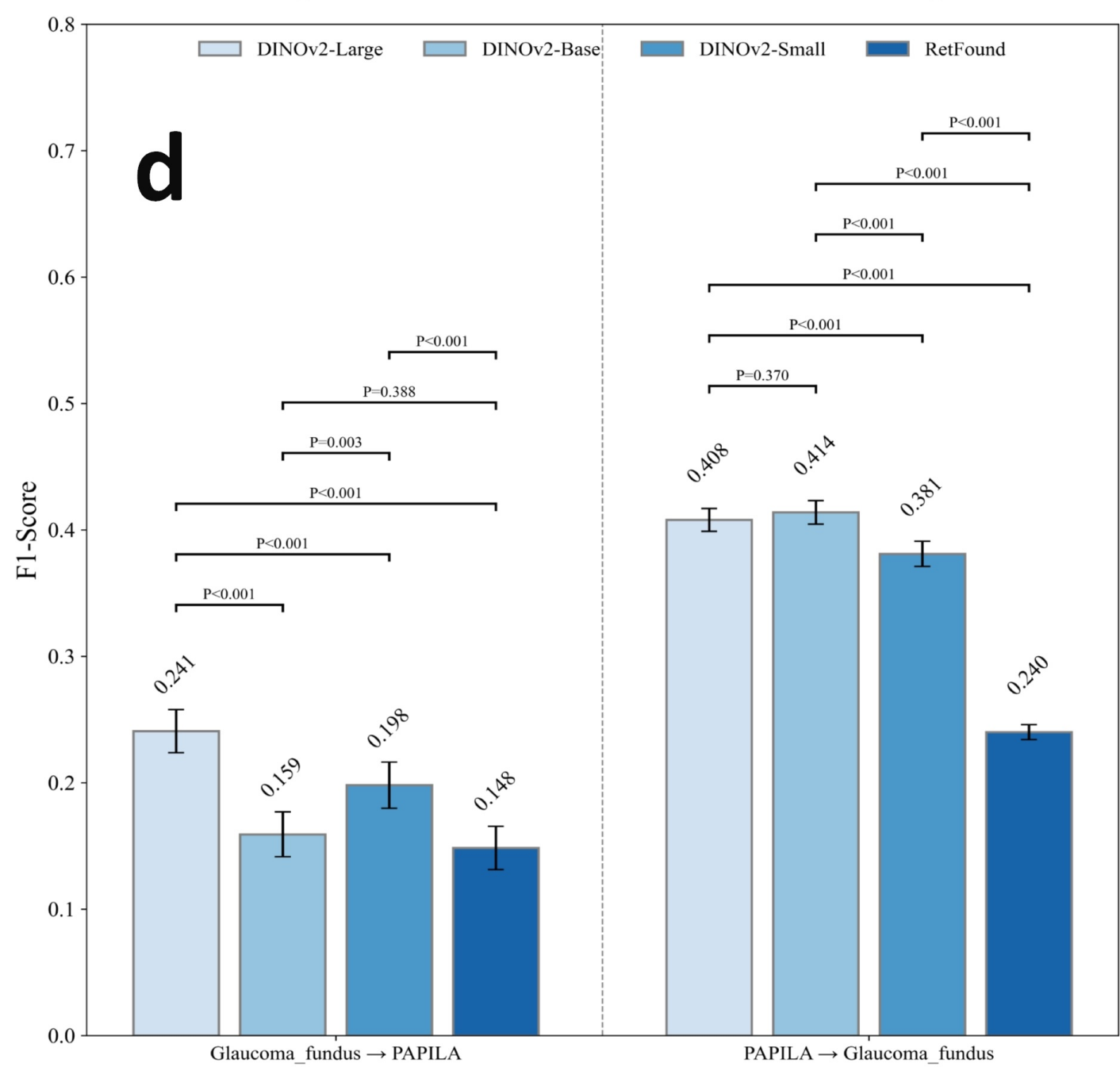
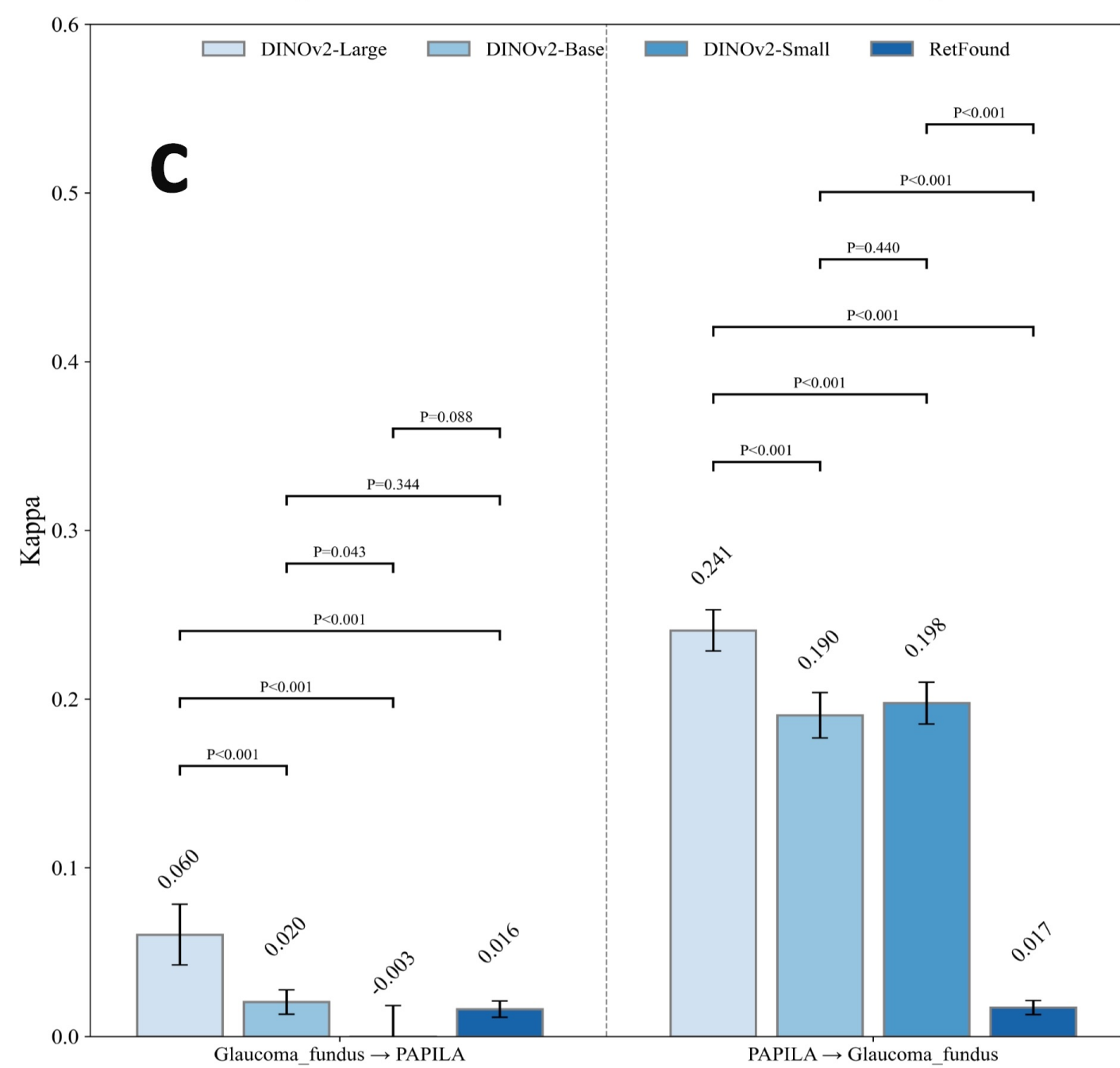
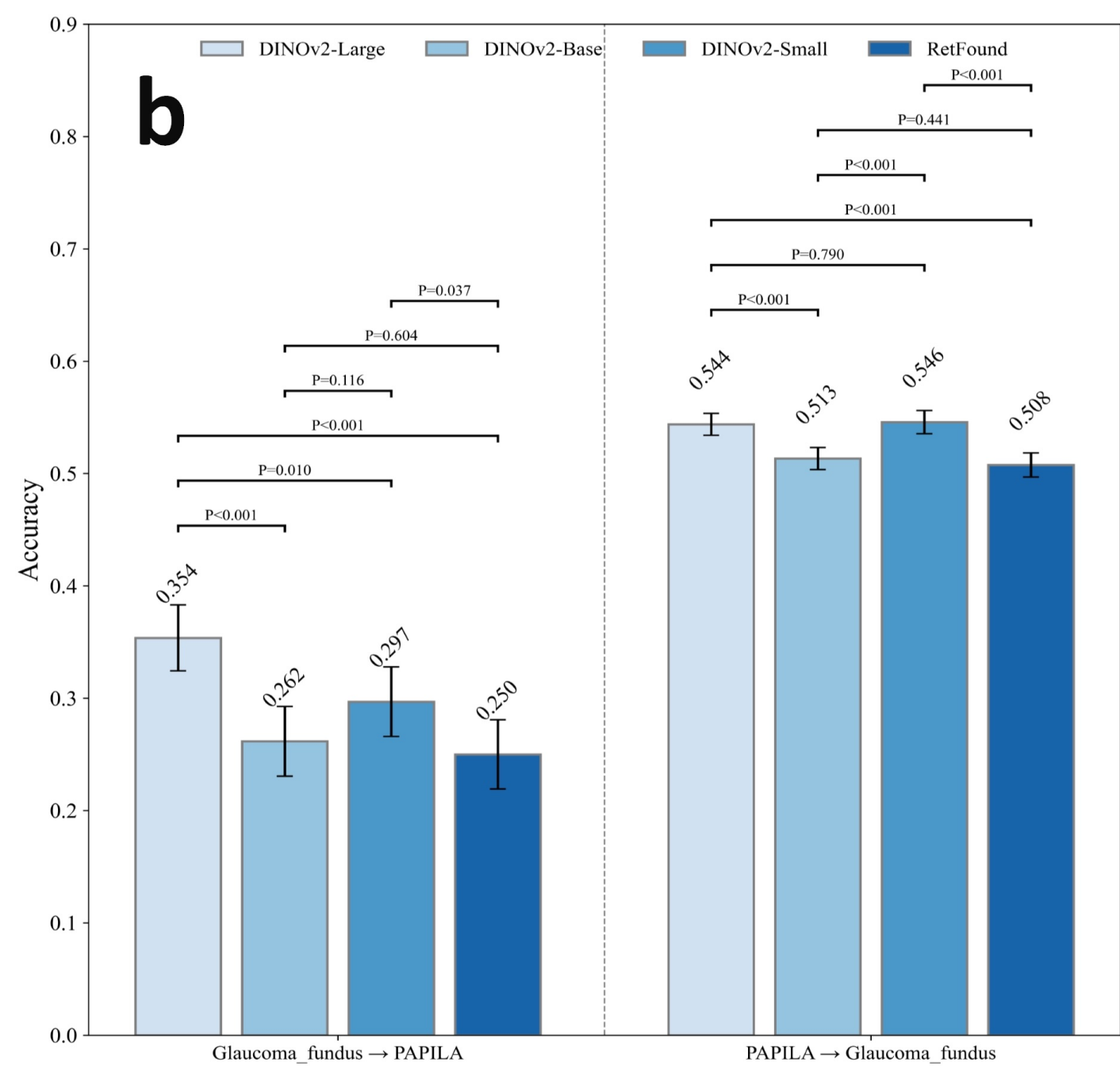
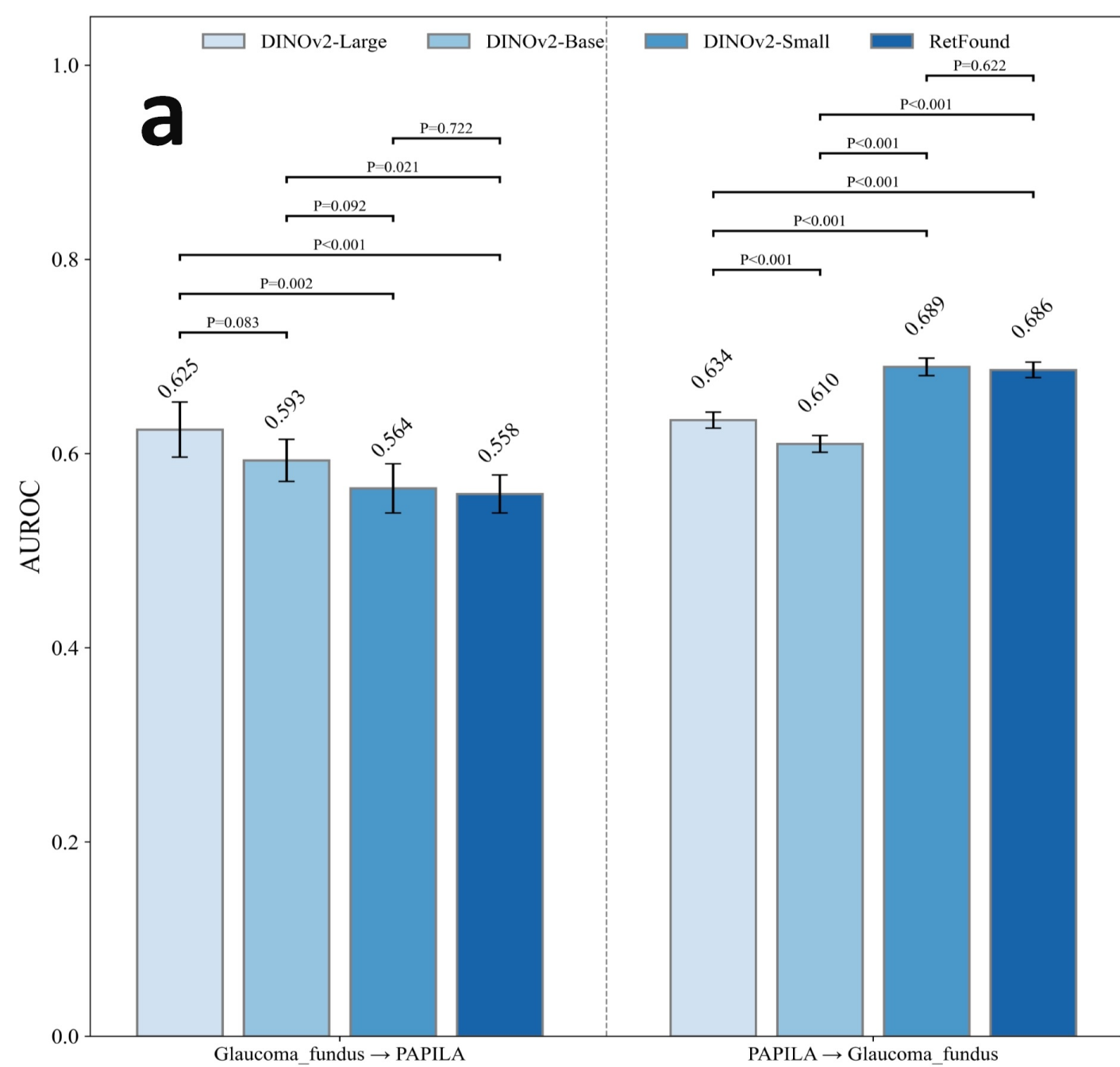
c Glaucoma diagnosis



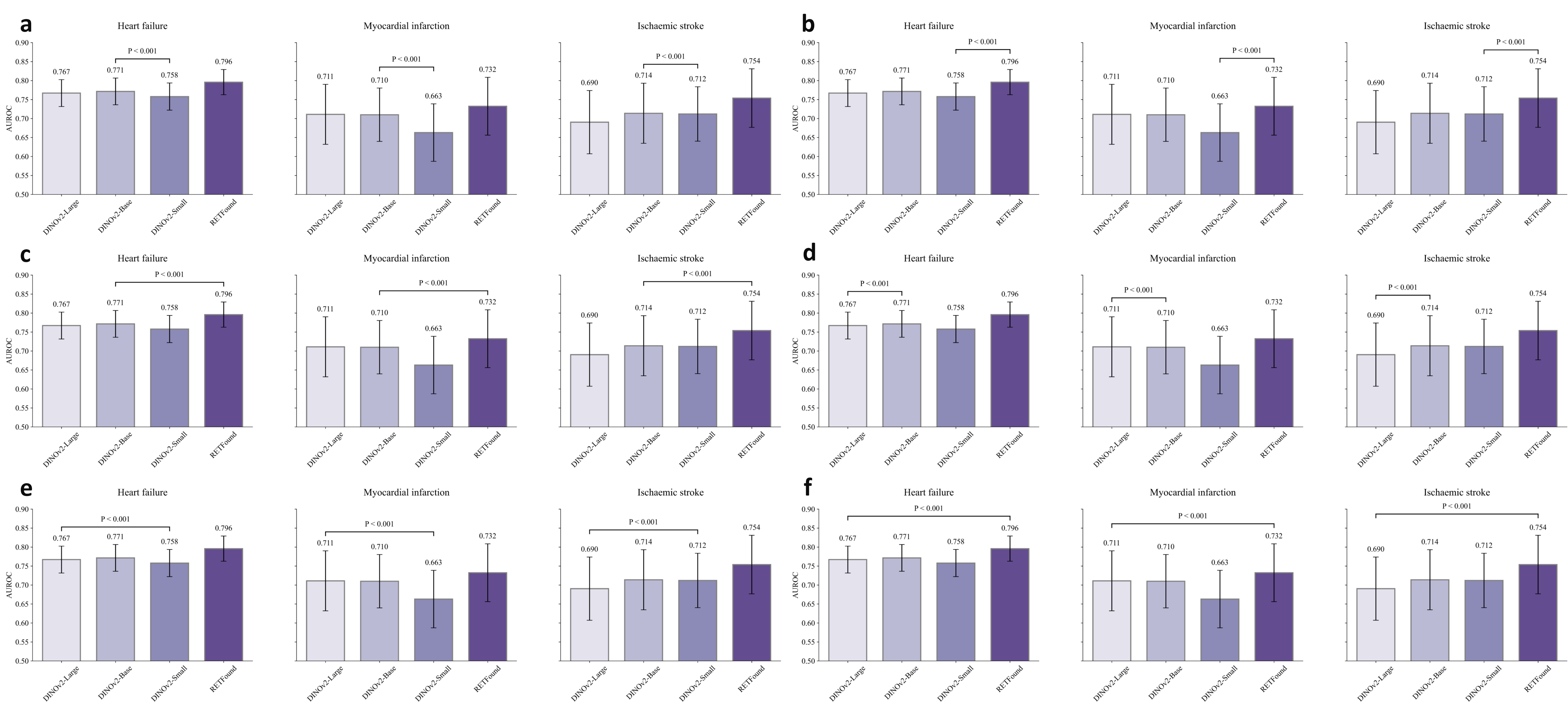
Extended Data Fig.2 Internal test confusion matrices of DINOv2 and RETFound models for ocular disease diagnosis tasks (Threshold:0.5). (a) diabetic retinopathy grading, (b) multi-category fundus disease classification, and (c) glaucoma detection across various datasets.



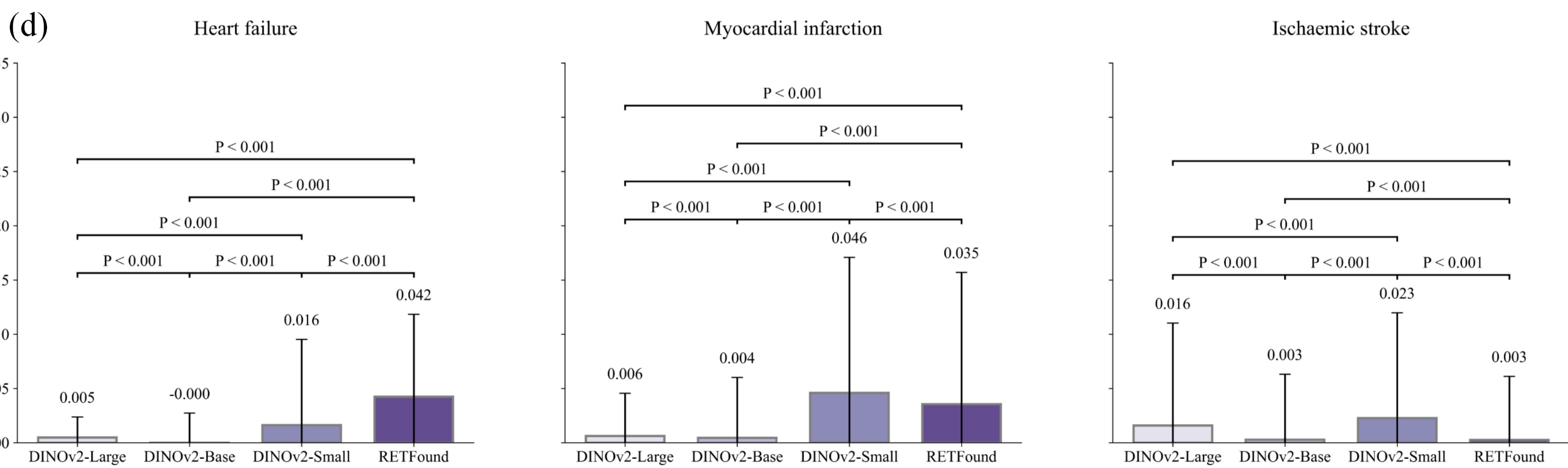
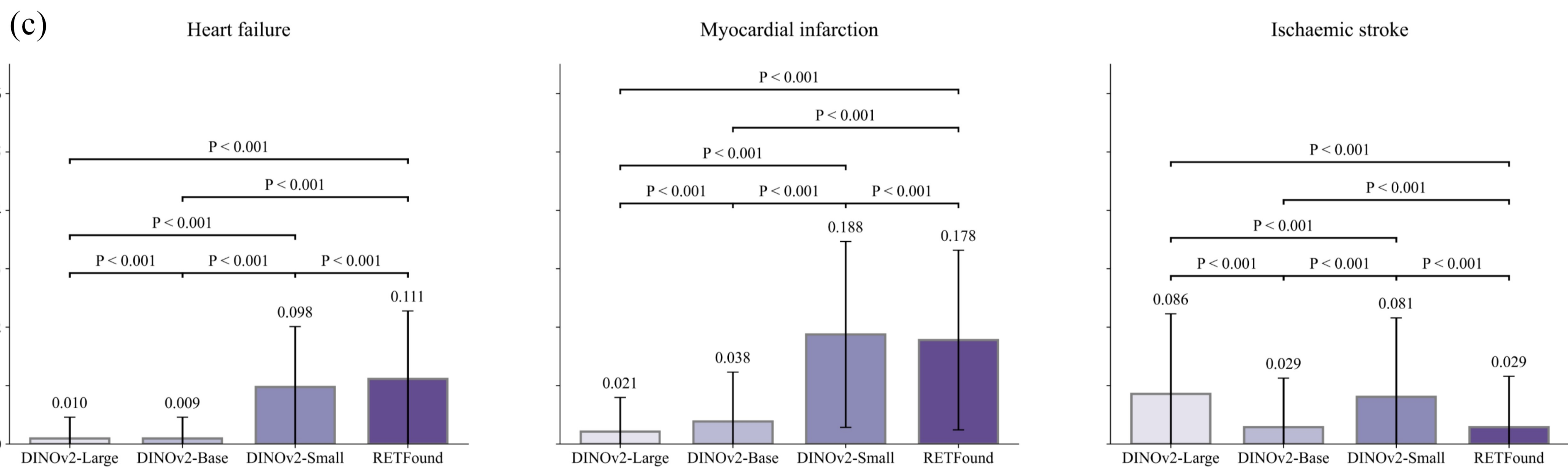
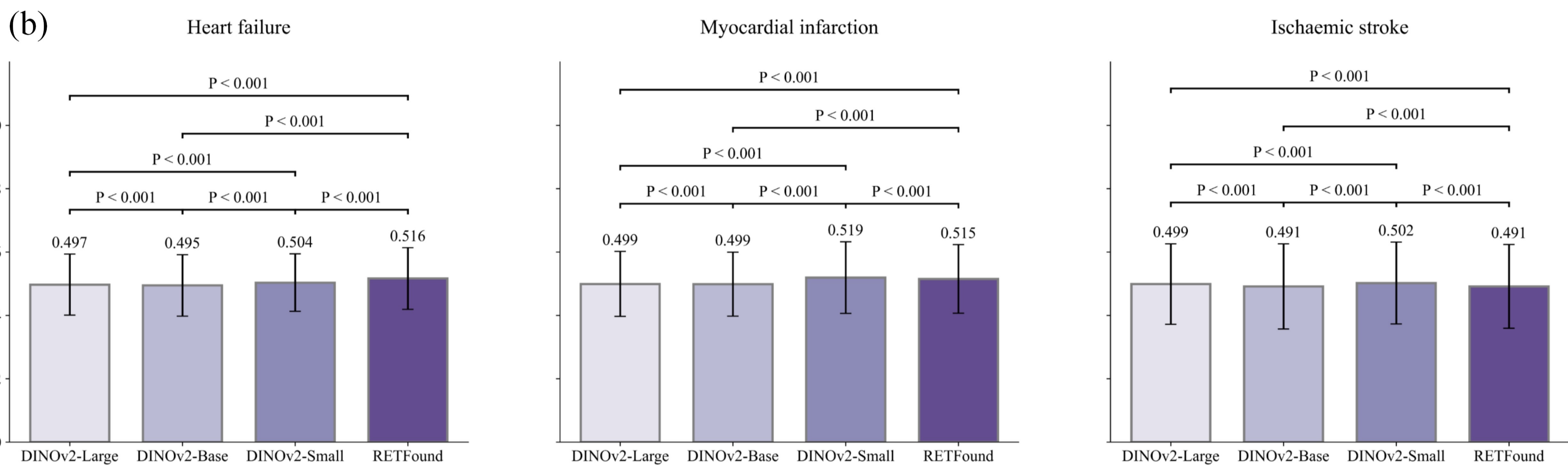
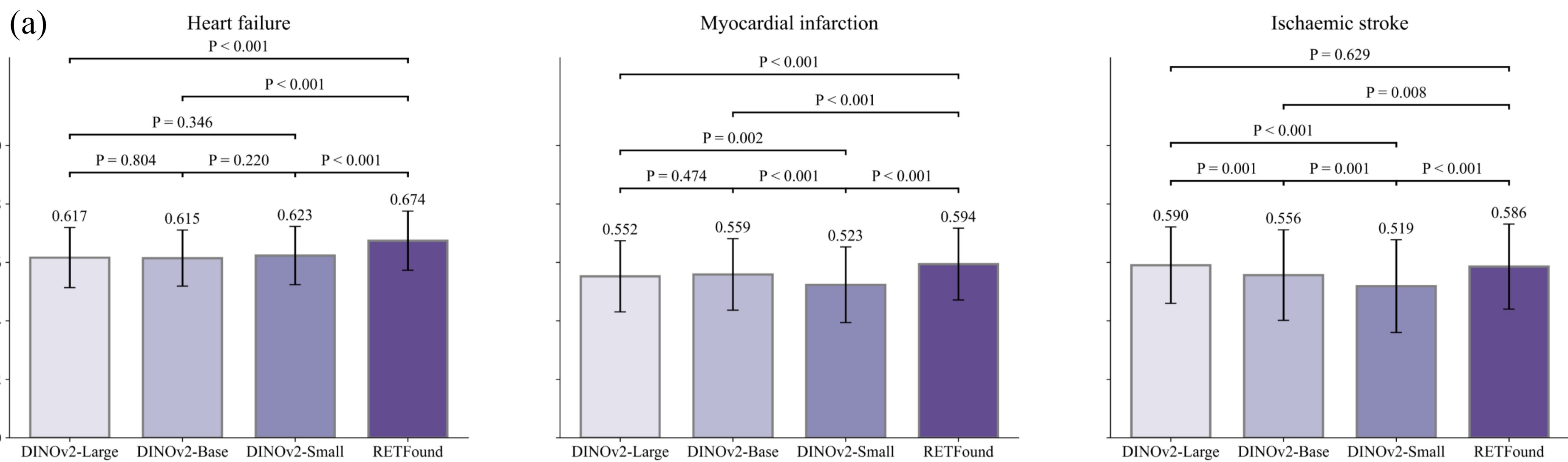
Extended Data Fig. 3. Performance of DINOv2 and RETFound models for DR classification tasks in the external tests. a-d) correspond to the AUROC, Accuracy, Kappa, and F1-Score metrics of the models. Each set of grouped bars represents models that were fine-tuned on one dataset, and externally evaluated on the other datasets for the task. In the DR diagnosis classification, models were fine-tuned on the APTOS2019 dataset and externally evaluated on IDRiD and MESSIDOR2 datasets, etc. For each scenario, the statistical significance of differences in metrics was evaluated using 100 bootstrap replicates by randomly sampling 20% of the data. Error bars indicate 95% confidence intervals, and bar centers represent the mean metric values.



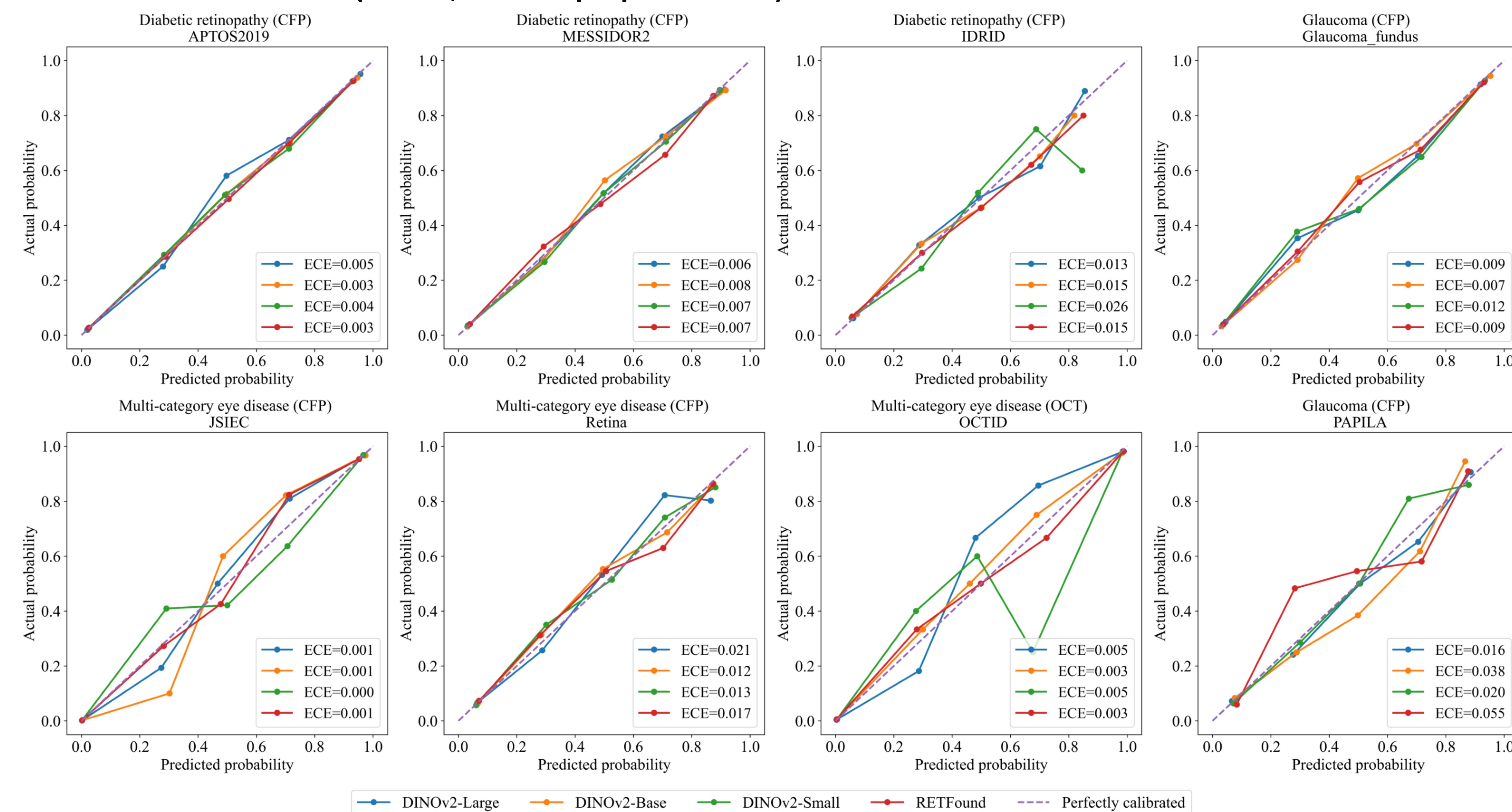
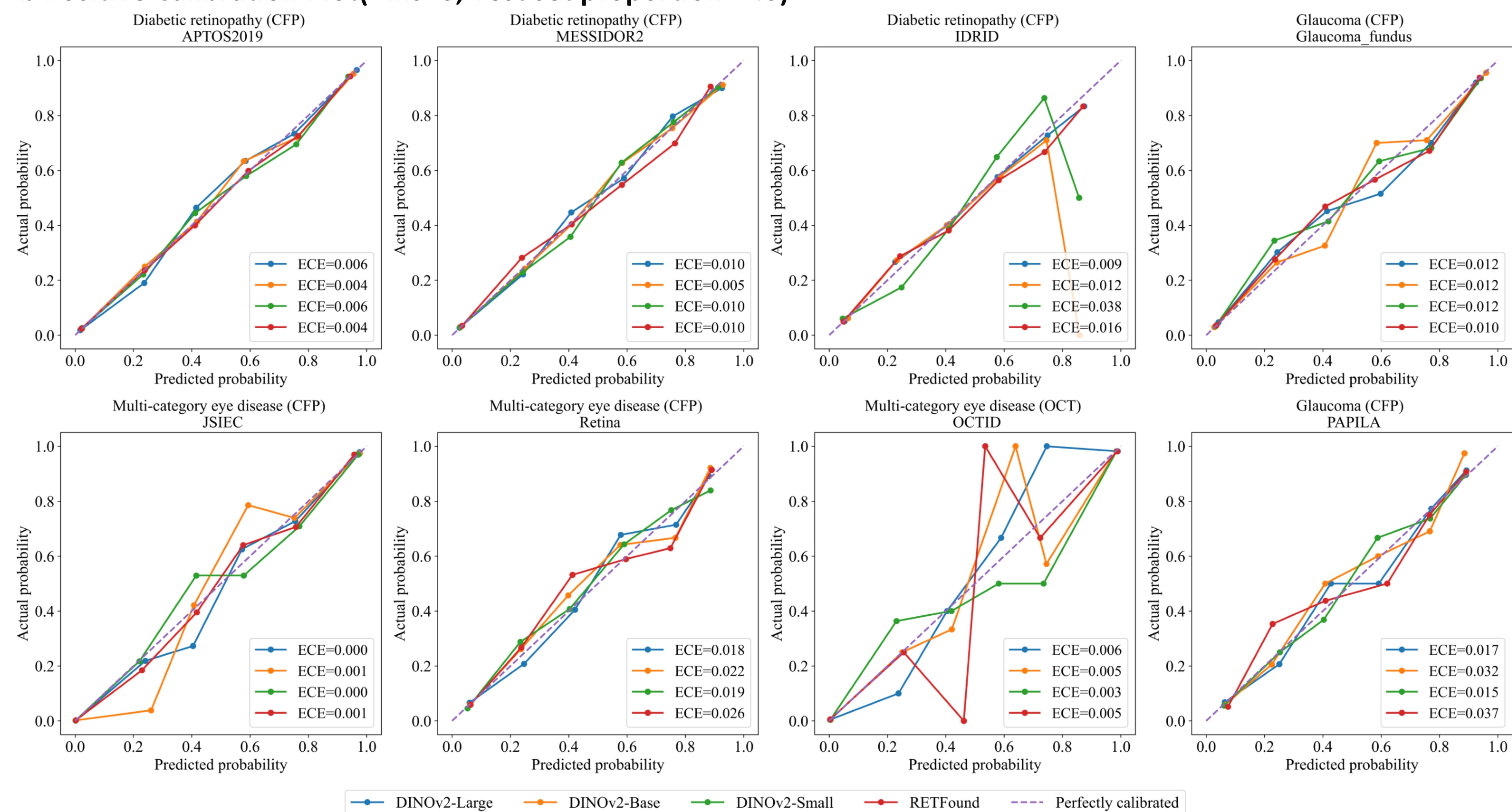
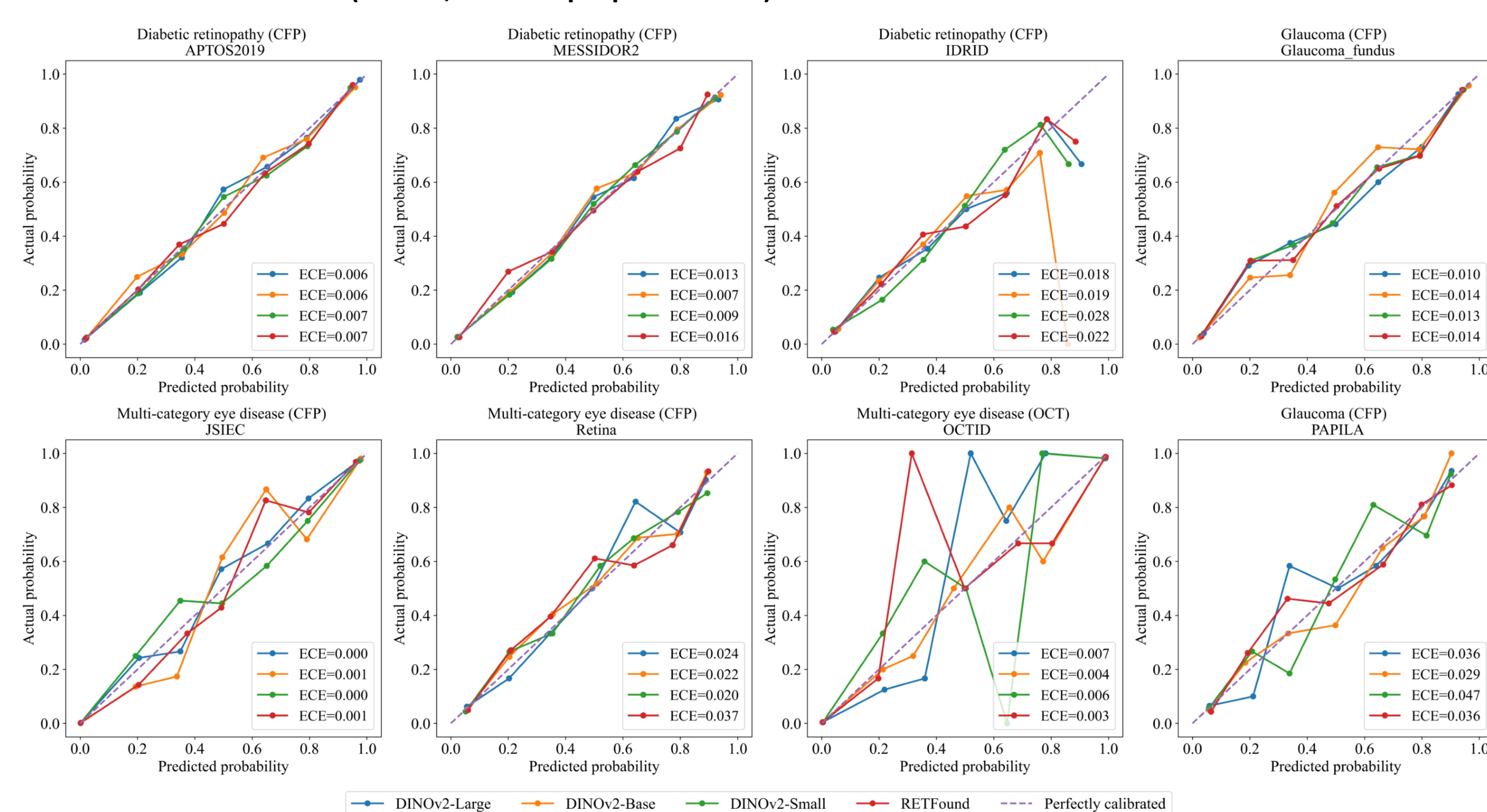
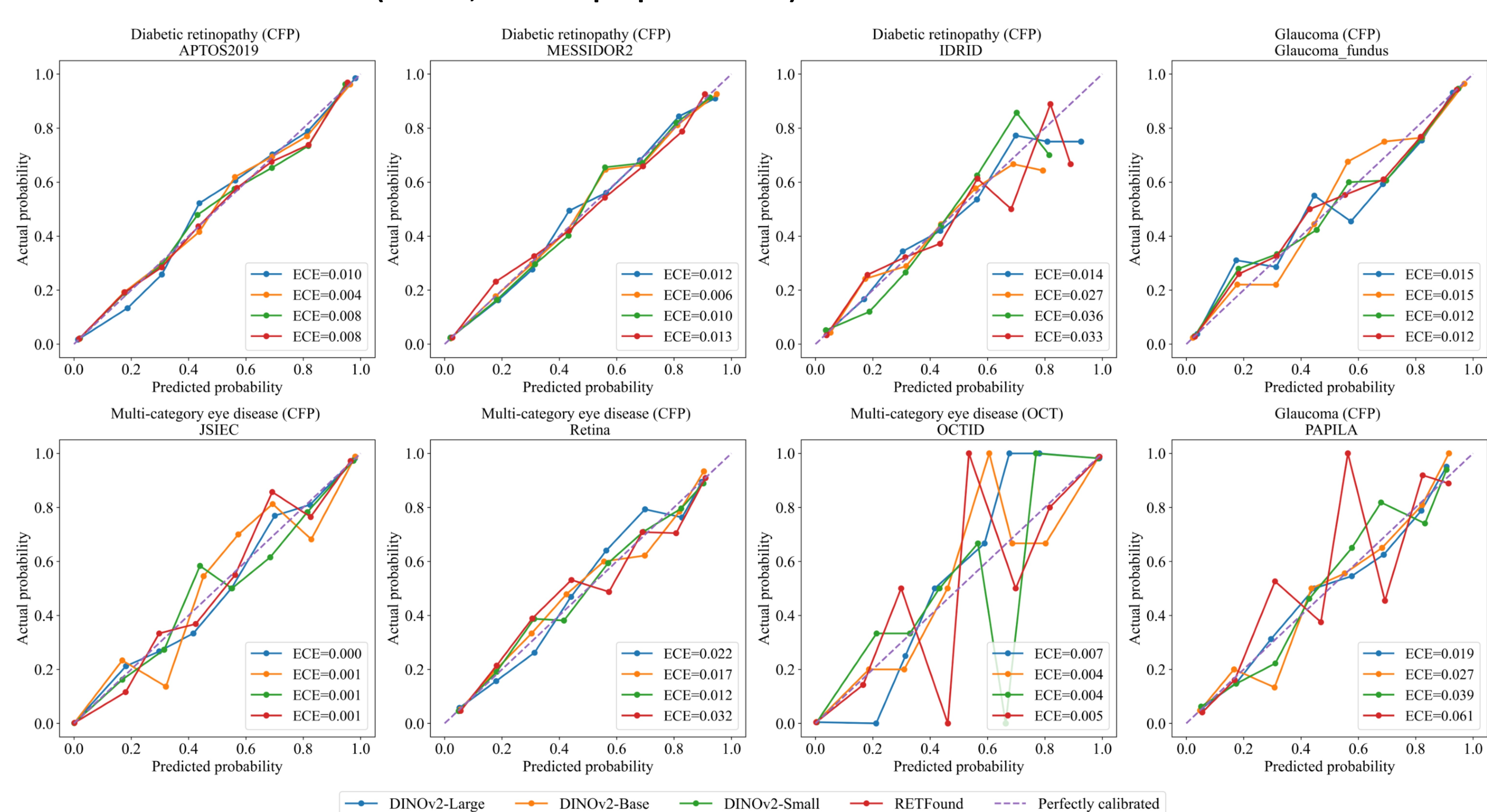
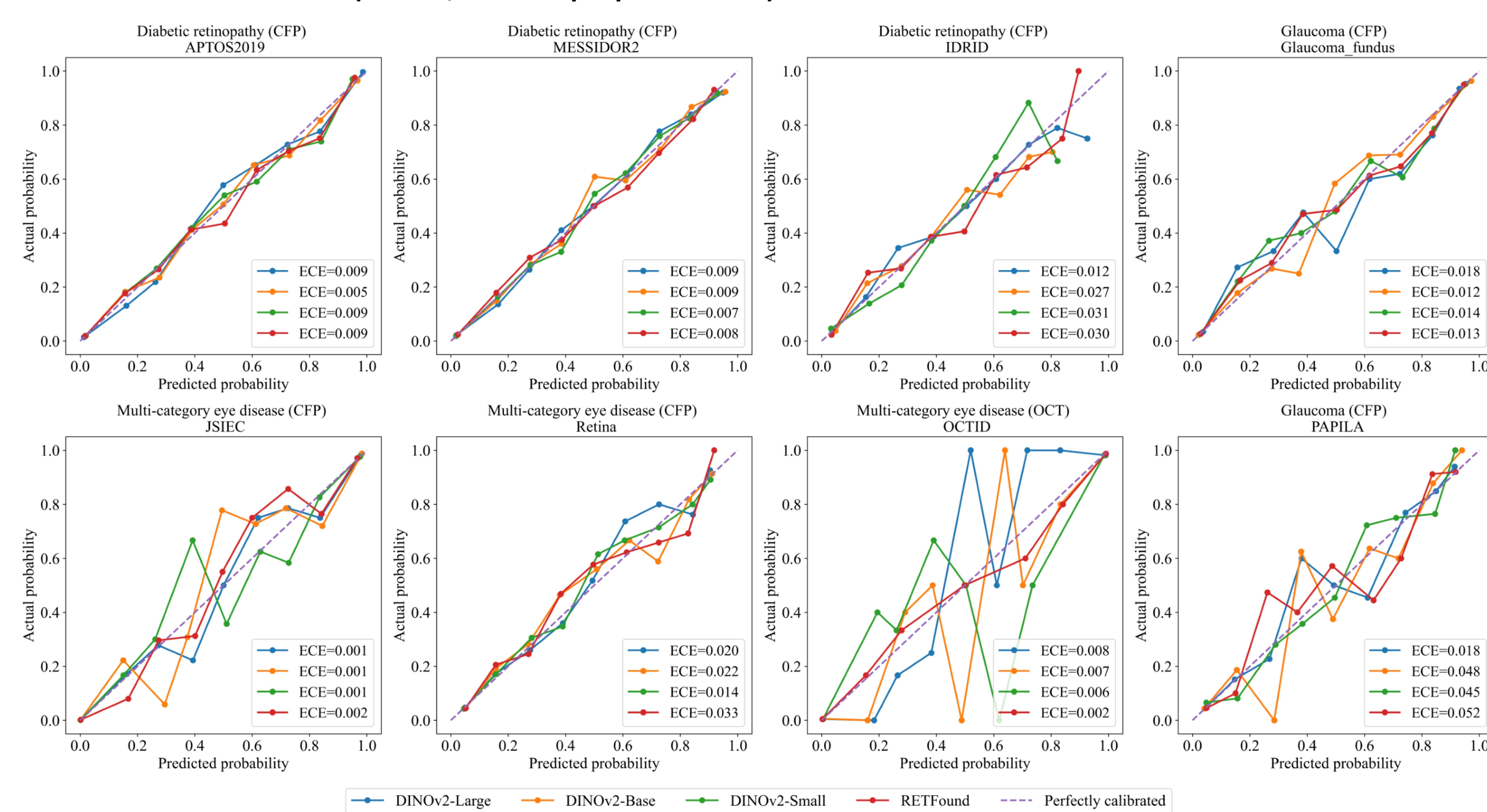
Extended Data Fig. 4. Performance of DINOv2 and RETFound models for glaucoma classification tasks in the external tests. a-d) correspond to the AUROC, Accuracy, Kappa, and F1-Score metrics of the models. Each set of grouped bars represents models that were fine-tuned on one dataset, and externally evaluated on the other datasets for the task. In the glaucoma diagnosis classification, fine-tuning was performed on either the Glaucoma_fundus or PAPILA dataset, then externally evaluated on the other dataset. For each scenario, the statistical significance of differences in metrics was evaluated using 100 bootstrap replicates by randomly sampling 20% of the data. Error bars indicate 95% confidence intervals, and bar centers represent the mean metric values.



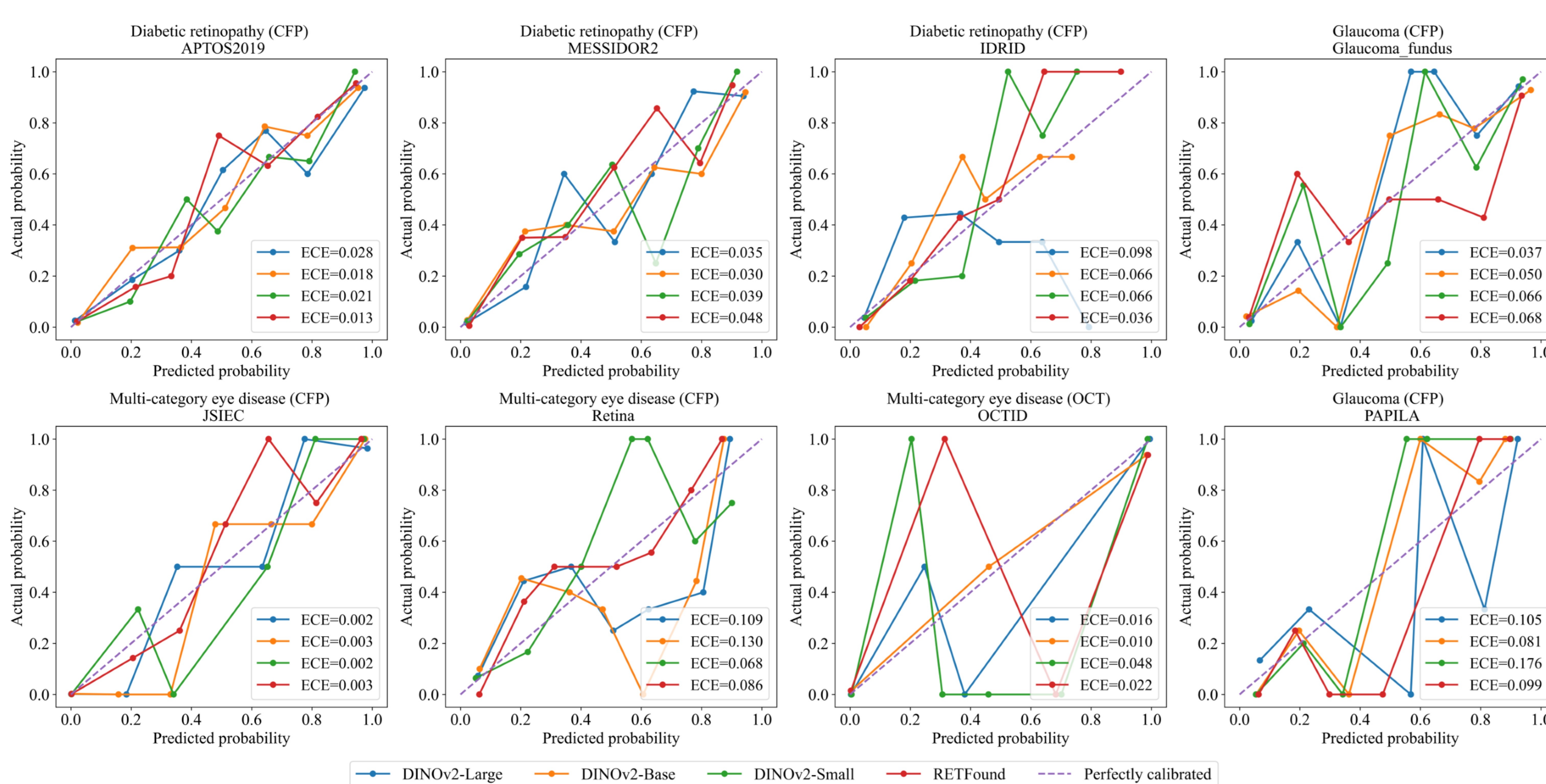
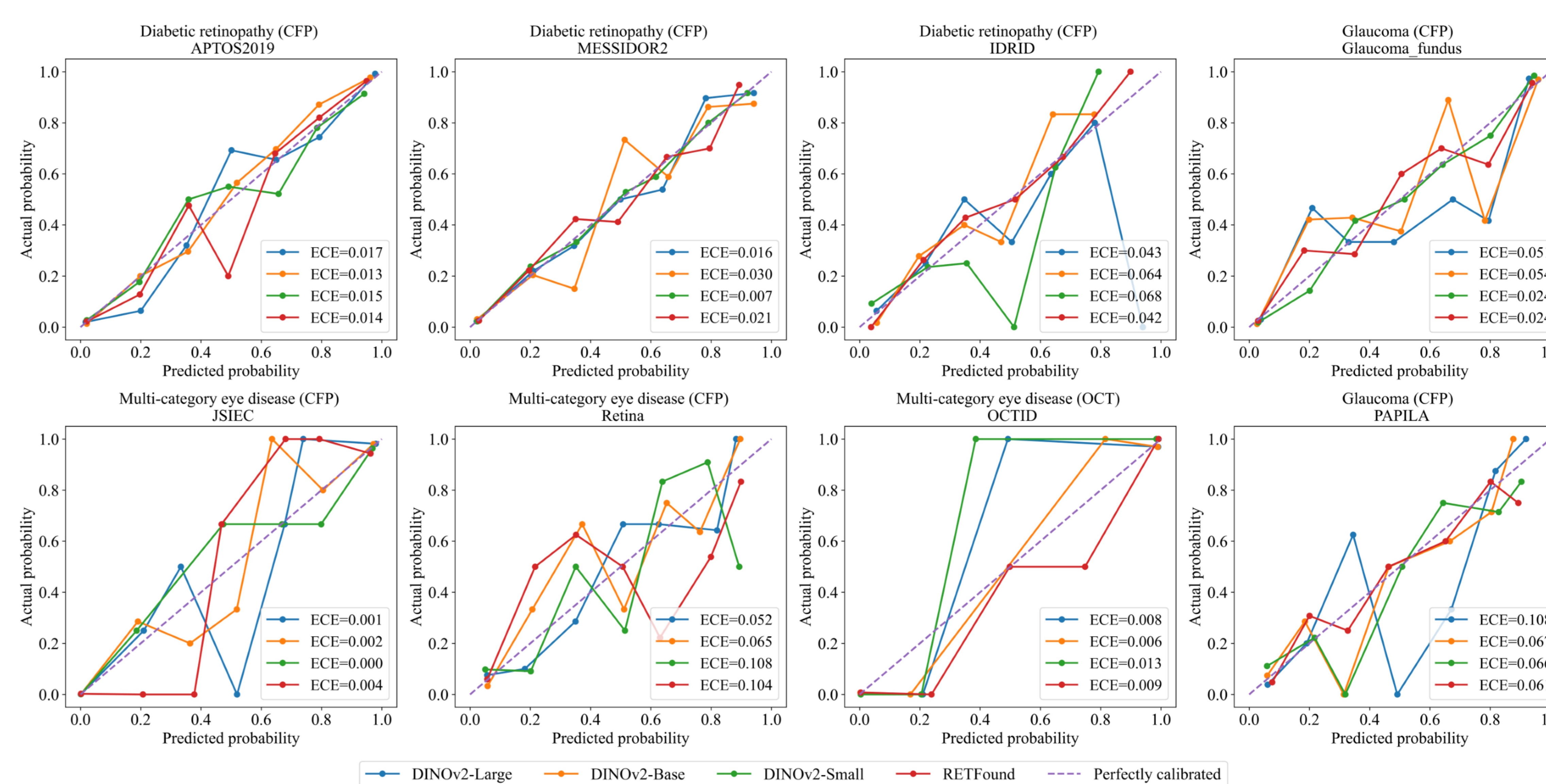
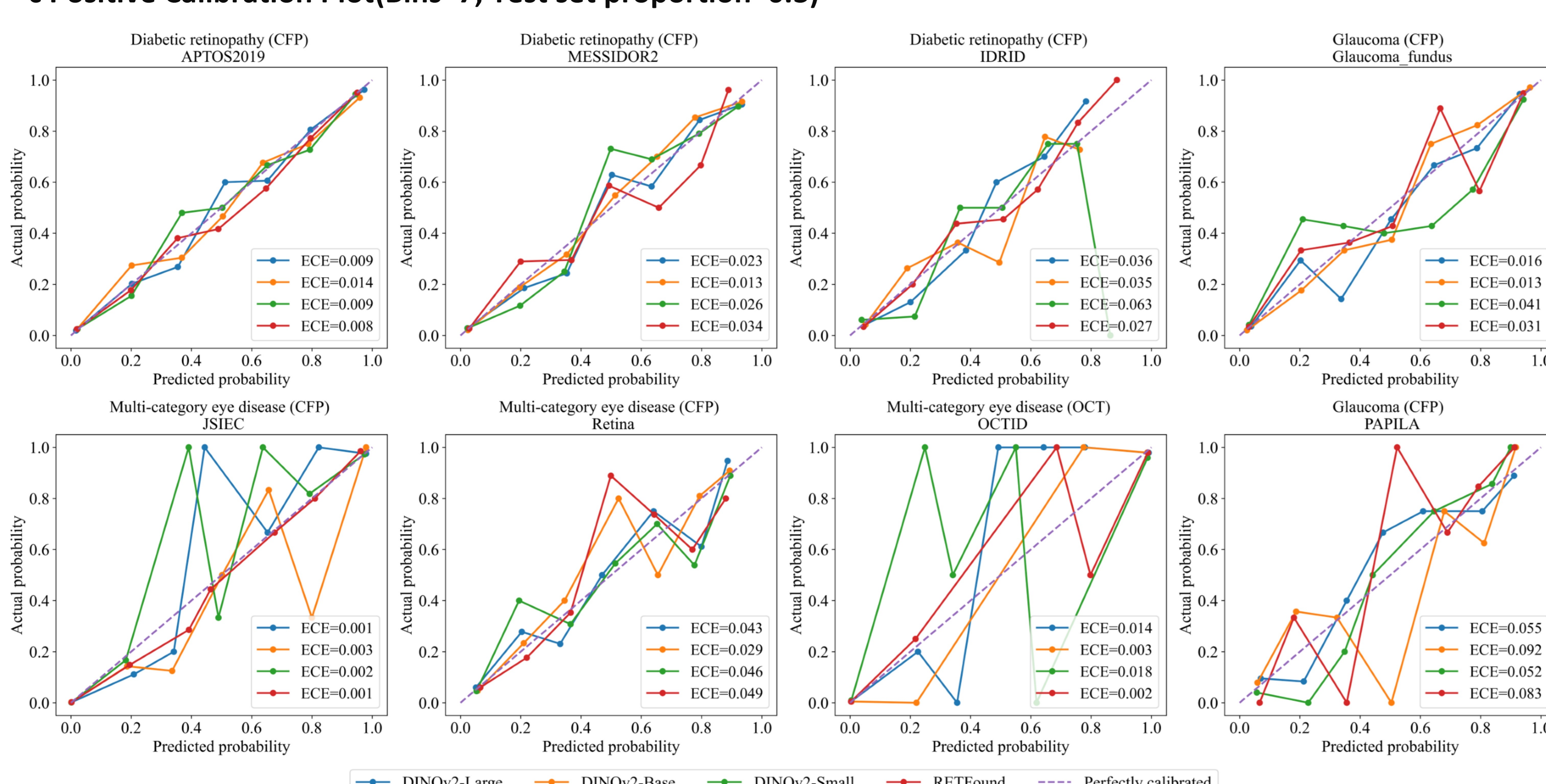
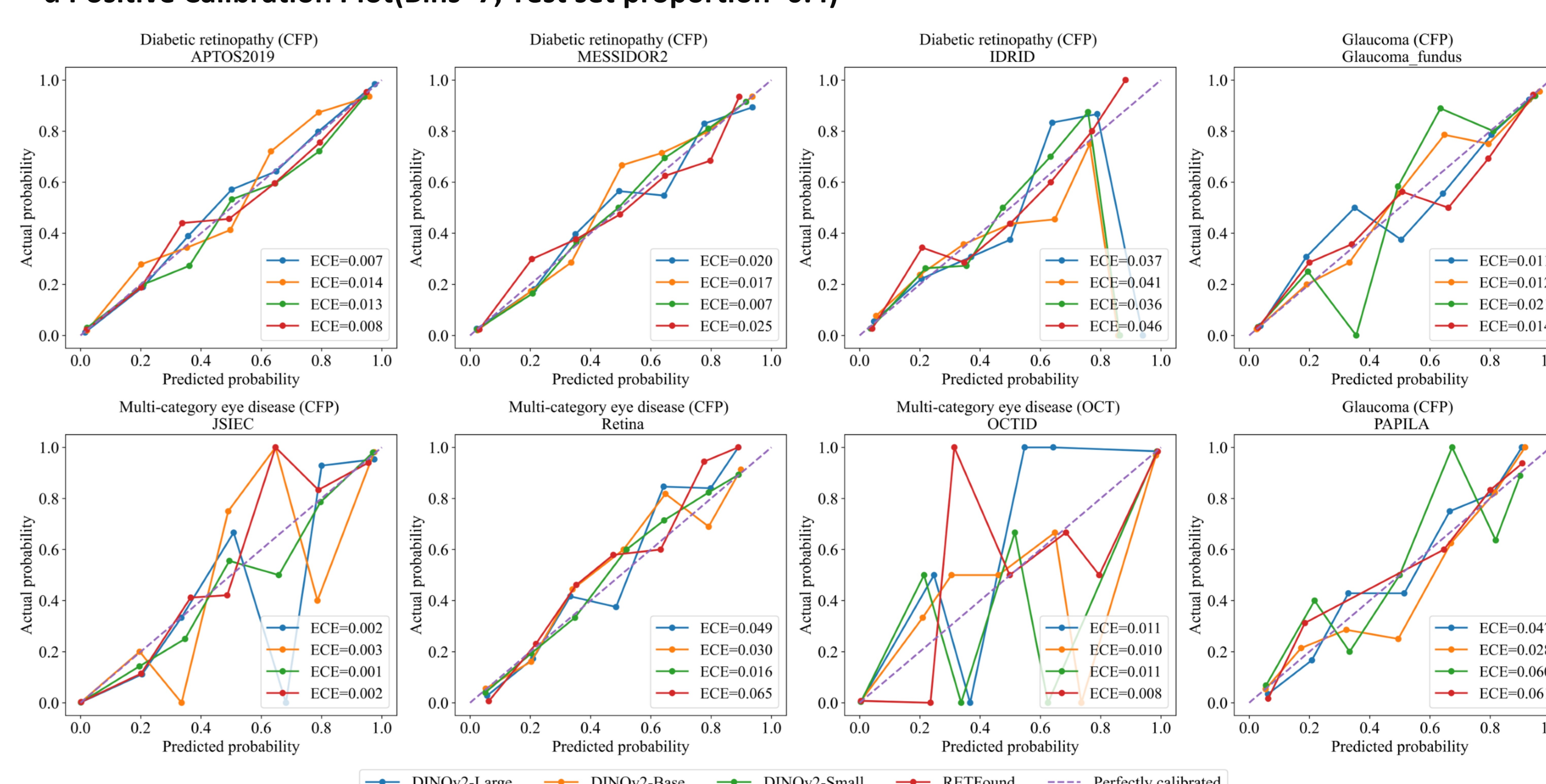
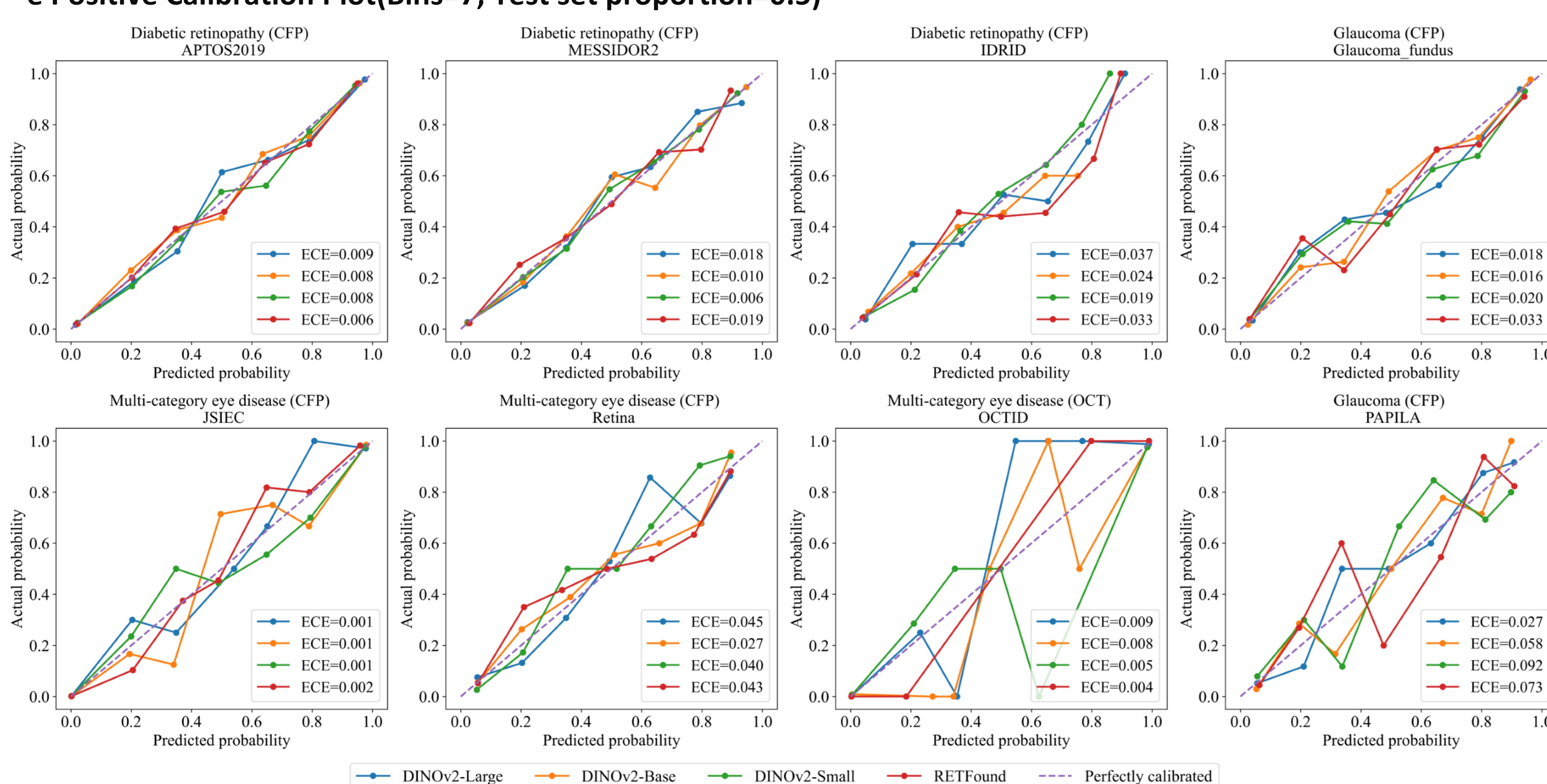
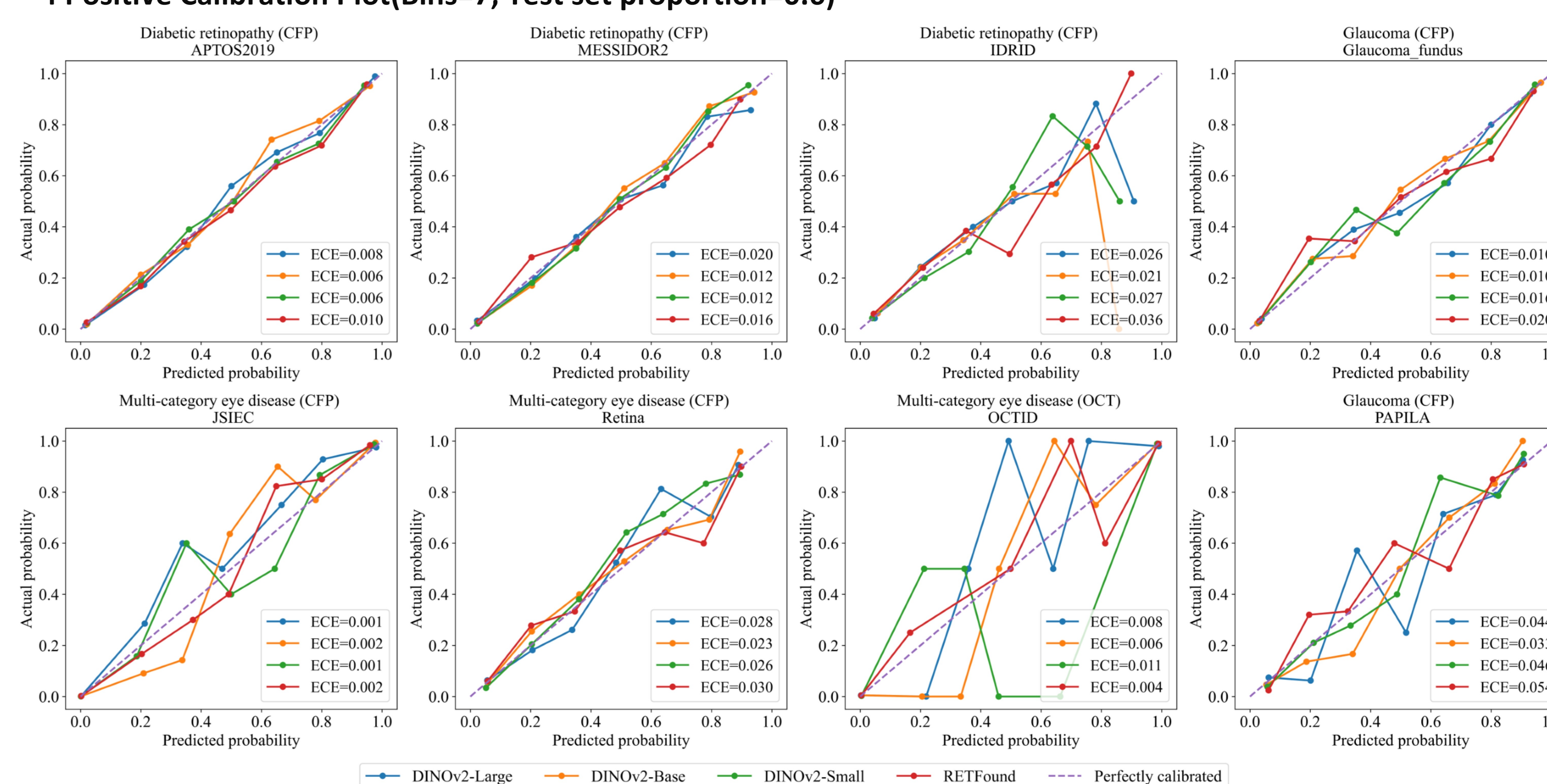
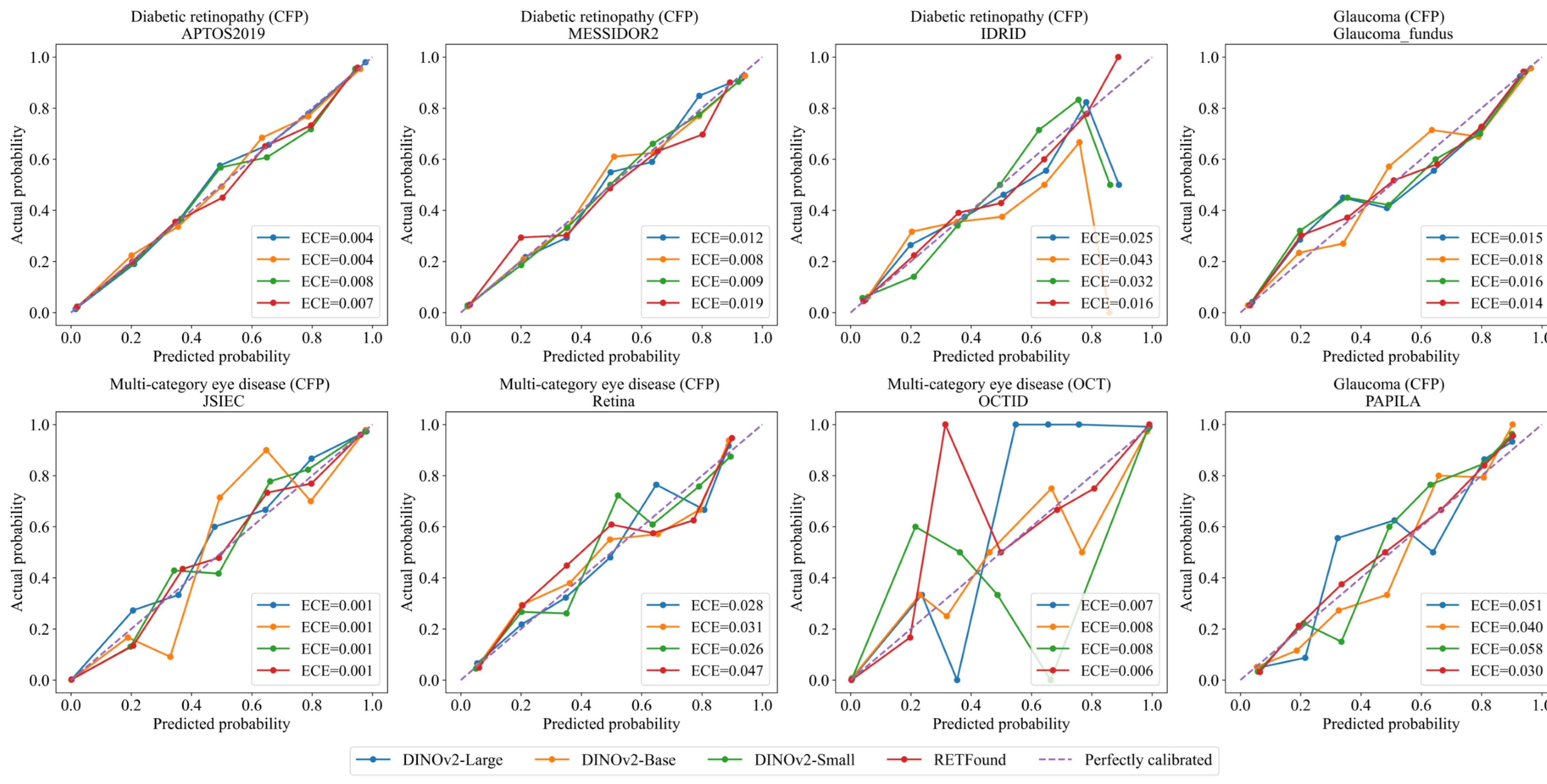
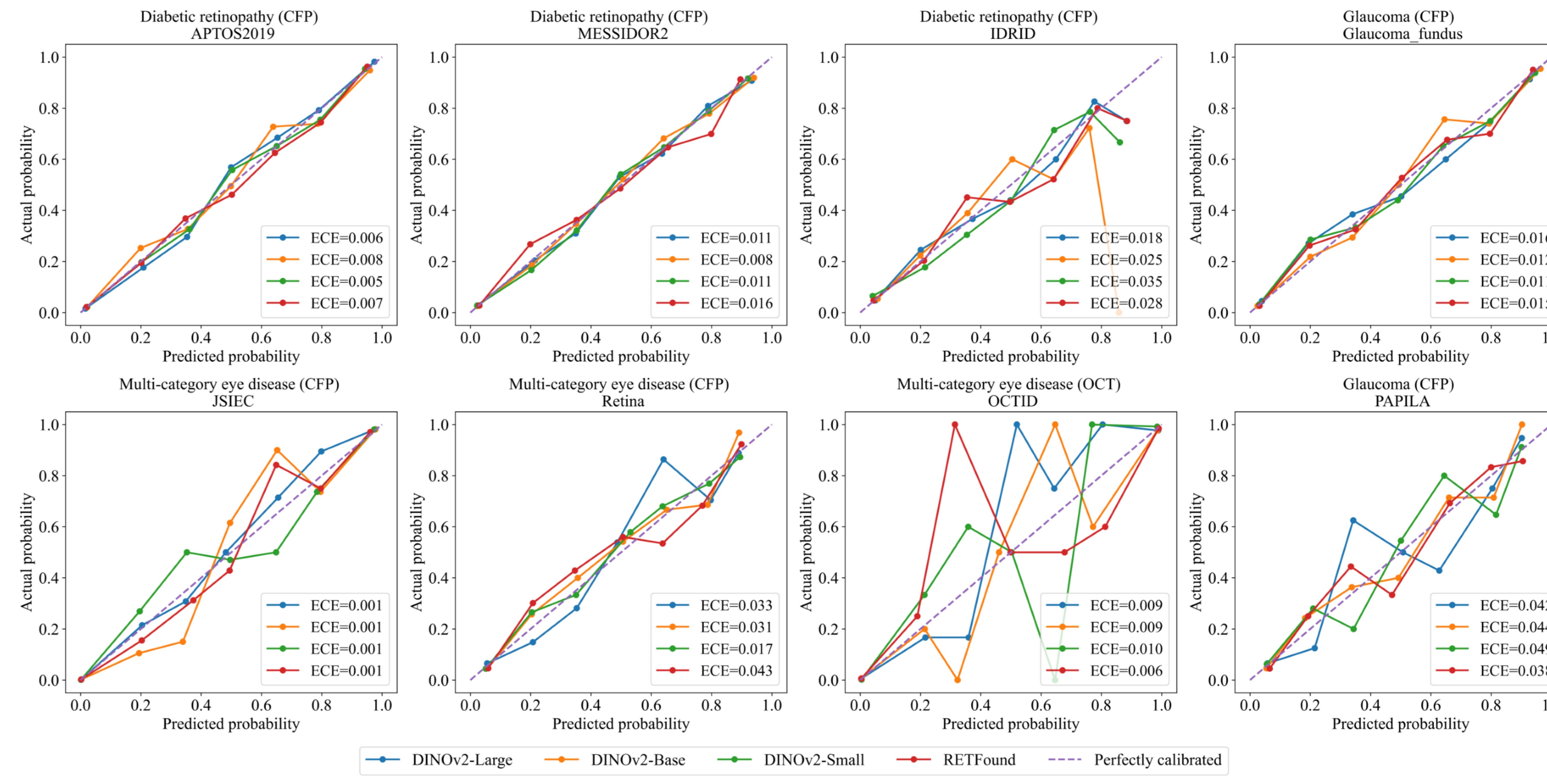
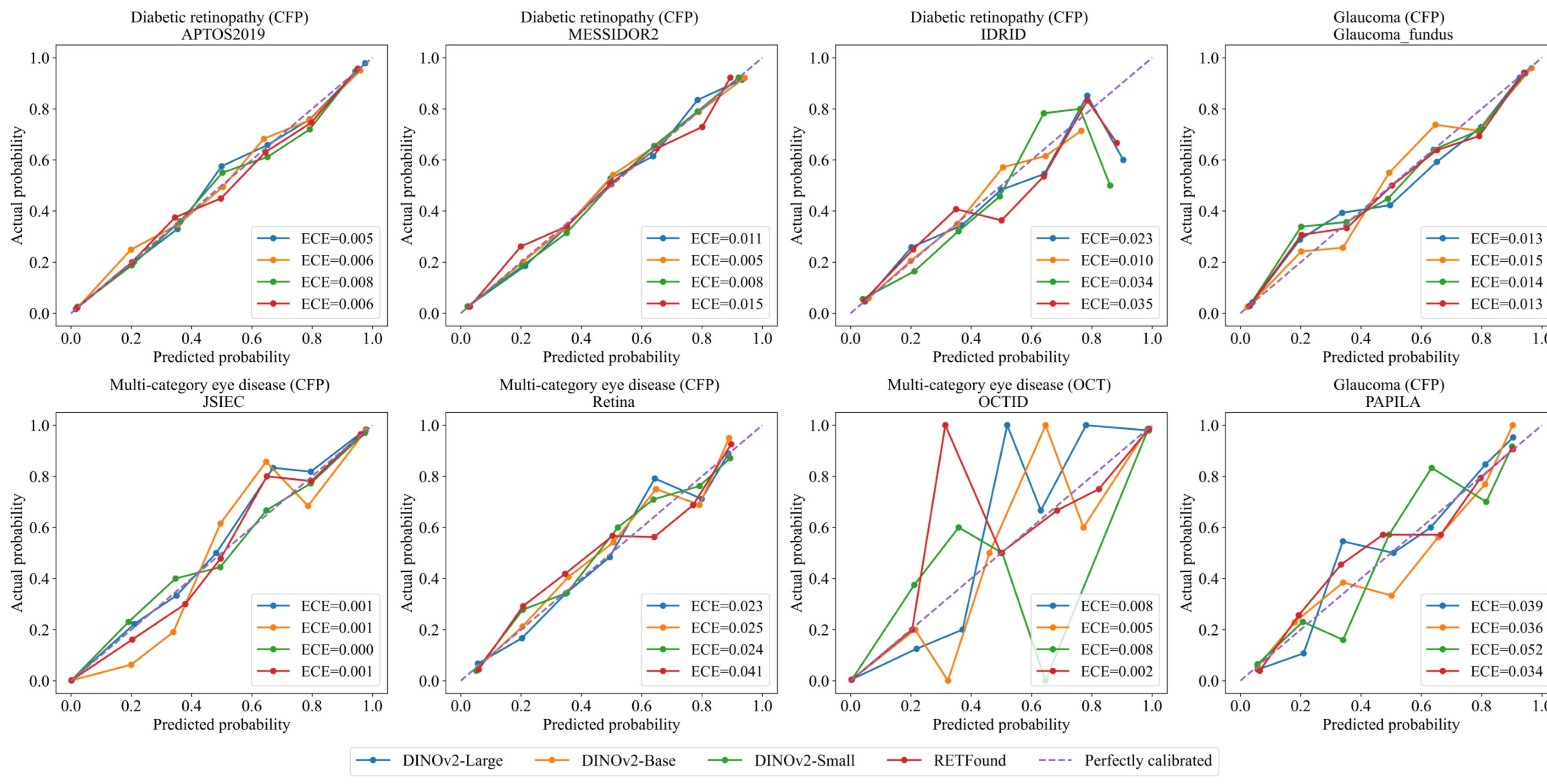
Extended Data Fig.5. Permuted pair-wise AUROC comparison between all models in predicting 3-year incidence of systemic diseases in the internal test (MEH-AlzEye). a) DINOv2-Base vs DINOv2-Small. b) DINOv2-Small vs RetFound. c) DINOv2-Base vs RetFound. d) DINOv2-Large vs DINOv2-Base. e) DINOv2-Large vs DINOv2-Small. f) DINOv2-Large vs RetFound. For each task and scenario, statistical significance of AUROC differences was evaluated using 100 bootstrap replicates, randomly sampling 20% of the data. Error bars show 95% confidence intervals, and bar centers represent the mean AUROC values.



Extended Data Fig. 6. External evaluation of diagnostic classification for three systemic diseases: heart failure, myocardial infarction, and ischemic stroke. illustrate the performance of models fine-tuned on the MEH-AlzEye dataset and externally evaluated on the UK Biobank dataset, using four key metrics: (a) AUROC, (b) Accuracy, (c) F1-Score, and (d) Kappa. Four FMs — DINOv2 Large, Base, Small, and RETFound—are systematically compared to assess their generalization capabilities for each disease. For each task and scenario, the statistical significance of differences in metrics was evaluated using 100 bootstrap replicates by randomly sampling 20% of the data. Error bars indicate 95% confidence intervals, and bar centers represent the mean metric values.

a Positive Calibration Plot(Bins=5; Test set proportion=1.0)**b Positive Calibration Plot(Bins=6; Test set proportion=1.0)****c Positive Calibration Plot(Bins=7; Test set proportion=1.0)****d Positive Calibration Plot(Bins=8; Test set proportion=1.0)****e Positive Calibration Plot(Bins=9; Test set proportion=1.0)**

Extended Data Fig.7. The positive calibration plots of the fundus disease diagnosis models under different numbers of bins. The calibration performance of the DINOv2-Large, DINOv2-Base, DINOv2-Small, and RETFound models on eight fundus disease datasets (OCTID, Retina, Glaucoma fundus, APTOS2019, PAPILA, MESSIDOR2, IDRID, and JSIEC) is shown. (a)-(e) correspond to the cases with 5, 6, 7, 8, and 9 bins, respectively. Each subplot shows the relationship between the actual probability and the predicted probability, along with the expected calibration error (ECE) for each model.

a Positive Calibration Plot(Bins=7; Test set proportion=0.1)**b Positive Calibration Plot(Bins=7; Test set proportion=0.2)****c Positive Calibration Plot(Bins=7; Test set proportion=0.3)****d Positive Calibration Plot(Bins=7; Test set proportion=0.4)****e Positive Calibration Plot(Bins=7; Test set proportion=0.5)****f Positive Calibration Plot(Bins=7; Test set proportion=0.6)****g Positive Calibration Plot(Bins=7; Test set proportion=0.7)****h Positive Calibration Plot(Bins=7; Test set proportion=0.8)****i Positive Calibration Plot(Bins=7; Test set proportion=0.9)****j Positive Calibration Plot(Bins=7; Test set proportion=0.9)**

Extended Data Fig.8. Positive Calibration Plots for Various Test Set Proportions (0.1-0.9) and Models on Eight Fundus Disease Datasets (OCTID, Retina, Glaucoma fundus, APTOS2019, PAPILA, MESSIDOR2, IDRID, and JSIEC). Each subplot displays the calibration performance for the DINOv2-Large, DINOv2-Base, DINOv2-Small, and RETFound models with 7 bins. The x-axis represents the predicted probability, while the y-axis represents the actual probability.

Supplementary table1

Disease category	Dataset name	Country	Imaging devices	Sub-category	Train	Validation	Test	In total(%)
Diabetic retinopathy	Indian Diabetic Retinopathy Image Dataset (IDRID)	India	VX-10 alpha digital fundus camera (Kowa)	No retinopathy: 107 Mild retinopathy: 16 Moderate retinopathy: 108 Severe retinopathy: 59 Proliferative retinopathy: 39 in total: 329	27 4 28 15 10 84	34 5 32 19 13 103	168(32.56%) 25(4.84%) 168(32.56%) 93(18.02%) 62(12.02) 516	
	MESSIDOR-2	France	TRC-NW6 non-mydiatic fundus camera (Topcon)	No retinopathy: 568 Mild retinopathy: 151 Moderate retinopathy: 193 Severe retinopathy: 41 Proliferative retinopathy: 19 in total: 972	143 38 49 11 5 246	306 81 105 23 11 526	1017(58.31%) 270(15.48%) 347(19.89%) 75(4.3%) 35(2.01%) 1744	
	Asia Pacific TeleOphthalmology Society 2019 (APTOS-2019)	India	a variety of camera models, not specified	No retinopathy: 1010 Mild retinopathy: 207 Moderate retinopathy: 559 Severe retinopathy: 108 Proliferative retinopathy: 164 in total: 2048	253 52 140 27 42 514	542 111 300 58 89 1100	1805(49.29%) 370(10.1%) 999(27.28%) 193(5.27%) 295(8.06%) 3662	
Glaucoma	PAPILA	Spain	TRC-NW400 non-mydiatic retinal camera (Topcon)	No glaucoma: 212 Suspected glaucoma: 57 Glaucoma: 43 in total: 312	54 14 11 79	67 17 14 98	333(68.1%) 88(17.99%) 68(13.9%) 489	
	Glaucoma Fundus	South Korea	AFC-330 non-mydiatic auto fundus camera (Nidek)	No glaucoma: 440 Early glaucoma: 161 Advanced glaucoma: 260 in total: 861	111 41 66 218	237 87 141 465	788(51.04%) 289(18.72%) 467(30.25%) 1544	
Multiple category disease	Joint Shantou International Eye Centre (JSIEC)	China	FF450 Plus IR Fundus Camera (ZEISS) and TRC-50DX Mydiatic Retinal Camera (Topcon)	Normal: 20 Tessellated fundus: 7 Large optic cup: 28 Non-referable DR: 9 Moderate nonproliferative DR: 27 Severe and proliferative DR: 21 Possible glaucoma: 7 Optic atrophy: 6 Severe hypertensive retinopathy: 8 Disc swelling and elevation: 7 Dragged Disc: 5 Congenital disc abnormality: 5 Retinitis pigmentosa: 12 Bietti crystalline dystrophy: 4 Peripheral retinal degeneration and break: 7 Myelinated nerve fiber: 5 Vitreous particles: 7 Fundus neoplasm: 4 Branch Retinal Vein Occlusion: 24 Central retinal vein occlusion: 12 Massive hard exudates: 7 Yellow-white spots-flecks: 16 Cotton-wool spots: 5 Vessel tortuosity: 7 Chorioretinal atrophy-coloboma: 8 Preretinal hemorrhage: 5	6 2 7 3 7 6 2 2 2 2 2 3 1 2 2 1 6 3 4 2 2 2 2 2 2 2 2 2 2	12 4 15 6 15 12 4 4 5 4 3 7 3 5 4 5 3 14 7 4 9 3 5 3 5 3	38(3.8%) 13(1.3%) 50(5%) 18(1.8%) 49(4.9%) 39(3.9%) 13(1.3%) 12(1.2%) 15(1.5%) 13(1.3%) 10(1%) 10(1%) 22(2.2%) 8(0.8%) 14(1.4%) 11(1.1%) 14(1.4%) 8(0.8%) 44(4.4%) 22(2.2%) 13(1.3%) 29(2.9%) 10(1%) 14(1.4%) 15(1.5%) 10(1%)	

				Fibrosis:	5	2	3	10(1%)
				Laser Spots:	11	3	6	20(2%)
				Silicon oil in eye:	10	3	6	19(1.9%)
				Blur fundus without PDR:	63	16	35	114(11.4%)
				Blur fundus with suspected PDR:	24	7	14	45(4.5%)
				Retinal artery occlusion:	8	3	5	16(1.6%)
				Rhegmatogenous retinal detachment:	31	8	18	57(5.7%)
				Central serous chorioretinopathy:	7	2	5	14(1.4%)
				Vogt-Koyanagi-Harada disease:	7	2	5	14(1.4%)
				Maculopathy:	40	11	23	74(7.4%)
				Epiretinal membrane:	14	4	8	26(2.6%)
				Macular hole:	12	4	7	23(2.3%)
				Pathological myopia:	29	8	17	54(5.4%)
				In total:	534	150	316	1000
	Retina	NR	NR	Normal:	168	42	90	300(49.92%)
				Cataract:	56	14	30	100(16.64%)
				Glaucoma:	56	14	31	101(16.81%)
				Other retinal diseases:	56	14	30	100(16.64%)
				In total:	336	84	181	601
	Optical Coherence Tomography Image Database (OCTID)	India	Cirrus HD-OCT machine (Carl Zeiss Meditec)	Control:	115	29	62	206(35.83%)
				AMD:	56	15	32	103(17.91%)
				DR:	30	8	17	55(9.57%)
				Macular hole:	59	15	33	107(18.61%)
				central serous chorioretinopathy:	58	15	31	104(18.09%)
				in total:	318	82	175	575

Supplementary table2

Study cohort	Function of data	Imaging device	Category	Number of individuals*	Number of eyes	Age - mean(SD)	Gender - Female(%)	Ethnicity
3-year incidence prediction of ischaemic stroke								
MEH-AlzEye	Model fine-tune and internal evaluation	TOPCON 3DOCT-2000SA	Stroke group	1263	1263	75.8(11.6)	671(53.1%)	White (41.9%); Asian or Asian British (20.3%); Black or Black British (10.4%); Others (11.9%); Unknown (14.5%)
			Control group	1263	1263	66.7(13.7)	653(51.7%)	White (37.1%); Asian or Asian British (16.2%); Black or Black British (9.7%); Others (16.2%); Unknown (20.8%)
UK Biobank	External evaluation	TOPCON 3DOCT-1000-Mk2	Stroke group	154	154	61.9(6.1)	95(61.7%)	White (93.5%); Asian or Asian British (0.6%); Black or Black British (2.6%); Others (2.5%); Unknown (0.8%)
			Control group	154	154	57.9(8)	69(44.8%)	White (88.3%); Asian or Asian British (3.9%); Black or Black British (0.6%); Others (5.2%); Unknown (2%)
3-year incidence prediction of myocardial infarction								
MEH-AlzEye	Model fine-tune and internal evaluation	TOPCON 3DOCT-2000SA	Myocardial infarction group	1403	1403	72.1(11.8)	596(42.4%)	White (34.2%); Asian or Asian British (33.2%); Black or Black British (7.5%); Others (13.6%); Unknown (11.5%)
			Control group	1403	1403	66.8(13.4)	704(50.2%)	White (37.2%); Asian or Asian British (16.7%); Black or Black British (9.6%); Others (16.9%); Unknown (19.6%)
UK Biobank	External evaluation	TOPCON 3DOCT-1000-Mk2	Myocardial infarction group	201	201	60.4(7)	151(75.1%)	White (93.5%); Asian or Asian British (4.4%); Others (2.1%)
			Control group	201	201	56.7(8.4)	104(51.7%)	White (91%); Asian or Asian British (3.9%); Others (5.1%)
3-year incidence prediction of heart failure								
MEH-AlzEye	Model fine-tune and internal evaluation	TOPCON 3DOCT-2000SA	Heart failure group	4055	4055	76.1(11.5)	2009(49.5%)	White (42.3%); Asian or Asian British (23%); Black or Black British (8.3%); Others (13.8%); Unknown (12.6%)
			Control group	4055	4055	66(13.5)	2123(52.3%)	White (37.4%); Asian or Asian British (17.2%); Black or Black British (9.14%); Others (15.8%); Unknown (20.4%)
UK Biobank	External evaluation	TOPCON 3DOCT-1000-Mk2	Heart failure group	248	248	61.9(6.2)	151(60.8%)	White (87.5%); Asian or Asian British (4.4%); Black or Black British (2.8%); Others (5.3%)
			Control group	248	248	57.1(7.9)	102(41.1%)	White (89.5%); Asian or Asian British (3.2%); Black or Black British (2.8%); Others (4.5%)

*All tasks are rigorously balanced with the same number of individuals in disease group and control group. For each patient, we only include the retinal images (CFP and OCT) from the left eye in one visit, to avoid potential bias by inconsistent individual visits.

Supplementary table 3

Performance of DINOv2 and RETFound for ocular disease diagnostic tasks in the internal tests.											
Tasks	Dataset	Model-1	Model-2	P-value-AUROC	Mean-AUROC-model-1	Mean-AUROC-model-2	Model-1 (1.96× Std)	Model-2 (1.96× Std)	Model-1 95% confidence interval	Model-2 95% confidence interval	Better-model
Diabetic retinopathy (CFP)(Task I)	APTOS2019	DINOv2-Large	DINOv2-Base	2.51E-16	0.951758039	0.937574685	0.001941429	0.002422636	[0.94981661, 0.95369947]	[0.93515205, 0.93999732]	DINOv2-Large
		DINOv2-Large	DINOv2-Small	1.11E-22	0.951758039	0.932268575	0.001941429	0.002827619	[0.94981661, 0.95369947]	[0.92944096, 0.93509619]	DINOv2-Large
		DINOv2-Large	RETFound	2.42E-07	0.951758039	0.943696072	0.001941429	0.002226187	[0.94981661, 0.95369947]	[0.94146989, 0.94592226]	DINOv2-Large
		DINOv2-Base	DINOv2-Small	0.005733748	0.937574685	0.932268575	0.002422636	0.002827619	[0.93515205, 0.93999732]	[0.92944096, 0.93509619]	DINOv2-Base
		DINOv2-Base	RETFound	0.000339642	0.937574685	0.943696072	0.002422636	0.002226187	[0.93515205, 0.93999732]	[0.94146989, 0.94592226]	RETFound
		DINOv2-Small	RETFound	2.84E-09	0.932268575	0.943696072	0.002827619	0.002226187	[0.92944096, 0.93509619]	[0.94146989, 0.94592226]	RETFound
	MESSIDOR2	DINOv2-Large	DINOv2-Base	0.383806913	0.906098518	0.90346367	0.003896471	0.004452455	[0.90220205, 0.90999499]	[0.89901122, 0.90791612]	DINOv2-Large
		DINOv2-Large	DINOv2-Small	0.034270383	0.906098518	0.899625487	0.003896471	0.004499132	[0.90220205, 0.90999499]	[0.89512635, 0.90412462]	DINOv2-Large
		DINOv2-Large	RETFound	4.49E-11	0.906098518	0.883482609	0.003896471	0.005021125	[0.90220205, 0.90999499]	[0.87846148, 0.88850373]	DINOv2-Large
		DINOv2-Base	DINOv2-Small	0.236069011	0.90346367	0.899625487	0.004452455	0.004499132	[0.89901122, 0.90791612]	[0.89512635, 0.90412462]	DINOv2-Base
		DINOv2-Base	RETFound	2.16E-08	0.90346367	0.883482609	0.004452455	0.005021125	[0.89901122, 0.90791612]	[0.87846148, 0.88850373]	DINOv2-Base
		DINOv2-Small	RETFound	5.02E-06	0.899625487	0.883482609	0.004499132	0.005021125	[0.89512635, 0.90412462]	[0.87846148, 0.88850373]	DINOv2-Small
	IDRID	DINOv2-Large	DINOv2-Base	6.04E-05	0.850284623	0.809158203	0.014298591	0.01349778	[0.83598603, 0.86458321]	[0.79566042, 0.82265598]	DINOv2-Large
		DINOv2-Large	DINOv2-Small	0.001543489	0.850284623	0.818019833	0.014298591	0.013543131	[0.83598603, 0.86458321]	[0.80447670, 0.83156296]	DINOv2-Large
		DINOv2-Large	RETFound	0.006624832	0.850284623	0.822709719	0.014298591	0.013544815	[0.83598603, 0.86458321]	[0.80916490, 0.83625453]	DINOv2-Large
		DINOv2-Base	DINOv2-Small	0.364787101	0.809158203	0.818019833	0.01349778	0.013543131	[0.79566042, 0.82265598]	[0.80447670, 0.83156296]	DINOv2-Small
		DINOv2-Base	RETFound	0.166385546	0.809158203	0.822709719	0.01349778	0.013544815	[0.79566042, 0.82265598]	[0.80916490, 0.83625453]	RETFound
		DINOv2-Small	RETFound	0.631823072	0.818019833	0.822709719	0.013543131	0.013544815	[0.80447670, 0.83156296]	[0.80916490, 0.83625453]	RETFound
Glaucoma (CFP)(Task II)	Glaucoma_fundus	DINOv2-Large	DINOv2-Base	1.03E-05	0.946914943	0.958162834	0.003546903	0.003335342	[0.94336804, 0.95046185]	[0.95482749, 0.96149818]	DINOv2-Base
		DINOv2-Large	DINOv2-Small	3.85E-05	0.946914943	0.957531514	0.003546903	0.003440251	[0.94336804, 0.95046185]	[0.95409126, 0.96097176]	DINOv2-Small
		DINOv2-Large	RETFound	0.022536669	0.946914943	0.940399136	0.003546903	0.004274603	[0.94336804, 0.95046185]	[0.93612453, 0.94467374]	DINOv2-Large
		DINOv2-Base	DINOv2-Small	0.796491033	0.958162834	0.957531514	0.003335342	0.003440251	[0.95482749, 0.96149818]	[0.95409126, 0.96097176]	DINOv2-Base
		DINOv2-Base	RETFound	9.79E-10	0.958162834	0.940399136	0.003335342	0.004274603	[0.95482749, 0.96149818]	[0.93612453, 0.94467374]	DINOv2-Base
		DINOv2-Small	RETFound	4.93E-09	0.957531514	0.940399136	0.003440251	0.004274603	[0.95409126, 0.96097176]	[0.93612453, 0.94467374]	DINOv2-Small
	PAPILA	DINOv2-Large	DINOv2-Base	0.269252218	0.838752968	0.849455466	0.013039377	0.013728546	[0.82571359, 0.85179234]	[0.83572692, 0.86318401]	DINOv2-Base
		DINOv2-Large	DINOv2-Small	0.052761363	0.838752968	0.820000547	0.013039377	0.013629747	[0.82571359, 0.85179234]	[0.80637080, 0.83363029]	DINOv2-Large
		DINOv2-Large	RETFound	0.241387133	0.838752968	0.850771761	0.013039377	0.015227598	[0.82571359, 0.85179234]	[0.83554416, 0.86599936]	RETFound
		DINOv2-Base	DINOv2-Small	0.003200557	0.849455466	0.820000547	0.013728546	0.013629747	[0.83572692, 0.86318401]	[0.80637080, 0.83363029]	DINOv2-Base
		DINOv2-Base	RETFound	0.899990033	0.849455466	0.850771761	0.013728546	0.015227598	[0.83572692, 0.86318401]	[0.83554416, 0.86599936]	RETFound
		DINOv2-Small	RETFound	0.003547782	0.820000547	0.850771761	0.013629747	0.015227598	[0.80637080, 0.83363029]	[0.83554416, 0.86599936]	RETFound
Multi-category eye disease (CFP)(Task III)	JSIEC	DINOv2-Large	DINOv2-Base	0.18568681	0.996843185	0.997652517	0.001077547	0.000515348	[0.99576564, 0.99792073]	[0.99713717, 0.99816786]	DINOv2-Base
		DINOv2-Large	DINOv2-Small	0.075377629	0.996843185	0.995402408	0.001077547	0.001155234	[0.99576564, 0.99792073]	[0.99424717, 0.99655764]	DINOv2-Large
		DINOv2-Large	RETFound	5.59E-05	0.996843185	0.993725557	0.001077547	0.001019759	[0.99576564, 0.99792073]	[0.99270580, 0.99474532]	DINOv2-Large
		DINOv2-Base	DINOv2-Small	0.000602898	0.997652517	0.995402408	0.000515348	0.001155234	[0.99713717, 0.99816786]	[0.99424717, 0.99655764]	DINOv2-Base
		DINOv2-Base	RETFound	1.72E-10	0.997652517	0.993725557	0.000515348	0.001019759	[0.99713717, 0.99816786]	[0.99270580, 0.99474532]	DINOv2-Base
		DINOv2-Small	RETFound	0.034165721	0.995402408	0.993725557	0.001155234	0.001019759	[0.99424717, 0.99655764]	[0.99270580, 0.99474532]	DINOv2-Small
	Retina	DINOv2-Large	DINOv2-Base	0.005549269	0.892482517	0.873826264	0.009035907	0.00940261	[0.88344661, 0.90151842]	[0.86442365, 0.88322887]	DINOv2-Large
		DINOv2-Large	DINOv2-Small	0.186518366	0.892482517	0.883089748	0.009035907	0.010547188	[0.88344661, 0.90151842]	[0.87254256, 0.89363694]	DINOv2-Large
		DINOv2-Large	RETFound	1.36E-10	0.892482517	0.84566736	0.009035907	0.010078122	[0.88344661, 0.90151842]	[0.83558924, 0.85574548]	DINOv2-Large
		DINOv2-Base	DINOv2-Small	0.200303564	0.873826264	0.883089748	0.00940261	0.010547188	[0.86442365, 0.88322887]	[0.87254256, 0.89363694]	DINOv2-Small
		DINOv2-Base	RETFound	8.80E-05	0.873826264	0.84566736	0.00940261	0.010078122	[0.86442365, 0.88322887]	[0.83558924, 0.85574548]	DINOv2-Base
		DINOv2-Small	RETFound	1.11E-06	0.883089748	0.84566736	0.010547188	0.010078122	[0.87254256, 0.89363694]	[0.83558924, 0.85574548]	DINOv2-Small
Multi-category eye disease (OCT)(Task IV)	OCTID	DINOv2-Large	DINOv2-Base	0.71595887	0.998647898	0.998513971	0.000465598	0.000549698	[0.99818230, 0.99911350]	[0.99796427, 0.99906367]	DINOv2-Large
		DINOv2-Large	DINOv2-Small	0.077988193	0.998647898	0.997921025	0.000465598	0.00065564	[0.99818230, 0.99911350]	[0.99726538, 0.99857666]	DINOv2-Large
		DINOv2-Large	RETFound	0.138391054	0.998647898	0.999080811	0.000465598	0.000329343	[0.99818230, 0.99911350]	[0.99875147, 0.99941015]	RETFound
		DINOv2-Base	DINOv2-Small	0.175903293	0.998513971	0.997921025	0.000549698	0.00065564	[0.99796427, 0.99906367]	[0.99726538, 0.99857666]	DINOv2-Base
		DINOv2-Base	RETFound	0.084517912	0.998513971	0.999080811	0.000549698	0.000329343	[0.99796427, 0.99906367]	[0.99875147, 0.99941015]	RETFound
		DINOv2-Small	RETFound	0.002230004	0.997921025	0.999080811	0.00065564	0.000329343	[0.99726538, 0.99857666]	[0.99875147, 0.99941015]	RETFound

Supplementary table 4

Performance of DINOv2 and RETFound models for DR classification tasks in the respective external tests sets. (AUROC)										
Dataset	Model-1	Model-2	P-value-AUROC	Mean-AUROC-model-1	Mean-AUROC-model-2	Model-1 (1.96× Std)	Model-2 (1.96× Std)	Model-1 95% confidence interval	Model-2 95% confidence interval	Better-model
APTOS2019->IDRID	DINOv2-Large	DINOv2-Base	7.54E-08	0.814894712	0.751048075	0.016168944	0.015495102	[0.79872577, 0.83106366]	[0.73555297, 0.76654318]	DINOv2-Large
	DINOv2-Large	DINOv2-Small	9.05E-05	0.814894712	0.769126873	0.016168944	0.01556535	[0.79872577, 0.83106366]	[0.75356152, 0.78469222]	DINOv2-Large
	DINOv2-Large	RetFound	0.157984523	0.814894712	0.799306837	0.016168944	0.014258117	[0.79872577, 0.83106366]	[0.78504872, 0.81356495]	DINOv2-Large
	DINOv2-Base	DINOv2-Small	0.10825856	0.751048075	0.769126873	0.015495102	0.01556535	[0.73555297, 0.76654318]	[0.75356152, 0.78469222]	DINOv2-Small
	DINOv2-Base	RetFound	1.20E-05	0.751048075	0.799306837	0.015495102	0.014258117	[0.73555297, 0.76654318]	[0.78504872, 0.81356495]	RetFound
	DINOv2-Small	RetFound	0.005578032	0.769126873	0.799306837	0.01556535	0.014258117	[0.75356152, 0.78469222]	[0.78504872, 0.81356495]	RetFound
APTOS2019->MESSIDOR2	DINOv2-Large	DINOv2-Base	1.11E-05	0.817161899	0.798800213	0.005531654	0.005750017	[0.81163025, 0.82269355]	[0.79305020, 0.80455023]	DINOv2-Large
	DINOv2-Large	DINOv2-Small	4.21E-07	0.817161899	0.795489543	0.005531654	0.005937929	[0.81163025, 0.82269355]	[0.78955161, 0.80142747]	DINOv2-Large
	DINOv2-Large	RetFound	8.98E-43	0.817161899	0.725082724	0.005531654	0.008538679	[0.81163025, 0.82269355]	[0.71654404, 0.73362140]	DINOv2-Large
	DINOv2-Base	DINOv2-Small	0.433367533	0.798800213	0.795489543	0.005750017	0.005937929	[0.79305020, 0.80455023]	[0.78955161, 0.80142747]	DINOv2-Base
	DINOv2-Base	RetFound	1.62E-31	0.798800213	0.725082724	0.005750017	0.008538679	[0.79305020, 0.80455023]	[0.71654404, 0.73362140]	DINOv2-Base
	DINOv2-Small	RetFound	3.66E-29	0.795489543	0.725082724	0.005937929	0.008538679	[0.78955161, 0.80142747]	[0.71654404, 0.73362140]	DINOv2-Small
IDRID->APTOS2019	DINOv2-Large	DINOv2-Base	7.38E-42	0.782651939	0.730185982	0.004206208	0.004135534	[0.77844573, 0.78685815]	[0.72605045, 0.73432152]	DINOv2-Large
	DINOv2-Large	DINOv2-Small	9.66E-17	0.782651939	0.807914771	0.004206208	0.003449966	[0.77844573, 0.78685815]	[0.80446481, 0.81136474]	DINOv2-Small
	DINOv2-Large	RetFound	8.93E-20	0.782651939	0.751758998	0.004206208	0.004224742	[0.77844573, 0.78685815]	[0.74753426, 0.75598374]	DINOv2-Large
	DINOv2-Base	DINOv2-Small	1.77E-71	0.730185982	0.807914771	0.004135534	0.003449966	[0.72605045, 0.73432152]	[0.80446481, 0.81136474]	DINOv2-Small
	DINOv2-Base	RetFound	1.62E-11	0.730185982	0.751758998	0.004135534	0.004224742	[0.72605045, 0.73432152]	[0.74753426, 0.75598374]	RetFound
	DINOv2-Small	RetFound	6.31E-50	0.807914771	0.751758998	0.003449966	0.004224742	[0.80446481, 0.81136474]	[0.74753426, 0.75598374]	DINOv2-Small
IDRID->MESSIDOR2	DINOv2-Large	DINOv2-Base	4.77E-17	0.792406649	0.729153167	0.007402616	0.011242586	[0.78500403, 0.79980926]	[0.71791058, 0.74039575]	DINOv2-Large
	DINOv2-Large	DINOv2-Small	0.73799821	0.792406649	0.790818807	0.007402616	0.005614187	[0.78500403, 0.79980926]	[0.78520462, 0.79643299]	DINOv2-Large
	DINOv2-Large	RetFound	0.02467032	0.792406649	0.803736121	0.007402616	0.006435731	[0.78500403, 0.79980926]	[0.79730039, 0.81017185]	RetFound
	DINOv2-Base	DINOv2-Small	3.27E-18	0.729153167	0.790818807	0.011242586	0.005614187	[0.71791058, 0.74039575]	[0.78520462, 0.79643299]	DINOv2-Small
	DINOv2-Base	RetFound	4.00E-23	0.729153167	0.803736121	0.011242586	0.006435731	[0.71791058, 0.74039575]	[0.79730039, 0.81017185]	RetFound
	DINOv2-Small	RetFound	0.003403927	0.790818807	0.803736121	0.005614187	0.006435731	[0.78520462, 0.79643299]	[0.79730039, 0.81017185]	RetFound
MESSIDOR2->APTOS2019	DINOv2-Large	DINOv2-Base	2.39E-16	0.749581951	0.770191173	0.002942438	0.003414495	[0.74663951, 0.75252439]	[0.76677668, 0.77360567]	DINOv2-Base
	DINOv2-Large	DINOv2-Small	8.74E-15	0.749581951	0.730548593	0.002942438	0.003328935	[0.74663951, 0.75252439]	[0.72721966, 0.73387753]	DINOv2-Large
	DINOv2-Large	RetFound	3.04E-67	0.749581951	0.806689273	0.002942438	0.003011751	[0.74663951, 0.75252439]	[0.80367752, 0.80970102]	RetFound
	DINOv2-Base	DINOv2-Small	2.02E-38	0.770191173	0.730548593	0.003414495	0.003328935	[0.76677668, 0.77360567]	[0.72721966, 0.73387753]	DINOv2-Base
	DINOv2-Base	RetFound	1.19E-36	0.770191173	0.806689273	0.003414495	0.003011751	[0.76677668, 0.77360567]	[0.80367752, 0.80970102]	RetFound
	DINOv2-Small	RetFound	5.95E-83	0.730548593	0.806689273	0.003328935	0.003011751	[0.72721966, 0.73387753]	[0.80367752, 0.80970102]	RetFound
MESSIDOR2->IDRID	DINOv2-Large	DINOv2-Base	0.344510419	0.74802221	0.756723537	0.012619461	0.012833378	[0.73540275, 0.76064167]	[0.74389016, 0.76955692]	DINOv2-Base
	DINOv2-Large	DINOv2-Small	5.16E-05	0.74802221	0.711291715	0.012619461	0.011971661	[0.73540275, 0.76064167]	[0.69932005, 0.72326338]	DINOv2-Large
	DINOv2-Large	RetFound	0.028550467	0.74802221	0.769332783	0.012619461	0.014118253	[0.73540275, 0.76064167]	[0.75521453, 0.78345104]	RetFound
	DINOv2-Base	DINOv2-Small	8.95E-07	0.756723537	0.711291715	0.012833378	0.011971661	[0.74389016, 0.76955692]	[0.69932005, 0.72326338]	DINOv2-Base
	DINOv2-Base	RetFound	0.196712808	0.756723537	0.769332783	0.012833378	0.014118253	[0.74389016, 0.76955692]	[0.75521453, 0.78345104]	RetFound
	DINOv2-Small	RetFound	4.30E-09	0.711291715	0.769332783	0.011971661	0.014118253	[0.69932005, 0.72326338]	[0.75521453, 0.78345104]	RetFound

Performance of DINOv2 and RETFound models for Glaucoma classification tasks in the respective external tests sets. (AUROC)										
Dataset	Model-1	Model-2	P-value-AUROC	Mean-AUROC-model-1	Mean-AUROC-model-2	Model-1 (1.96× Std)	Model-2 (1.96× Std)	Model-1 95% confidence interval	Model-2 95% confidence interval	Better-model
Glaucoma_fundus->PAPILA	DINOv2-Large	DINOv2-Base	0.083225738	0.62468719	0.592960098	0.028381566	0.021683442	[0.59630562, 0.65306876]	[0.57127666, 0.61464354]	DINOv2-Large
	DINOv2-Large	DINOv2-Small	0.002095539	0.62468719	0.564190431	0.028381566	0.025320886	[0.59630562, 0.65306876]	[0.53886955, 0.58951132]	DINOv2-Large
	DINOv2-Large	RetFound	0.000214577	0.62468719	0.558380264	0.028381566	0.019549439	[0.59630562, 0.65306876]	[0.53883082, 0.57792970]	DINOv2-Large
	DINOv2-Base	DINOv2-Small	0.092314952	0.592960098	0.564190431	0.021683442	0.025320886	[0.57127666, 0.61464354]	[0.53886955, 0.58951132]	DINOv2-Base
	DINOv2-Base	RetFound	0.021277032	0.592960098	0.558380264	0.021683442	0.019549439	[0.57127666, 0.61464354]	[0.53883082, 0.57792970]	DINOv2-Base
	DINOv2-Small	RetFound	0.72222735	0.564190431	0.558380264	0.025320886	0.019549439	[0.53886955, 0.58951132]	[0.53883082, 0.57792970]	DINOv2-Small
PAPILA->Glaucoma_fundus	DINOv2-Large	DINOv2-Base	8.47E-05	0.634425018	0.60998002	0.008315351	0.008564431	[0.62610967, 0.64274037]	[0.60141559, 0.61854445]	DINOv2-Large
	DINOv2-Large	DINOv2-Small	8.57E-16	0.634425018	0.689266211	0.008315351	0.009017336	[0.62610967, 0.64274037]	[0.68024887, 0.69828355]	DINOv2-Small

	DINOv2-Large	RetFound	6.39E-16	0.634425018	0.686236092	0.008315351	0.007984311	[0.62610967, 0.64274037]	[0.67825178, 0.69422040]	RetFound
	DINOv2-Base	DINOv2-Small	8.50E-27	0.60998002	0.689266211	0.008564431	0.009017336	[0.60141559, 0.61854445]	[0.68024887, 0.69828355]	DINOv2-Small
	DINOv2-Base	RetFound	1.28E-27	0.60998002	0.686236092	0.008564431	0.007984311	[0.60141559, 0.61854445]	[0.67825178, 0.69422040]	RetFound
	DINOv2-Small	RetFound	0.622484758	0.689266211	0.686236092	0.009017336	0.007984311	[0.68024887, 0.69828355]	[0.67825178, 0.69422040]	DINOv2-Small

Performance of DINOv2 and RETFound models for DR classification tasks in the respective external tests sets. (Accuracy)										
Dataset	Model-1	Model-2	P-value-Accuracy	Mean-Accuracy-model-1	Mean-Accuracy-model-2	Model-1 (1.96× Std)	Model-2 (1.96× Std)	Model-1 95% confidence interval	Model-2 95% confidence interval	Better-model
APTOS2019->IDRID	DINOv2-Large	DINOv2-Base	6.91E-07	0.4845	0.4025	0.021788936	0.022519332	[0.46271106, 0.50628894]	[0.37998067, 0.42501933]	DINOv2-Large
	DINOv2-Large	DINOv2-Small	2.36E-05	0.4845	0.417	0.021788936	0.021408282	[0.46271106, 0.50628894]	[0.39559172, 0.43840828]	DINOv2-Large
	DINOv2-Large	RetFound	4.03E-05	0.4845	0.415	0.021788936	0.024025197	[0.46271106, 0.50628894]	[0.39097480, 0.43902520]	DINOv2-Large
	DINOv2-Base	DINOv2-Small	0.361479466	0.4025	0.417	0.022519332	0.021408282	[0.37998067, 0.42501933]	[0.39559172, 0.43840828]	DINOv2-Small
	DINOv2-Base	RetFound	0.457745734	0.4025	0.415	0.022519332	0.024025197	[0.37998067, 0.42501933]	[0.39097480, 0.43902520]	RetFound
	DINOv2-Small	RetFound	0.903167948	0.417	0.415	0.021408282	0.024025197	[0.39559172, 0.43840828]	[0.39097480, 0.43902520]	DINOv2-Small
APTOS2019->MESSIDOR2	DINOv2-Large	DINOv2-Base	0.788157988	0.672095238	0.670190476	0.010225032	0.009379058	[0.66187021, 0.68232027]	[0.66081142, 0.67956953]	DINOv2-Large
	DINOv2-Large	DINOv2-Small	6.75E-08	0.672095238	0.632285714	0.010225032	0.009428613	[0.66187021, 0.68232027]	[0.62285710, 0.64171433]	DINOv2-Large
	DINOv2-Large	RetFound	9.71E-10	0.672095238	0.625904762	0.010225032	0.009701589	[0.66187021, 0.68232027]	[0.61620317, 0.63560635]	DINOv2-Large
	DINOv2-Base	DINOv2-Small	7.59E-08	0.670190476	0.632285714	0.009379058	0.009428613	[0.66081142, 0.67956953]	[0.62285710, 0.64171433]	DINOv2-Base
	DINOv2-Base	RetFound	9.23E-10	0.670190476	0.625904762	0.009379058	0.009701589	[0.66081142, 0.67956953]	[0.61620317, 0.63560635]	DINOv2-Base
	DINOv2-Small	RetFound	0.356366965	0.632285714	0.625904762	0.009428613	0.009701589	[0.62285710, 0.64171433]	[0.61620317, 0.63560635]	DINOv2-Small
IDRID->APTOS2019	DINOv2-Large	DINOv2-Base	5.85E-66	0.565227273	0.450272727	0.006307787	0.005903949	[0.55891949, 0.57153506]	[0.44436878, 0.45617668]	DINOv2-Large
	DINOv2-Large	DINOv2-Small	3.15E-12	0.565227273	0.599227273	0.006307787	0.006373135	[0.55891949, 0.57153506]	[0.59285414, 0.60560041]	DINOv2-Small
	DINOv2-Large	RetFound	0.028023154	0.565227273	0.555318182	0.006307787	0.006100613	[0.55891949, 0.57153506]	[0.54921757, 0.56141880]	DINOv2-Large
	DINOv2-Base	DINOv2-Small	9.60E-84	0.450272727	0.599227273	0.005903949	0.006373135	[0.44436878, 0.45617668]	[0.59285414, 0.60560041]	DINOv2-Small
	DINOv2-Base	RetFound	3.39E-61	0.450272727	0.555318182	0.005903949	0.006100613	[0.44436878, 0.45617668]	[0.54921757, 0.56141880]	RetFound
	DINOv2-Small	RetFound	1.32E-18	0.599227273	0.555318182	0.006373135	0.006100613	[0.59285414, 0.60560041]	[0.54921757, 0.56141880]	DINOv2-Small
IDRID->MESSIDOR2	DINOv2-Large	DINOv2-Base	0.00260899	0.565333333	0.543904762	0.009865063	0.009613448	[0.55546827, 0.57519840]	[0.53429131, 0.55351821]	DINOv2-Large
	DINOv2-Large	DINOv2-Small	0.059577698	0.565333333	0.578857143	0.009865063	0.009918649	[0.55546827, 0.57519840]	[0.56893849, 0.58877579]	DINOv2-Small
	DINOv2-Large	RetFound	0.007553065	0.565333333	0.585428571	0.009865063	0.010752536	[0.55546827, 0.57519840]	[0.57467604, 0.59618111]	RetFound
	DINOv2-Base	DINOv2-Small	1.52E-06	0.543904762	0.578857143	0.009613448	0.009918649	[0.53429131, 0.55351821]	[0.56893849, 0.58877579]	DINOv2-Small
	DINOv2-Base	RetFound	5.73E-08	0.543904762	0.585428571	0.009613448	0.010752536	[0.53429131, 0.55351821]	[0.57467604, 0.59618111]	RetFound
	DINOv2-Small	RetFound	0.379674564	0.578857143	0.585428571	0.009918649	0.010752536	[0.56893849, 0.58877579]	[0.57467604, 0.59618111]	RetFound
MESSIDOR2->APTOS2019	DINOv2-Large	DINOv2-Base	4.47E-27	0.412363636	0.464954546	0.005558795	0.006013571	[0.40680484, 0.41792243]	[0.45894097, 0.47096812]	DINOv2-Base
	DINOv2-Large	DINOv2-Small	8.80E-22	0.412363636	0.367090909	0.005558795	0.006013338	[0.40680484, 0.41792243]	[0.36107757, 0.37310425]	DINOv2-Large
	DINOv2-Large	RetFound	8.60E-92	0.412363636	0.577227273	0.005558795	0.006599868	[0.40680484, 0.41792243]	[0.57062740, 0.58382714]	RetFound
	DINOv2-Base	DINOv2-Small	1.31E-56	0.464954546	0.367090909	0.006013571	0.006013338	[0.45894097, 0.47096812]	[0.36107757, 0.37310425]	DINOv2-Base
	DINOv2-Base	RetFound	3.07E-62	0.464954546	0.577227273	0.006013571	0.006599868	[0.45894097, 0.47096812]	[0.57062740, 0.58382714]	RetFound
	DINOv2-Small	RetFound	7.07E-108	0.367090909	0.577227273	0.006013338	0.006599868	[0.36107757, 0.37310425]	[0.57062740, 0.58382714]	RetFound
MESSIDOR2->IDRID	DINOv2-Large	DINOv2-Base	2.03E-06	0.345	0.422	0.020683678	0.022859029	[0.32431632, 0.36568368]	[0.39914097, 0.44485903]	DINOv2-Base
	DINOv2-Large	DINOv2-Small	0.392798625	0.345	0.358	0.020683678	0.021385612	[0.32431632, 0.36568368]	[0.33661439, 0.37938561]	DINOv2-Small
	DINOv2-Large	RetFound	0.004704222	0.345	0.3885	0.020683678	0.021482243	[0.32431632, 0.36568368]	[0.36701776, 0.40998224]	RetFound
	DINOv2-Base	DINOv2-Small	8.69E-05	0.422	0.358	0.022859029	0.021385612	[0.39914097, 0.44485903]	[0.33661439, 0.37938561]	DINOv2-Base
	DINOv2-Base	RetFound	0.03761029	0.422	0.3885	0.022859029	0.021482243	[0.39914097, 0.44485903]	[0.36701776, 0.40998224]	DINOv2-Base
	DINOv2-Small	RetFound	0.049985744	0.358	0.3885	0.021385612	0.021482243	[0.33661439, 0.37938561]	[0.36701776, 0.40998224]	RetFound

Performance of DINOv2 and RETFound models for Glaucoma classification tasks in the respective external tests sets. (Accuracy)										
Dataset	Model-1	Model-2	P-value-Accuracy	Mean-Accuracy-model-1	Mean-Accuracy-model-2	Model-1 (1.96× Std)	Model-2 (1.96× Std)	Model-1 95% confidence interval	Model-2 95% confidence interval	Better-model
Glaucoma_fundus->PAPILA	DINOv2-Large	DINOv2-Base	3.69E-05	0.353684211	0.261578948	0.029400594	0.031049836	[0.32428362, 0.38308480]	[0.23052911, 0.29262878]	DINOv2-Large
	DINOv2-Large	DINOv2-Small	0.009747866	0.353684211	0.296842105	0.029400594	0.030948063	[0.32428362, 0.38308480]	[0.26589404, 0.32779017]	DINOv2-Large
	DINOv2-Large	RetFound	3.49E-06	0.353684211	0.25	0.029400594	0.030768845	[0.32428362, 0.38308480]	[0.21923115, 0.28076885]	DINOv2-Large
	DINOv2-Base	DINOv2-Small	0.11648965	0.261578948	0.296842105	0.031049836	0.030948063	[0.23052911, 0.29262878]	[0.26589404, 0.32779017]	DINOv2-Small

	DINOV2-Base	RetFound	0.604216744	0.261578948	0.25	0.031049836	0.030768845	[0.23052911, 0.29262878]	[0.21923115, 0.28076885]	DINOV2-Base
	DINOV2-Small	RetFound	0.036659659	0.296842105	0.25	0.030948063	0.030768845	[0.26589404, 0.32779017]	[0.21923115, 0.28076885]	DINOV2-Small
PAPILA->Glaucoma_fundus	DINOV2-Large	DINOV2-Base	2.43E-05	0.543763441	0.513333333	0.009808883	0.009700175	[0.53395456, 0.55357232]	[0.50363316, 0.52303351]	DINOV2-Large
	DINOV2-Large	DINOV2-Small	0.790197901	0.543763441	0.545698925	0.009808883	0.010322015	[0.53395456, 0.55357232]	[0.53537691, 0.55602094]	DINOV2-Small
	DINOV2-Large	RetFound	2.26E-06	0.543763441	0.507634409	0.009808883	0.01072666	[0.53395456, 0.55357232]	[0.49690775, 0.51836107]	DINOV2-Large
	DINOV2-Base	DINOV2-Small	1.27E-05	0.513333333	0.545698925	0.009700175	0.010322015	[0.50363316, 0.52303351]	[0.53537691, 0.55602094]	DINOV2-Small
	DINOV2-Base	RetFound	0.440826928	0.513333333	0.507634409	0.009700175	0.01072666	[0.50363316, 0.52303351]	[0.49690775, 0.51836107]	DINOV2-Base
	DINOV2-Small	RetFound	1.19E-06	0.545698925	0.507634409	0.010322015	0.01072666	[0.53537691, 0.55602094]	[0.49690775, 0.51836107]	DINOV2-Small

Performance of DINOV2 and RETFound models for DR classification tasks in the respective external tests sets. (Kappa)										
Dataset	Model-1	Model-2	P-value-Kappa	Mean-Kappa-model-1	Mean-Kappa-model-2	Model-1 (1.96× Std)	Model-2 (1.96× Std)	Model-1 95% confidence interval	Model-2 95% confidence interval	Better-model
APTOS2019->IDRID	DINOV2-Large	DINOV2-Base	1.90E-07	0.306296874	0.207026347	0.026410271	0.024517463	[0.27988660, 0.33270715]	[0.18250888, 0.23154381]	DINOV2-Large
	DINOV2-Large	DINOV2-Small	9.60E-06	0.306296874	0.219666033	0.026410271	0.026438811	[0.27988660, 0.33270715]	[0.19322722, 0.24610484]	DINOV2-Large
	DINOV2-Large	RetFound	8.05E-06	0.306296874	0.21767796	0.026410271	0.027162608	[0.27988660, 0.33270715]	[0.19051535, 0.24484057]	DINOV2-Large
	DINOV2-Base	DINOV2-Small	0.492842378	0.207026347	0.219666033	0.024517463	0.026438811	[0.18250888, 0.23154381]	[0.19322722, 0.24610484]	DINOV2-Small
	DINOV2-Base	RetFound	0.568950316	0.207026347	0.21767796	0.024517463	0.027162608	[0.18250888, 0.23154381]	[0.19051535, 0.24484057]	RetFound
	DINOV2-Small	RetFound	0.918226785	0.219666033	0.21767796	0.026438811	0.027162608	[0.19322722, 0.24610484]	[0.19051535, 0.24484057]	DINOV2-Small
APTOS2019->MESSIDOR2	DINOV2-Large	DINOV2-Base	0.776390524	0.362499679	0.365509903	0.015315765	0.013991577	[0.34718391, 0.37781544]	[0.35151833, 0.37950148]	DINOV2-Base
	DINOV2-Large	DINOV2-Small	7.71E-10	0.362499679	0.296967512	0.015315765	0.012652363	[0.34718391, 0.37781544]	[0.28431515, 0.30961988]	DINOV2-Large
	DINOV2-Large	RetFound	4.46E-15	0.362499679	0.267432397	0.015315765	0.015671044	[0.34718391, 0.37781544]	[0.25176135, 0.28310344]	DINOV2-Large
	DINOV2-Base	DINOV2-Small	1.93E-11	0.365509903	0.296967512	0.013991577	0.012652363	[0.35151833, 0.37950148]	[0.28431515, 0.30961988]	DINOV2-Base
	DINOV2-Base	RetFound	7.05E-17	0.365509903	0.267432397	0.013991577	0.015671044	[0.35151833, 0.37950148]	[0.25176135, 0.28310344]	DINOV2-Base
	DINOV2-Small	RetFound	0.004493466	0.296967512	0.267432397	0.012652363	0.015671044	[0.28431515, 0.30961988]	[0.25176135, 0.28310344]	DINOV2-Small
IDRID->APTOS2019	DINOV2-Large	DINOV2-Base	1.24E-61	0.385961631	0.256800082	0.007666724	0.006980128	[0.37829491, 0.39362836]	[0.24981995, 0.26378021]	DINOV2-Large
	DINOV2-Large	DINOV2-Small	5.20E-07	0.385961631	0.415484834	0.007666724	0.008096504	[0.37829491, 0.39362836]	[0.40738833, 0.42358134]	DINOV2-Small
	DINOV2-Large	RetFound	8.35E-13	0.385961631	0.342692081	0.007666724	0.007998584	[0.37829491, 0.39362836]	[0.33469350, 0.35069067]	DINOV2-Large
	DINOV2-Base	DINOV2-Small	1.98E-73	0.256800082	0.415484834	0.006980128	0.008096504	[0.24981995, 0.26378021]	[0.40738833, 0.42358134]	DINOV2-Small
	DINOV2-Base	RetFound	4.26E-37	0.256800082	0.342692081	0.006980128	0.007998584	[0.24981995, 0.26378021]	[0.33469350, 0.35069067]	RetFound
	DINOV2-Small	RetFound	6.40E-27	0.415484834	0.342692081	0.008096504	0.007998584	[0.40738833, 0.42358134]	[0.33469350, 0.35069067]	DINOV2-Small
IDRID->MESSIDOR2	DINOV2-Large	DINOV2-Base	0.007391012	0.301641174	0.276810684	0.013363929	0.012030122	[0.28827725, 0.31500510]	[0.26478056, 0.28884081]	DINOV2-Large
	DINOV2-Large	DINOV2-Small	0.014597017	0.301641174	0.276265914	0.013363929	0.015128558	[0.28827725, 0.31500510]	[0.26113736, 0.29139447]	DINOV2-Large
	DINOV2-Large	RetFound	0.000960211	0.301641174	0.266825553	0.013363929	0.015355034	[0.28827725, 0.31500510]	[0.25147052, 0.28218059]	DINOV2-Large
	DINOV2-Base	DINOV2-Small	0.956001548	0.276810684	0.276265914	0.012030122	0.015128558	[0.26478056, 0.28884081]	[0.26113736, 0.29139447]	DINOV2-Base
	DINOV2-Base	RetFound	0.316939368	0.276810684	0.266825553	0.012030122	0.015355034	[0.26478056, 0.28884081]	[0.25147052, 0.28218059]	DINOV2-Base
	DINOV2-Small	RetFound	0.391718464	0.276265914	0.266825553	0.015128558	0.015355034	[0.26113736, 0.29139447]	[0.25147052, 0.28218059]	DINOV2-Small
MESSIDOR2->APTOS2019	DINOV2-Large	DINOV2-Base	9.90E-24	0.23222036	0.286052429	0.006168354	0.00680714	[0.22605201, 0.23838871]	[0.27924529, 0.29285957]	DINOV2-Base
	DINOV2-Large	DINOV2-Small	1.80E-27	0.23222036	0.174641595	0.006168354	0.006380734	[0.22605201, 0.23838871]	[0.16826086, 0.18102233]	DINOV2-Large
	DINOV2-Large	RetFound	9.35E-80	0.23222036	0.39888877	0.006168354	0.008210674	[0.22605201, 0.23838871]	[0.39067810, 0.40709944]	RetFound
	DINOV2-Base	DINOV2-Small	6.33E-59	0.286052429	0.174641595	0.00680714	0.006380734	[0.27924529, 0.29285957]	[0.16826086, 0.18102233]	DINOV2-Base
	DINOV2-Base	RetFound	1.61E-51	0.286052429	0.39888877	0.00680714	0.008210674	[0.27924529, 0.29285957]	[0.39067810, 0.40709944]	RetFound
	DINOV2-Small	RetFound	4.74E-101	0.174641595	0.39888877	0.006380734	0.008210674	[0.16826086, 0.18102233]	[0.39067810, 0.40709944]	RetFound
MESSIDOR2->IDRID	DINOV2-Large	DINOV2-Base	6.90E-06	0.13534334	0.222828655	0.023760674	0.028512162	[0.11158267, 0.15910401]	[0.19431649, 0.25134082]	DINOV2-Base
	DINOV2-Large	DINOV2-Small	0.464140016	0.13534334	0.148525749	0.023760674	0.026006435	[0.11158267, 0.15910401]	[0.12251931, 0.17453218]	DINOV2-Small
	DINOV2-Large	RetFound	0.262769918	0.13534334	0.15662336	0.023760674	0.02854281	[0.11158267, 0.15910401]	[0.12808055, 0.18516617]	RetFound
	DINOV2-Base	DINOV2-Small	0.000212419	0.222828655	0.148525749	0.028512162	0.026006435	[0.19431649, 0.25134082]	[0.12251931, 0.17453218]	DINOV2-Base
	DINOV2-Base	RetFound	0.001516293	0.222828655	0.15662336	0.028512162	0.02854281	[0.19431649, 0.25134082]	[0.12808055, 0.18516617]	DINOV2-Base
	DINOV2-Small	RetFound	0.681497309	0.148525749	0.15662336	0.026006435	0.02854281	[0.12251931, 0.17453218]	[0.12808055, 0.18516617]	RetFound

Performance of DINOV2 and RETFound models for Glaucoma classification tasks in the respective external tests sets. (Kappa)										
Dataset	Model-1	Model-2	P-value-Kappa	Mean-Kappa-model-1	Mean-Kappa-model-2	Model-1 (1.96× Std)	Model-2 (1.96× Std)	Model-1 95% confidence interval	Model-2 95% confidence interval	Better-model

Glaucoma_fundus->PAPILA	DINOV2-Large	DINOV2-Base	7.45E-05	0.060401358	0.020407359	0.017998387	0.007162807	[0.04240297, 0.07839974]	[0.01324455, 0.02757017]	DINOV2-Large
	DINOV2-Large	DINOV2-Small	1.32E-05	0.060401358	-0.00261723	0.017998387	0.020976805	[0.04240297, 0.07839974]	[-0.02359403, 0.01835958]	DINOV2-Large
	DINOV2-Large	RetFound	6.13E-06	0.060401358	0.016228597	0.017998387	0.004809331	[0.04240297, 0.07839974]	[0.01141927, 0.02103793]	DINOV2-Large
	DINOV2-Base	DINOV2-Small	0.043090554	0.020407359	-0.00261723	0.007162807	0.020976805	[0.01324455, 0.02757017]	[-0.02359403, 0.01835958]	DINOV2-Base
	DINOV2-Base	RetFound	0.343613813	0.020407359	0.016228597	0.007162807	0.004809331	[0.01324455, 0.02757017]	[0.01141927, 0.02103793]	DINOV2-Base
	DINOV2-Small	RetFound	0.087660715	-0.00261723	0.016228597	0.020976805	0.004809331	[-0.02359403, 0.01835958]	[0.01141927, 0.02103793]	RetFound
PAPILA->Glaucoma_fundus	DINOV2-Large	DINOV2-Base	1.62E-07	0.240681342	0.190402866	0.012196454	0.013427262	[0.22848489, 0.25287780]	[0.17697560, 0.20383013]	DINOV2-Large
	DINOV2-Large	DINOV2-Small	2.45E-06	0.240681342	0.197612647	0.012196454	0.012395832	[0.22848489, 0.25287780]	[0.18521682, 0.21000848]	DINOV2-Large
	DINOV2-Large	RetFound	1.23E-84	0.240681342	0.017166361	0.012196454	0.004135942	[0.22848489, 0.25287780]	[0.01303042, 0.02130230]	DINOV2-Large
	DINOV2-Base	DINOV2-Small	0.440276802	0.190402866	0.197612647	0.013427262	0.012395832	[0.17697560, 0.20383013]	[0.18521682, 0.21000848]	DINOV2-Small
	DINOV2-Base	RetFound	5.69E-61	0.190402866	0.017166361	0.013427262	0.004135942	[0.17697560, 0.20383013]	[0.01303042, 0.02130230]	DINOV2-Base
	DINOV2-Small	RetFound	1.87E-68	0.197612647	0.017166361	0.012395832	0.004135942	[0.18521682, 0.21000848]	[0.01303042, 0.02130230]	DINOV2-Small

Performance of DINOV2 and RETFound models for DR classification tasks in the respective external tests sets. (F1-Score)										
Dataset	Model-1	Model-2	P-value-F1-Score	Mean-F1-Score-model-1	Mean-F1-Score-model-2	Model-1 (1.96× Std)	Model-2 (1.96× Std)	Model-1 95% confidence interval	Model-2 95% confidence interval	Better-model
APTOS2019->IDRID	DINOV2-Large	DINOV2-Base	1.30E-07	0.402438421	0.311559914	0.023881267	0.022066465	[0.37855715, 0.42631969]	[0.28949345, 0.33362638]	DINOV2-Large
	DINOV2-Large	DINOV2-Small	0.000253922	0.402438421	0.341127672	0.023881267	0.021678433	[0.37855715, 0.42631969]	[0.31944924, 0.36280611]	DINOV2-Large
	DINOV2-Large	RetFound	6.03E-08	0.402438421	0.307648176	0.023881267	0.02275206	[0.37855715, 0.42631969]	[0.28489612, 0.33040024]	DINOV2-Large
	DINOV2-Base	DINOV2-Small	0.062477965	0.311559914	0.341127672	0.022066465	0.021678433	[0.28949345, 0.33362638]	[0.31944924, 0.36280611]	DINOV2-Small
	DINOV2-Base	RetFound	0.80910946	0.311559914	0.307648176	0.022066465	0.02275206	[0.28949345, 0.33362638]	[0.28489612, 0.33040024]	DINOV2-Base
	DINOV2-Small	RetFound	0.038071845	0.341127672	0.307648176	0.021678433	0.02275206	[0.31944924, 0.36280611]	[0.28489612, 0.33040024]	DINOV2-Small
APTOS2019->MESSIDOR2	DINOV2-Large	DINOV2-Base	0.425012706	0.415469744	0.426281952	0.019937076	0.017471994	[0.39553267, 0.43540682]	[0.40880996, 0.44375395]	DINOV2-Base
	DINOV2-Large	DINOV2-Small	0.12557269	0.415469744	0.394574958	0.019937076	0.017643336	[0.39553267, 0.43540682]	[0.37693162, 0.41221829]	DINOV2-Large
	DINOV2-Large	RetFound	1.46E-06	0.415469744	0.351253089	0.019937076	0.015629003	[0.39553267, 0.43540682]	[0.33562409, 0.36688209]	DINOV2-Large
	DINOV2-Base	DINOV2-Small	0.013130835	0.426281952	0.394574958	0.017471994	0.017643336	[0.40880996, 0.44375395]	[0.37693162, 0.41221829]	DINOV2-Base
	DINOV2-Base	RetFound	2.18E-09	0.426281952	0.351253089	0.017471994	0.015629003	[0.40880996, 0.44375395]	[0.33562409, 0.36688209]	DINOV2-Base
	DINOV2-Small	RetFound	0.000398617	0.394574958	0.351253089	0.017643336	0.015629003	[0.37693162, 0.41221829]	[0.33562409, 0.36688209]	DINOV2-Small
IDRID->APTOS2019	DINOV2-Large	DINOV2-Base	2.68E-27	0.404705899	0.342075957	0.007019561	0.006689263	[0.39768634, 0.41172546]	[0.33538669, 0.34876522]	DINOV2-Large
	DINOV2-Large	DINOV2-Small	0.000729673	0.404705899	0.387588169	0.007019561	0.006804395	[0.39768634, 0.41172546]	[0.38078377, 0.39439256]	DINOV2-Large
	DINOV2-Large	RetFound	4.02E-08	0.404705899	0.376411606	0.007019561	0.006703976	[0.39768634, 0.41172546]	[0.36970763, 0.38311558]	DINOV2-Large
	DINOV2-Base	DINOV2-Small	1.93E-17	0.342075957	0.387588169	0.006689263	0.006804395	[0.33538669, 0.34876522]	[0.38078377, 0.39439256]	DINOV2-Small
	DINOV2-Base	RetFound	2.11E-11	0.342075957	0.376411606	0.006689263	0.006703976	[0.33538669, 0.34876522]	[0.36970763, 0.38311558]	RetFound
	DINOV2-Small	RetFound	0.022879776	0.387588169	0.376411606	0.006804395	0.006703976	[0.38078377, 0.39439256]	[0.36970763, 0.38311558]	DINOV2-Small
IDRID->MESSIDOR2	DINOV2-Large	DINOV2-Base	3.79E-12	0.412181561	0.346392364	0.013717574	0.010743689	[0.39846399, 0.42589914]	[0.33564867, 0.35713605]	DINOV2-Large
	DINOV2-Large	DINOV2-Small	0.811347661	0.412181561	0.410001785	0.013717574	0.011461305	[0.39846399, 0.42589914]	[0.39854048, 0.42146309]	DINOV2-Large
	DINOV2-Large	RetFound	1.25E-06	0.412181561	0.361850606	0.013717574	0.014176098	[0.39846399, 0.42589914]	[0.34767451, 0.37602670]	DINOV2-Large
	DINOV2-Base	DINOV2-Small	1.51E-13	0.346392364	0.410001785	0.010743689	0.011461305	[0.33564867, 0.35713605]	[0.39854048, 0.42146309]	DINOV2-Small
	DINOV2-Base	RetFound	0.090070224	0.346392364	0.361850606	0.010743689	0.014176098	[0.33564867, 0.35713605]	[0.34767451, 0.37602670]	RetFound
	DINOV2-Small	RetFound	5.52E-07	0.410001785	0.361850606	0.011461305	0.014176098	[0.39854048, 0.42146309]	[0.34767451, 0.37602670]	DINOV2-Small
MESSIDOR2->APTOS2019	DINOV2-Large	DINOV2-Base	9.77E-15	0.328980028	0.368773596	0.006582649	0.006581859	[0.32239738, 0.33556268]	[0.36219174, 0.37535546]	DINOV2-Base
	DINOV2-Large	DINOV2-Small	2.08E-20	0.328980028	0.283137951	0.006582649	0.005631632	[0.32239738, 0.33556268]	[0.27750632, 0.28876958]	DINOV2-Large
	DINOV2-Large	RetFound	3.82E-41	0.328980028	0.419049794	0.006582649	0.007878664	[0.32239738, 0.33556268]	[0.41117113, 0.42692846]	RetFound
	DINOV2-Base	DINOV2-Small	1.33E-47	0.368773596	0.283137951	0.006581859	0.005631632	[0.36219174, 0.37535546]	[0.27750632, 0.28876958]	DINOV2-Base
	DINOV2-Base	RetFound	3.72E-18	0.368773596	0.419049794	0.006581859	0.007878664	[0.36219174, 0.37535546]	[0.41117113, 0.42692846]	RetFound
	DINOV2-Small	RetFound	1.48E-69	0.283137951	0.419049794	0.005631632	0.007878664	[0.27750632, 0.28876958]	[0.41117113, 0.42692846]	RetFound
MESSIDOR2->IDRID	DINOV2-Large	DINOV2-Base	8.46E-06	0.247418978	0.317448612	0.020014592	0.02236652	[0.22740439, 0.26743357]	[0.29508209, 0.33981513]	DINOV2-Base
	DINOV2-Large	DINOV2-Small	0.013156377	0.247418978	0.284893101	0.020014592	0.021474404	[0.22740439, 0.26743357]	[0.26341870, 0.30636750]	DINOV2-Small
	DINOV2-Large	RetFound	0.02365527	0.247418978	0.279442042	0.020014592	0.018895574	[0.22740439, 0.26743357]	[0.26054647, 0.29833762]	RetFound
	DINOV2-Base	DINOV2-Small	0.040908977	0.317448612	0.284893101	0.02236652	0.021474404	[0.29508209, 0.33981513]	[0.26341870, 0.30636750]	DINOV2-Base
	DINOV2-Base	RetFound	0.011716545	0.317448612	0.279442042	0.02236652	0.018895574	[0.29508209, 0.33981513]	[0.26054647, 0.29833762]	DINOV2-Base

	DINOv2-Small	RetFound	0.709164106	0.284893101	0.279442042	0.021474404	0.018895574	[0.26341870, 0.30636750]	[0.26054647, 0.29833762]	DINOv2-Small
--	--------------	----------	-------------	-------------	-------------	-------------	-------------	--------------------------	--------------------------	--------------

Performance of DINOv2 and RETFound models for Glaucoma classification tasks in the respective external tests sets. (F1-Score)										
Dataset	Model-1	Model-2	P-value-F1-Score	Mean-F1-Score-model-1	Mean-F1-Score-model-2	Model-1 (1.96× Std)	Model-2 (1.96× Std)	Model-1 95% confidence interval	Model-2 95% confidence interval	Better-model
Glaucoma_fundus->PAPILA	DINOv2-Large	DINOv2-Base	6.48E-10	0.240803987	0.15920351	0.017124957	0.017682916	[0.22367903, 0.25792894]	[0.14152059, 0.17688643]	DINOv2-Large
	DINOv2-Large	DINOv2-Small	0.000984878	0.240803987	0.198061131	0.017124957	0.018277476	[0.22367903, 0.25792894]	[0.17978365, 0.21633861]	DINOv2-Large
	DINOv2-Large	RetFound	2.35E-12	0.240803987	0.148328036	0.017124957	0.017139381	[0.22367903, 0.25792894]	[0.13118865, 0.16546742]	DINOv2-Large
	DINOv2-Base	DINOv2-Small	0.003097008	0.15920351	0.198061131	0.017682916	0.018277476	[0.14152059, 0.17688643]	[0.17978365, 0.21633861]	DINOv2-Small
	DINOv2-Base	RetFound	0.387766209	0.15920351	0.148328036	0.017682916	0.017139381	[0.14152059, 0.17688643]	[0.13118865, 0.16546742]	DINOv2-Base
	DINOv2-Small	RetFound	0.000136684	0.198061131	0.148328036	0.018277476	0.017139381	[0.17978365, 0.21633861]	[0.13118865, 0.16546742]	DINOv2-Small
PAPILA->Glaucoma_fundus	DINOv2-Large	DINOv2-Base	0.369772932	0.407926781	0.41386198	0.009034928	0.009264528	[0.39889185, 0.41696171]	[0.40459745, 0.42312651]	DINOv2-Base
	DINOv2-Large	DINOv2-Small	0.00011979	0.407926781	0.381055055	0.009034928	0.00922927	[0.39889185, 0.41696171]	[0.37113213, 0.39097798]	DINOv2-Large
	DINOv2-Large	RetFound	1.27E-76	0.407926781	0.240015258	0.009034928	0.005934523	[0.39889185, 0.41696171]	[0.23408073, 0.24594978]	DINOv2-Large
	DINOv2-Base	DINOv2-Small	4.14E-06	0.41386198	0.381055055	0.009264528	0.00922927	[0.40459745, 0.42312651]	[0.37113213, 0.39097798]	DINOv2-Base
	DINOv2-Base	RetFound	7.73E-78	0.41386198	0.240015258	0.009264528	0.005934523	[0.40459745, 0.42312651]	[0.23408073, 0.24594978]	DINOv2-Base
	DINOv2-Small	RetFound	2.78E-60	0.381055055	0.240015258	0.00922927	0.005934523	[0.37113213, 0.39097798]	[0.23408073, 0.24594978]	DINOv2-Small

Supplementary table 5

External evaluation of diagnostic classification for three systemic diseases: heart failure, myocardial infarction, and ischemic stroke. (Fine-tuned on the MEH-AlzEye dataset and externally evaluated on the UK Biobank dataset)					
Prediction of 3-year incidence of systemic diseases	Model	Mean-AUROC	Std-AUROC	95% confidence interval (AUROC)	P-value-AUROC
Heart failure	DINOV2-large	0.616550439	0.052492615	[0.51286131 0.69927789]	3.27E-13
	DINOV2-base	0.614764891	0.04893961	[0.5242533 0.70824468]	1.31E-14
	DINOV2-small	0.62344994	0.050827706	[0.52895008 0.70306097]	4.11E-11
	RetFound	0.674403192	0.051742297	[0.58099382 0.76361821]	1
Myocardial infarction	DINOV2-large	0.552436324	0.061984335	[0.42005501 0.67112587]	5.13E-06
	DINOV2-base	0.55875252	0.062519093	[0.43410835 0.67759359]	0.00010521
	DINOV2-small	0.52335581	0.065928218	[0.41645705 0.65232665]	5.52E-13
	RetFound	0.593976445	0.062699356	[0.47715234 0.71804276]	1
Ischaemic stroke	DINOV2-large	0.590414434	0.066680004	[0.4725209 0.72539117]	0.629429638
	DINOV2-base	0.556479383	0.079120379	[0.40612701 0.69528842]	0.00823233
	DINOV2-small	0.518707029	0.080968619	[0.36069913 0.66021212]	6.78E-09
	RetFound	0.585570588	0.074155322	[0.44381267 0.70308874]	1

Prediction of 3-year incidence of systemic diseases	Model	Mean-Accuracy	Std-Accuracy	95% confidence interval (Accuracy)	P-value-Accuracy
Heart failure	DINOV2-large	0.497070707	0.049139	[0.4040404 0.58585859]	0.006242461
	DINOV2-base	0.494545455	0.049359121	[0.39873737 0.58585859]	0.002096471
	DINOV2-small	0.503535354	0.046340964	[0.41414141 0.58585859]	0.05947122
	RetFound	0.516464646	0.049580528	[0.40883838 0.60606061]	1
Myocardial infarction	DINOV2-large	0.49925	0.052285873	[0.425 0.6065625]	0.042237435
	DINOV2-base	0.49875	0.051493325	[0.4184375 0.6125]	0.034827399
	DINOV2-small	0.519375	0.057645875	[0.4184375 0.6375]	0.575496743
	RetFound	0.514875	0.055218175	[0.425 0.6190625]	1
Ischaemic stroke	DINOV2-large	0.499016393	0.064762191	[0.37704918 0.61516393]	0.422925053
	DINOV2-base	0.491311475	0.06855733	[0.36065574 0.59877049]	0.986475949
	DINOV2-small	0.502131148	0.06596828	[0.37704918 0.60655738]	0.262122196
	RetFound	0.49147541	0.067352115	[0.36065574 0.59016393]	1

Prediction of 3-year incidence of systemic diseases	Model	Mean-kappa	Std-Kappa	95% confidence interval (Kappa)	P-value-Kappa
Heart failure	DINOV2-large	0.004892988	0.009556864	[0. 0.02740014]	1.68E-17
	DINOV2-base	-0.000159602	0.013965524	[-0.02025606 0.02740014]	3.39E-20
	DINOV2-small	0.016272031	0.040264879	[-0.06195586 0.09463056]	5.65E-06
	RetFound	0.04247833	0.038749165	[-0.02605629 0.10934256]	1
Myocardial infarction	DINOV2-large	0.006174373	0.020121919	[-0.03811214 0.04482542]	1.28E-05
	DINOV2-base	0.004469216	0.028369215	[-0.04963789 0.06877792]	1.02E-05
	DINOV2-small	0.045954117	0.06372518	[-0.0619945 0.19140833]	0.242722089
	RetFound	0.035487054	0.061963211	[-0.06280488 0.16978721]	1
Ischaemic stroke	DINOV2-large	0.015810036	0.04815832	[-0.06564036 0.10956153]	0.022809005
	DINOV2-base	0.00286251	0.030768506	[-0.06510786 0.0662434]	0.980283435
	DINOV2-small	0.022761557	0.049480339	[-0.06602199 0.14985019]	0.000690651
	RetFound	0.002756071	0.02975036	[-0.05468253 0.06821936]	1

Prediction of 3-year incidence of systemic diseases	Model	Mean-F1-Score	Std-F1-Score	95% confidence interval (F1 Score)	P-value-F1-Score
Heart failure	DINOV2-large	0.009520717	0.018509458	[0. 0.04659091]	2.14E-38
	DINOV2-base	0.00948408	0.01845145	[0. 0.04659091]	1.99E-38
	DINOV2-small	0.097584024	0.052707528	[0. 0.22277417]	0.087016435
	RetFound	0.111306978	0.059369273	[0. 0.21780632]	1
Myocardial infarction	DINOV2-large	0.021378444	0.029674949	[0. 0.09418605]	3.12E-45
	DINOV2-base	0.038493255	0.043108542	[0. 0.12785326]	5.38E-36
	DINOV2-small	0.187509938	0.081223551	[0.04208777 0.33045455]	0.400947467
	RetFound	0.177954895	0.078482694	[0.04298611 0.33333333]	1
Ischaemic stroke	DINOV2-large	0.085890994	0.069861936	[0. 0.22908497]	8.25E-11
	DINOV2-base	0.028693545	0.042923513	[0. 0.12711694]	0.992958985
	DINOV2-small	0.080631393	0.069045483	[0. 0.25]	2.02E-09
	RetFound	0.028748405	0.044429014	[0. 0.129375]	1

Supplementary table 6

Internal test analysis of label efficiency for ocular disease							
Tasks	Dataset	Models	Ratio of training data	Mean-Accuracy	Lower (95% CI)	Upper (95% CI)	
Diabetic retinopathy (CFP) (Task I)	APTOS2019	DINOv2-Large	1	0.951465852	0.94981336	0.953118344	
			0.9	0.954284965	0.952735937	0.955833993	
			0.5	0.944426521	0.942780039	0.946073002	
			0.2	0.933959713	0.932157866	0.93576156	
			0.1	0.930941596	0.928809764	0.933073429	
		DINOv2-Base	1	0.936351716	0.934145191	0.938558241	
			0.9	0.944440156	0.942516742	0.946363569	
			0.5	0.936548798	0.934541783	0.938555813	
			0.2	0.929889658	0.927732354	0.932046962	
			0.1	0.931255703	0.929168051	0.933343356	
		DINOv2-Small	1	0.930314087	0.927888162	0.932740012	
			0.9	0.947154576	0.945284942	0.94902421	
			0.5	0.923793368	0.921132346	0.92645439	
			0.2	0.934558022	0.93252477	0.936591273	
			0.1	0.929568088	0.927508372	0.931627805	
		RETFFound	1	0.939822436	0.937721886	0.941922986	
			0.9	0.949499022	0.948017382	0.950980662	
			0.5	0.942160085	0.940491833	0.943828337	
			0.2	0.934077194	0.932179683	0.935974706	
			0.1	0.922840515	0.920693016	0.924988014	
	MESSIDOR2	DINOv2-Large	1	0.908719086	0.905694377	0.911743795	
			0.9	0.904464586	0.901294515	0.907634657	
			0.5	0.89928073	0.895559028	0.903002433	
			0.2	0.882409773	0.878436252	0.886383295	
			0.1	0.887819135	0.883621771	0.892016499	
		DINOv2-Base	1	0.905444362	0.902183631	0.908705092	
			0.9	0.897278964	0.893644836	0.900913091	
			0.5	0.89860737	0.895249285	0.901965455	
			0.2	0.866961283	0.86266163	0.871260936	
			0.1	0.86103474	0.857168183	0.864901297	
		DINOv2-Small	1	0.90023287	0.896937198	0.903528542	
			0.9	0.903351072	0.899965579	0.906736566	
			0.5	0.887053405	0.883496771	0.890610038	
			0.2	0.881857458	0.877929473	0.885785442	
			0.1	0.867902029	0.864076952	0.871727106	
		RETFFound	1	0.877161621	0.873329853	0.880993388	
			0.9	0.880241266	0.876133844	0.884348688	
			0.5	0.873010467	0.868886649	0.877134285	
			0.2	0.782969017	0.775264521	0.790673513	
			0.1	0.716208601	0.707626364	0.724790839	
	IDRID	DINOv2-Large	1	0.849550824	0.836798561	0.862303088	
			0.9	0.832674547	0.820604588	0.844744507	
			0.5	0.843560486	0.832909687	0.854211285	
			0.2	0.774295001	0.763004826	0.785585176	
			0.1	0.767989466	0.756998186	0.778980746	
		DINOv2-Base	1	0.809584459	0.797362599	0.821806319	
			0.9	0.836735621	0.824879996	0.848591246	
			0.5	0.845087724	0.834298868	0.85587658	
			0.2	0.791739722	0.779508902	0.803970542	
			0.1	0.786067005	0.77452214	0.797611871	
		DINOv2-Small	1	0.813365522	0.802288202	0.824442843	
			0.9	0.821725373	0.809445416	0.834005331	
			0.5	0.849906489	0.839704403	0.860108575	
			0.2	0.749863896	0.736722717	0.763005075	
			0.1	0.785364492	0.77185427	0.798874714	
		RETFFound	1	0.816212149	0.805223275	0.827201023	
			0.9	0.817945506	0.806618304	0.829272709	
			0.5	0.823924331	0.813404531	0.83444413	
			0.2	0.706859157	0.696183033	0.71753528	
			0.1	0.6902515	0.677649081	0.70285392	
	Glaucoma (CFP) (Task II)	Glaucoma_fundus	DINOv2-Large	1	0.946962852	0.944069524	0.94985618
				0.9	0.945233848	0.942296617	0.94817108
				0.5	0.900609573	0.895179324	0.906039823
				0.2	0.886401427	0.88206236	0.890740494
				0.1	0.876524079	0.871786892	0.881261265
			DINOv2-Base	1	0.958459087	0.955797374	0.961120801
				0.9	0.955443733	0.952709217	0.958178248
				0.5	0.933893323	0.930476009	0.937310637
				0.2	0.91137089	0.907738525	0.915003255
				0.1	0.881531944	0.877365191	0.885698697
			DINOv2-Small	1	0.958914963	0.956344053	0.961485874
				0.9	0.950364272	0.947293773	0.953434772
				0.5	0.932214531	0.928464175	0.935964888
				0.2	0.909953119	0.905873946	0.914032291
				0.1	0.881812573	0.877410361	0.886214786
			RETFFound	1	0.936582461	0.932788136	0.940376786
				0.9	0.941821623	0.938721707	0.94492154
				0.5	0.924794484	0.921036088	0.928552879

	PAPILA	DINOv2-Large	0.2	0.909311689	0.905545197	0.913078182
			0.1	0.877153952	0.872683328	0.881624576
			1	0.837469526	0.822065296	0.852873756
			0.9	0.870860226	0.857868831	0.88385162
			0.5	0.803865296	0.788000542	0.819730051
			0.2	0.709619843	0.68932851	0.729911176
		DINOv2-Base	0.1	0.684301977	0.665850163	0.702753792
			1	0.848937405	0.834577345	0.863297464
			0.9	0.843527115	0.828311399	0.85874283
			0.5	0.781472511	0.76450071	0.798444313
			0.2	0.759139352	0.738148761	0.780129943
			0.1	0.671228865	0.653063511	0.689394218
		DINOv2-Small	1	0.823173644	0.808433994	0.837913295
			0.9	0.840305766	0.826482129	0.854129404
			0.5	0.782118739	0.764029368	0.80020811
			0.2	0.730391779	0.708937106	0.751846451
0.1	0.682047573		0.664523971	0.699571174		
1	0.855098211		0.83850796	0.871688461		
RETFFound	0.9	0.865889991	0.850470167	0.881309815		
	0.5	0.828344441	0.814429144	0.842259738		
	0.2	0.745938604	0.729739113	0.762138095		
	0.1	0.642343706	0.623692028	0.660995384		
	1	0.996259428	0.995209715	0.99730914		
	0.9	0.996863418	0.996399206	0.99732763		
Multi-category eye disease (CFP) (Task III)	JSIEC	DINOv2-Large	0.5	0.993579316	0.992778063	0.994380569
			0.2	0.937732637	0.934309679	0.941155595
			0.1	0.841064781	0.835565947	0.846563615
			1	0.99741418	0.996994986	0.997833374
			0.9	0.996466781	0.996064852	0.99686871
		DINOv2-Base	0.5	0.991510993	0.9904749	0.992547086
			0.2	0.940908332	0.937395489	0.944421174
			0.1	0.855685972	0.850568889	0.860803055
			1	0.994724424	0.993613538	0.99583531
			0.9	0.994226266	0.9933023	0.995150233
		DINOv2-Small	0.5	0.992542606	0.991808356	0.993276855
			0.2	0.927130699	0.923030272	0.931231127
			0.1	0.863685827	0.858546253	0.8688254
			1	0.992973165	0.992098769	0.993847561
			0.9	0.986826482	0.985464454	0.988188511
		RETFFound	0.5	0.975704305	0.973682984	0.977725626
0.2	0.862624784		0.857523629	0.867725939		
0.1	0.811254295		0.80568571	0.816822879		
1	0.892156716		0.884470855	0.899842578		
0.9	0.888046082		0.87980944	0.896282724		
Multi-category eye disease (CFP) (Task III)	Retina	DINOv2-Large	0.5	0.884879414	0.876404596	0.893354232
			0.2	0.82496095	0.816402384	0.833519516
			0.1	0.706921456	0.695745758	0.718097153
			1	0.872930905	0.864447411	0.881414398
			0.9	0.836491285	0.826138134	0.846844435
		DINOv2-Base	0.5	0.860676029	0.851146109	0.870205949
			0.2	0.772162442	0.762043826	0.782281058
			0.1	0.714862766	0.70285455	0.726870981
			1	0.879877579	0.870727099	0.88902806
			0.9	0.877110654	0.867434484	0.886786824
		DINOv2-Small	0.5	0.866802766	0.857838937	0.875766596
			0.2	0.738074927	0.726878314	0.74927154
			0.1	0.752727194	0.741250957	0.76420343
			1	0.846217071	0.838112985	0.854321157
			0.9	0.814922393	0.804824063	0.825020722
		RETFFound	0.5	0.766784432	0.756315623	0.77725324
0.2	0.708590362		0.697370701	0.719810023		
0.1	0.673307904		0.662461075	0.684154733		
1	0.998765842		0.998426536	0.999105149		
0.9	0.998333458		0.997912742	0.998754174		
Multi-category eye disease (OCT) (Task IV)	OCTID	DINOv2-Large	0.5	0.994705781	0.993571983	0.995839579
			0.2	0.984473799	0.982192183	0.986755415
			0.1	0.873700515	0.867673503	0.879727527
			1	0.998563591	0.998143479	0.998983704
			0.9	0.995829385	0.994794819	0.996863952
		DINOv2-Base	0.5	0.993373447	0.991911532	0.994835362
			0.2	0.989797136	0.987482752	0.992111519
			0.1	0.949847901	0.943415614	0.956280188
			1	0.99808642	0.997650284	0.998522555
			0.9	0.997639679	0.997093584	0.998185775
		DINOv2-Small	0.5	0.993299748	0.992228481	0.994371016
			0.2	0.987898604	0.985949136	0.989848072
			0.1	0.946218988	0.941411335	0.951026641
			1	0.999288969	0.999080532	0.999497407
			0.9	0.93239682	0.925657866	0.939135774
		RETFFound	0.5	0.875518602	0.868911712	0.882125491
0.2	0.840791849		0.833197215	0.848386484		
0.1	0.767680718		0.759287489	0.776073948		

Supplementary table 7

AUROC Performance of all models in predicting 3-year incidence of systemic diseases using retinal images in the internal test (MEH-AlzEye dataset).						
Ratio of training data	Prediction of 3-year incidence of systemic diseases	Models	Mean-AUROC	Std-AUROC	95% confidence interval	P-value-AUROC
1	Heart failure	DINOV2-large	0.767103307	0.018100313	[0.73246627 0.80013376]	7.39E-24
		DINOV2-base	0.771440432	0.017978413	[0.73773338 0.80653686]	8.31E-19
		DINOV2-small	0.757836845	0.018275136	[0.72525449 0.78962458]	5.54E-35
		RetFound	0.795852679	0.01697335	[0.76659377 0.82737053]	1
	Myocardial infarction	DINOV2-large	0.711063532	0.040337169	[0.63846958 0.78407478]	0.000202234
		DINOV2-base	0.709930652	0.035852982	[0.63991474 0.78242482]	3.65E-05
		DINOV2-small	0.662948138	0.038643885	[0.58653423 0.7272883]	3.95E-27
		RetFound	0.732383852	0.038871084	[0.66251299 0.80530279]	1
	Ischaemic stroke	DINOV2-large	0.690448191	0.0424947	[0.60627614 0.7730664]	6.45E-22
		DINOV2-base	0.713816749	0.040382842	[0.63287334 0.78933099]	2.85E-11
		DINOV2-small	0.711994708	0.036599553	[0.64107752 0.77271921]	5.06E-13
		RetFound	0.75379559	0.039365003	[0.68353624 0.83777143]	1
0.9	Heart failure	DINOV2-large	0.773330317	0.017571946	[0.74096091 0.80591433]	1.67E-05
		DINOV2-base	0.775320345	0.016556081	[0.74752039 0.80730642]	0.000252327
		DINOV2-small	0.757053467	0.018479368	[0.7255414 0.79682323]	4.06E-21
		RetFound	0.784432056	0.017817314	[0.75412065 0.81623446]	1
	Myocardial infarction	DINOV2-large	0.691502487	0.039036201	[0.61480887 0.76983415]	7.85E-12
		DINOV2-base	0.711099255	0.039004178	[0.6428712 0.78337979]	0.000370074
		DINOV2-small	0.684561357	0.042702474	[0.60068298 0.76019244]	4.01E-14
		RetFound	0.730517254	0.036366396	[0.66860255 0.79928615]	1
	Ischaemic stroke	DINOV2-large	0.723108332	0.040682925	[0.64967974 0.79878416]	3.66E-09
		DINOV2-base	0.714462998	0.038252859	[0.63741429 0.78426498]	7.19E-14
		DINOV2-small	0.712770475	0.037045508	[0.64723986 0.78255286]	3.78E-15
		RetFound	0.756331803	0.034779941	[0.7003056 0.82647338]	1
0.5	Heart failure	DINOV2-large	0.759741106	0.01761729	[0.72755039 0.79401549]	9.73E-24
		DINOV2-base	0.766063579	0.017599521	[0.73272927 0.7994287]	1.22E-16
		DINOV2-small	0.749301608	0.01953179	[0.7152216 0.78786288]	1.16E-33
		RetFound	0.789675821	0.019020564	[0.75108652 0.8228312]	1
	Myocardial infarction	DINOV2-large	0.703289479	0.038535499	[0.63791339 0.77793802]	1.78E-08
		DINOV2-base	0.719610375	0.037377446	[0.65735178 0.78313722]	0.004920641
		DINOV2-small	0.69773964	0.039085192	[0.63310185 0.77501443]	8.32E-11
		RetFound	0.734471611	0.036137145	[0.67122391 0.80445636]	1
	Ischaemic stroke	DINOV2-large	0.714154413	0.040920185	[0.64212021 0.7927289]	0.000441472
		DINOV2-base	0.719895194	0.037427842	[0.65133351 0.7909192]	0.008115952
		DINOV2-small	0.685694786	0.043564133	[0.60410829 0.76108761]	1.29E-14
		RetFound	0.734291112	0.03831536	[0.6728642 0.81024822]	1
0.2	Heart failure	DINOV2-large	0.736179149	0.018840212	[0.70188816 0.77503092]	3.17E-38
		DINOV2-base	0.746951988	0.018566649	[0.71146138 0.78522841]	1.30E-25
		DINOV2-small	0.742199768	0.017559095	[0.71000322 0.77501757]	1.22E-32
		RetFound	0.777619732	0.017045668	[0.75025791 0.81528719]	1
	Myocardial infarction	DINOV2-large	0.640658819	0.040836561	[0.57325811 0.71924933]	1.54E-29
		DINOV2-base	0.653632483	0.039995016	[0.58898771 0.72581584]	8.62E-23
		DINOV2-small	0.617444389	0.042870237	[0.54223134 0.69170573]	6.84E-41
		RetFound	0.714788468	0.03696176	[0.64853358 0.77960953]	1
	Ischaemic stroke	DINOV2-large	0.661216821	0.044380689	[0.58208234 0.75234193]	3.72E-21
		DINOV2-base	0.707374163	0.039852431	[0.6407423 0.77730993]	0.00254215
		DINOV2-small	0.689844118	0.040179436	[0.61446023 0.7753263]	4.34E-09
		RetFound	0.724595167	0.039407063	[0.64717858 0.79285185]	1
0.1	Heart failure	DINOV2-large	0.709533219	0.021329543	[0.6679498 0.75319835]	2.06E-52
		DINOV2-base	0.741219129	0.019805344	[0.70376075 0.78166091]	1.54E-19
		DINOV2-small	0.721315612	0.022830667	[0.67437131 0.76619689]	6.38E-38
		RetFound	0.768061141	0.017616053	[0.73933527 0.80436007]	1
	Myocardial infarction	DINOV2-large	0.634880503	0.041575356	[0.56131556 0.71419843]	5.23E-26
		DINOV2-base	0.635921892	0.041067037	[0.56144705 0.71050117]	1.08E-25
		DINOV2-small	0.634276097	0.042878191	[0.56158319 0.72046003]	1.03E-25
		RetFound	0.705456509	0.039555541	[0.63145063 0.7789849]	1
	Ischaemic stroke	DINOV2-large	0.65289561	0.045410758	[0.56806513 0.74880495]	2.33E-18
		DINOV2-base	0.699016549	0.042661851	[0.61600495 0.7903517]	0.027034844
		DINOV2-small	0.676559575	0.041674081	[0.59533108 0.76729804]	5.93E-09
		RetFound	0.712236682	0.040827658	[0.63600531 0.79120195]	1

Supplementary table 8

Parameters and computational costs associated with different FMs					
Model	Parameters (M)	FLOPs (G)	Total Inference Time (s)	Average Inference Time (s)	Max Memory Usage (MB)
dinov2_small	21.520512	5.5247232	0.480681419	0.004806814	153.6621094
dinov2_base	85.508352	21.9635497	0.636247158	0.006362472	403.3408203
dinov2_large	302.91456	77.81712282	1.698586226	0.016985862	1236.862305
RETFound	303.10708	59.68569549	1.478601933	0.014786019	1232.889648

*For inference time on 100 fundus images (224 × 224 resolution, using 1 × A100 GPU)